

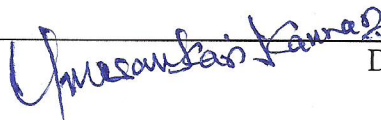
**Development of Deterministic and Stochastic Methods
for Physics Analysis of High-Temperature Reactors**

Homi Bhabha National Institute

Recommendations of the Viva Voce Committee

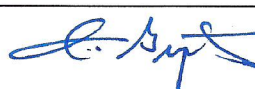
As members of the Viva Voce Committee, we certify that we have read the dissertation prepared by INDRAJEET SINGH entitled "DEVELOPMENT OF DETERMINISTIC AND STOCHASTIC METHODS FOR PHYSICS ANALYSIS OF HIGH-TEMPERATURE REACTORS" and recommend that it may be accepted as fulfilling the thesis requirement for the award of Degree of Doctor of Philosophy.

Chairman - Prof. Umasankari Kannan



Date: 29/6/2021

Guide / Convener - Prof. Anurag Gupta



Date: 29/6/2021

Examiner - Prof. R. S. Keshavamurthy



Date: 29/06/2021

Member 1- Prof. Palani Selvam



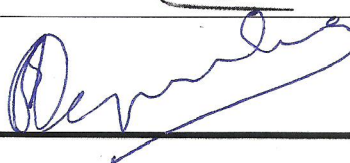
Date: 29/06/2021

Member 2- Prof. K. Devan



Date: 29/06/2021

Invitee- Prof. S. B. Degweker



Date: 29/06/2021

Final approval and acceptance of this thesis is contingent upon the candidate's submission of the final copies of the thesis to HBNI.

I/We hereby certify that I/we have read this thesis prepared under my/our direction and recommend that it may be accepted as fulfilling the thesis requirement.

Date: 29-June-2021

Place: MUMBAI



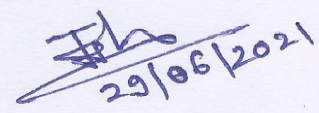
Prof. Anurag Gupta

Guide

STATEMENT BY AUTHOR

This dissertation has been submitted in partial fulfillment of requirements for an advanced degree at Homi Bhabha National Institute (HBNI) and is deposited in the Library to be made available to borrowers under rules of the HBNI.

Brief quotations from this dissertation are allowable without special permission, provided that accurate acknowledgement of source is made. Requests for permission for extended quotation from or reproduction of this manuscript in whole or in part may be granted by the Competent Authority of HBNI when in his or her judgment the proposed use of the material is in the interests of scholarship. In all other instances, however, permission must be obtained from the author.



Indrajeet Singh

DECLARATION

I, hereby declare that the investigation presented in the thesis has been carried out by me. The work is original and has not been submitted earlier as a whole or in part for a degree / diploma at this or any other Institution / University.


29/06/2021
Indrajeet Singh

List of Publications arising from the thesis

Journal

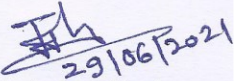
1. "A New Collision Probability Approach for Solution of the Transport Equation in the Random Medium of High-Plutonium-Content HTR Lattice Cells", Indrajeet Singh, S. B. Degweker & Anurag Gupta, Nucl. Sci. and Eng., Volume 189, 2018 - Issue 2, Pages 101-119. <https://doi.org/10.1080/00295639.2017.1402568>
2. "Treatment of Double Heterogeneity in the Resonance and Thermal Energy Regions in High-Temperature Reactors", Indrajeet Singh, S. B. Degweker and Anurag Gupta, Nucl. Sci. & Eng., Volume 189, 2018 - Issue 3, Pages 243-258. <https://doi.org/10.1080/00295639.2017.1388092>
3. "A New Approach to Monte Carlo in High Temperature Reactors", Indrajeet Singh, S. B. Degweker, Amod Kishore Mallick and Anurag Gupta, Nucl. Sci. & Eng., Volume 193, 2019 - Issue 8. Pages 868-883, <https://doi.org/10.1080/00295639.2019.1576453>

National Conference

1. "Preliminary Study of OTTO Fuel Cycle for IHTR-20 MWth" Indrajeet Singh, Anurag Gupta and Umasankari Kannan, Advances in Reactor Physics (ARP-2017), Mumbai, India, Dec. 06-09, 2017, DS11.044, P-367

Others

2. "Studies on Reactivity Coefficients of Thorium- Based Fuel (Th-233U)O₂ with Molten Salt (Flibe) Cooled Pebble," Indrajeet Singh, Anurag Gupta and Umasankari Kannan, Nucl. Sci. & Eng., Volume 191, 2018 - Issue 2, Pages 161-177 <https://doi.org/10.1080/00295639.2018.1463745>


29/06/2021
Indrajeet Singh

**Dedicated
to
My Teachers and Parents**

ACKNOWLEDGEMENTS

I would like to take this opportunity to convey my thanks of gratitude towards several people without their direct or indirect support this work would not have been possible.

I would like to express my great appreciation and deepest regards to my thesis supervisor Dr S.B. Degweker for all his support, motivations, encouragements and guidance. I sincerely thank him for providing me the opportunity to carry out my research under his professional expertise. I will always be indebted to him for all he taught to me, untiring efforts to clarify my doubts and invaluable help in writing the thesis.

I sincerely thank my co-guide Dr Anurag Gupta, Head RPAS, RPDD for his care, motivation, encouragement and for providing all the freedom I needed to work in my own ways. He is my guide after superannuation of Dr S. B. Degweker. I am particularly thankful to Dr Umasankari Kannan, Head RPDD and chairman of my doctoral committee for her insightful comments and technical suggestions. I am thankful to Dr Palani Selvem, BARC and Dr Deven, IGCAR for their time, suggestions, efforts in reviewing my progress of the research and serving on my doctoral committee.

I am grateful to Shri Amod Kishore Mallick and Smt. Argala Srivastava, RPDD for always being helpful and friendly for any problem. I sincerely acknowledge to Shri D.K. Dwivedi, Shri Kapil Deo, Shri A. K. Srivastava, Shri Amit Thakur, Shri Vishal Bharti and Shri Arindam Chakraborti for all their support and help. I want to thanks to RPDD colleagues and friends in BARC for all their help and encouragements.

Thanks are due to my cousin and friend Sunil Singh for his time, support and encouragements. I would like to record high respect and admiration to my parents for their unconditional love and several cheerful sacrifices for my success. I highly appreciate to numerous friends for being supportive, giving unforgettable happy moments in my life and having faith in me.

Thanks, finally but not least, to my son Viresh and wife Chandra Prabha for providing emotional support and great care during the work of this thesis. Above all, I pray and thanks to God Almighty for blessing me the mental ability, courage and knowledge to complete this work.

CONTENTS

ACKNOWLEDGEMENTS	7
CONTENTS.....	8
SYNOPSIS.....	13
LIST OF FIGURES	23
LIST OF TABLES	26
CHAPTER 1 INTRODUCTION: HIGH TEMPERATURE REACTORS.....	28
1.1 NEED OF NUCLEAR ENERGY	28
1.2 WHY HIGH TEMPERATURE REACTORS.....	30
1.3 EXPERIENCE WITH HTRS	31
1.4 CURRENTLY OPERATING AND FUTURE HTRS	32
1.5 HTR TYPES AND FUEL ELEMENTS	33
1.5.1 Pebble-bed Type	34
1.5.2 Prismatic Block Type.....	34
1.5.3 TRISO.....	35
1.5.4 Fuel Pebble	35
1.5.5 Fuel Compact.....	36
1.6 NUCLEAR HYDROGEN PRODUCTION	36
1.7 REACTOR PHYSICS DESIGN OBJECTIVES	38
1.8 SPECIAL PROBLEMS OF HTR DESIGN AND THESIS OUTLINE	40
CHAPTER 2 REVIEW OF NEUTRONICS METHODS: CURRENTLY USED IN TRADITIONAL REACTORS AND HTRS	43
2.1 INTRODUCTION	43
2.2 NEUTRONICS METHODOLOGY.....	44
2.3 NEUTRON TRANSPORT EQUATION	46

2.4	MULTI-STEP METHODOLOGY.....	49
2.4.1	Multi-group approximation.....	51
2.4.2	Self-Shielding Methods	55
2.4.3	Equivalence Principle	56
2.4.4	Subgroup Method	59
2.5	DETERMINISTIC METHODS: SOLUTION OF THE TRANSPORT EQUATION	59
2.5.1	Spherical Harmonics Method (PN).....	60
2.5.2	Discrete Ordinates Method (DSN)	60
2.5.3	Method of Characteristics (MOC)	62
2.5.4	Integral Transport Theory Based Methods	62
	<i>The Collision Probability Method</i>	63
	<i>The Interface Current Method ($J \pm$)</i>	65
	<i>Calculation of Collision Probabilities</i>	67
	<i>Properties of Collision Probabilities</i>	70
2.5.5	Solution of Collision Probability Equations	71
2.6	FUEL BURN-UP	72
2.7	MONTE CARLO METHODS FOR NEUTRON TRANSPORT	73
2.7.1	Pseudo Random Numbers and Generators.....	74
2.7.2	Sampling Methods	75
2.7.3	Neutron Tracking in Finite Geometry.....	77
2.7.4	Statistical Estimators.....	79
2.7.5	Statistical Error	80
2.8	REVIEW OF EXISTING METHODS USED IN HTRs CALCULATIONS	82
2.8.1	Calculation of Dancoff Factors in HTR.....	83
2.8.2	Deterministic Approach to HTRs	83
2.8.3	Monte Carlo Approach to HTRs.....	85
2.9	THESIS OBJECTIVE	86

CHAPTER 3	STOCHASTIC LOADING IN THE HTR FUEL ELEMENTS: DANCOFF	
	FACTOR CALCULATION IN THE FUEL PEBBLE AND COMPACT	88
3.1	INTRODUCTION	88
3.2	STOCHASTIC LOADING SCHEMES	91
3.2.1	The RSA and modified (fast) RSA methods and its limitations	91
3.2.2	The Cyclic Lattice Randomization Method	92
3.3	DANCOFF FACTOR CALCULATION.....	95
3.3.1	Monte Carlo Tracking.....	95
3.4	COMPARISON WITH REFERENCE RESULTS.....	97
3.4.1	Infinite Medium Dancoff Factor.....	97
3.4.2	Finite Medium Dancoff Factor	99
	<i>Intra-Pebble Dancoff factor</i>	100
	<i>Intra-compact Dancoff factor</i>	101
3.5	CONCLUSIONS.....	105
CHAPTER 4	BOXER3 MODEL OF HTR LATTICE CELL: TREATMENT OF DOUBLE	
	HETEROGENEITY IN THE RESONANCE AND THERMAL ENERGY REGIONS	106
4.1	INTRODUCTION	106
4.2	THE PROBLEM OF HIGH PU CONTENT FUEL	109
4.3	SELF-SHIELDING BY EQUIVALENT SPHERICAL SHELL: THEORY	109
4.4	THE LATTICE CODE BOXER3 AND ITS MODIFICATION FOR HTR CELLS	113
4.4.1	Geometry and Cross-Section Data.....	114
4.5	ANALYSIS OF HTR BENCHMARKS	116
4.5.1	Results with Self-Shielding Treatment in Epithermal Groups.....	117
4.5.2	Results with the Equivalent Spherical Shell Model.....	119
4.5.3	Results of the Equivalent Spherical Shell Model for the Bende's HTR problems.....	119
4.6	CONCLUSIONS.....	121

CHAPTER 5 NEUTRON TRANSPORT IN STOCHASTIC MEDIA: COLLISION

PROBABILITY METHOD FOR PEBBLE WITH RANDOM FUEL DISTRIBUTION..... 123

5.1	INTRODUCTION	123
5.2	APPLICATION OF BOXER3 CODE TO THE HTR LATTICE CELL.....	125
5.3	MODIFICATION FOR CALCULATION OF VARIOUS PROBABILITIES FOR A HETEROGENEOUS FUEL ZONE	127
5.4	COLLISION PROBABILITY INTEGRANDS FOR HETEROGENEOUS RANDOM FUEL GRAPHITE MIXTURE...	128
5.5	FIRST METHOD FOR CALCULATING INTEGRANDS IN THE CP CALCULATIONS	130
5.5.1	Contribution to Fuel Kernel to Kernel Probability $PFF(L)$	130
5.5.2	Contribution to Fuel Kernel to Mesh Surface Probability $PFB(L)$	135
5.5.3	Contribution to Mesh Surface to Surface Probability $PBB(L)$	136
5.6	ALTERNATIVE METHOD FOR OBTAINING INTEGRANDS IN THE CP CALCULATIONS	137
5.6.1	Integrand for the Mesh Surface-to-Surface Probability $PBB(L)$	137
5.6.2	Integrands for the Collision Probabilities $PBF(L)$ and $PBM(L)$	138
5.6.3	Integrands for the Collision Probabilities $PFF(L)$ and $PFM(L)$	139
5.6.4	Integrands for the Collision Probabilities $PMF(L)$ $PMB(L)$ and $PMM(L)$	140
5.7	CORRECTIONS TO THE DISTRIBUTION OF FUEL KERNELS DUE TO THE COATINGS	141
5.8	RESULTS AND DISCUSSIONS.....	148
5.8.1	Analysis of an OECD Benchmark	149
5.8.2	Analysis of Other Benchmarks	153
5.9	CONCLUSIONS	154

CHAPTER 6 A NEW APPROACH TO MONTE CARLO IN HTRS: SAMPLING

KERNEL POSITION DURING A RANDOM WALK PROCESS..... 156

6.1	INTRODUCTION	156
6.2	THEORETICAL BASIS OF THE METHOD: THE NEW ALGORITHM FOR NEUTRON TRACKING FOR POISSON STATISTICS OF KERNELS.....	158
6.2.1	The Next Collision of a Neutron Starting at a Point in the Graphite Matrix.....	158
6.2.2	The next collision of a neutron starting at a point in the fuel kernel.....	160

6.2.3	Sampling of the collision point in a fuel kernel	161
6.3	THE NEW ALGORITHM FOR NEUTRON TRACKING FOR COATING CORRECTED POISSON STATISTICS OF KERNELS	167
6.3.1	The next collision of a neutron starting at a randomly chosen point in the graphite matrix	168
6.4	IMPLEMENTATION FOR A PEBBLE-BED HTR LATTICE CELL	169
6.4.1	The algorithm used in development of PebMC Code	170
6.4.2	White Boundary Condition used in PebMC Code	172
6.4.3	Track length estimator used with the first algorithm	174
6.4.4	Alternative algorithm for sampling collision point	176
6.5	EXTENSION TO PEBBLE BED HTR CORE CALCULATIONS	178
6.6	RESULTS	178
6.6.1	Brief description of the benchmarks studied.....	179
6.6.2	Comparison of the k_{∞} obtained using Monte Carlo with BOXER3 results.....	180
6.6.3	Effect of using reduced track length $(1 - \lambda l)$ in graphite matrix.....	181
6.6.4	Study of the need for tracking within a kernel	182
6.6.5	Alternative method for sampling the point of collision	183
6.6.6	Studies on the effect of the coatings	184
6.6.7	Discussion of the results	185
6.7	CONCLUSIONS	186
CHAPTER 7	SUMMARY AND CONCLUSIONS.....	187
7.1	SUMMARY AND CONCLUSIONS.....	187
7.2	FUTURE WORK.....	190
	<i>APPENDIX-A</i>	<i>191</i>
	<i>APPENDIX-B</i>	<i>194</i>
	<i>REFERENCES</i>	<i>196</i>

List of Figures

Figure 1-1: Schematic of TRISO and fuel pebbles in pebble-bed design.....	35
Figure 1-2: TRISO and Fuel Compact in the Prismatic HTR designs.....	36
Figure 1-3: Sulfur–Iodine thermo-chemical cycle with HTR nuclear heat source	37
Figure 2-1: Variation of Total microscopic continuous cross-section of U^{238}	45
Figure 2-2: Neutrons location at r in d^3r volume element and motion in direction cone $d\Omega$ around Ω	46
Figure 2-3: Spatial coordinate along the direction of trajectory.	48
Figure 2-4: A multi-step reactor physics analysis procedure.....	50
Figure 3-1 TRISO particles arranged in a FCC lattice (a) and (b) after randomisation of the lattice structure using the CLR method.	94
Figure 3-2 Variation of the infinite-medium Dancoff Factor with packing fraction: comparison between various methods.....	98
Figure 3-3 Variation of the intra-infinite compact Dancoff Factor with packing fraction: comparison between various methods	99
Figure 3-4: Random packing of TRISO in the fuel pebble (a) and fuel compact (b) for finite medium Dancoff factor calculation.	100
Figure 3-5: Variation of the intra-pebble Dancoff factor with packing fraction: comparison between various methods.....	101
Figure 3-6: Intra-finite compact Dancoff factor with volume packing fraction of TRISO particles at H/D ratio equal to 2	102
Figure 3-7: Intra-finite compact Dancoff factor with volume packing fraction of TRISO particles at H/D ratio equal to 5.	102

Figure 3-8: Intra-finite compact Dancoff factor with volume packing fraction of TRISO particles at H/D ratio equal to 10.	103
Figure 3-9: Intra-finite compact Dancoff factor with volume packing fraction of TRISO particles at H/D ratio equal to 20.	103
Figure 3-10: Intra-finite compact Dancoff factor with volume packing fraction of TRISO particles at H/D ratio equal to 50.	104
Figure 3-11: Intra-finite compact Dancoff factor with volume packing fraction of TRISO particles at H/D ratio equal to 100.	104
Figure 4-1: Double heterogeneous fuel pebble and equivalent spherical shell model.	110
Figure 4-2: Schematic of fuel pebble (a) as it exists; (b) as modeled in BOXER3 code.....	114
Figure 5-1: Schematic of fuel pebble used in BOXER3 code.	126
Figure 5-2: Variation of Q_{FL} with distance (L): Comparison between Eq. (5.58) and Monte Carlo for smaller kernel radius (0.012cm) and lower kernel density (15000 Kernels). The result based on the assumption of Poisson statistics is also included.	145
Figure 5-3: Variation of Q_{FL} with distance (L): Comparison between Eq. (5.58) and Monte Carlo for larger kernel radius (0.025cm) and higher kernel density (30000 Kernels). The result based on the assumption of Poisson statistics is also included.	146
Figure 5-4: Variation of k_{∞} as a function of fuel burn-up for the benchmark defined in the phase 2a.	151
Figure 5-5: Variation of Plutonium isotopes density as a function of fuel burn-up for the benchmark defined in the phase 2a.	152
Figure 5-6: Variation of Americium isotopes density as a function of fuel burn-up for the benchmark defined in the phase 2a.	152

Figure 5-7: Variation of Curium isotopes density as a function of fuel burn-up for the benchmark defined in the phase 2a..... 153

Figure 6-1: The cylindrical coordinates (ρ,z) of the point of collision within the fuel kernel. 164

Figure 6-2: (a) HTR pebble unit cell (b) Graphite matrix with TRISO particles (c) Different coating layers of TRISO particle 173

List of Tables

Table 3-1 Average relative deviations for CLR and RSA schemes from the reference results	105
Table 4-1 Finite medium Dancoff using CLR method and Bell Factors for Benchmark Problems [40], [65]	117
Table 4-2 Comparison of BOXER Results with the Reference Values [40], [65]	117
Table 4-3 Iteration scheme used for Equivalent spherical model to study Bende's PuO ₂ fueled pebble with 0.01 cm kernel radius	120
Table 4-4 Iteration scheme used for Equivalent spherical model to study Bende's PuO ₂ fueled pebble with 0.011 cm kernel radius	120
Table 5-1 Results of BOXER3 code with new method of self-shielding and comparison with other codes	149
Table 5-2 Comparison of k_{∞} of pebble with MCNP results.....	154
Table 6-1 Comparison of k_{∞} obtained using Monte Carlo and BOXER3. Numbers in brackets show % deviation from the reference result.	180
Table 6-2 Effect of using reduced track length $(1 - \lambda l)$ in graphite matrix. Numbers in brackets show % deviation from the reference result.	181
Table 6-3 Results showing the need for tracking within a kernel. Numbers in brackets show % deviation from the reference result.	182
Table 6-4 Effect of different methods of tracking within a kernel. Numbers in brackets show % deviation from the reference result.	183
Table 6-5 Results using alternative method for sampling the point of collision. Numbers in brackets show % deviation from the reference result.	184

Table 6-6 The effect of the kernel distribution. Numbers in brackets show % deviation from the reference result.....185

SUMMARY AND CONCLUSIONS

This chapter summarises the highlights of the results obtained in this thesis and outline the ways the present work can be extended in the future.

1.1 Summary and Conclusions

HTRs present unusual challenges concerning the neutronic simulations. It might appear that both deterministic and stochastic methods are inapt to deal efficiently with the peculiar configuration of HTRs. The major challenge is to devise a new efficient method to perform neutron transport in random dispersion of fuel lumps. This also includes resonance self-shielding both in thermal and resonance regions in HTR lattice cell calculations. To provide an appreciation of these challenges, we first gave an overview of HTRs in Chapter 1.

In Chapter 2, traditional neutronics methods and literature review on specific methods used in HTR neutronic calculations were discussed. Two comprehensive objectives of the thesis were defined in Section [2.9](#). The first is that the thesis sought to improve upon the existing tools to treat HTRs unusual challenges. The second is to develop new deterministic and stochastic methodologies as well as computational tools for HTR analysis. This includes the development of new theoretical models, algorithms and computer codes based on the models, and analysis of benchmark problems.

Chapter 3 presented a new method for computing the Dancoff factors using the Monte Carlo method for the treatment of resonance self-shielding in the resonance energy region. We have described the development of a new scheme (CLR) method using the Monte Carlo to generate the randomly distributed TRISO particles in the fuel zones of the pebble and the

compact shaped graphite. The principal advantage of the method described in the thesis is that it can be used for low as well as high particle densities ($\sim 70\%$). This method is implemented in the Monte Carlo program, called **MCDanc**. The method is very efficient as the randomisation scheme is based on nearest neighbours search algorithm to eliminate any overlapping of particles. This method can also be used to randomly stack pebbles to form pebble-bed in the reactor core for neutronics simulations.

The **MCDanc** program is used to compute the Dancoff factors to conserve the resonance self-shielding in pebble-bed HTR lattice cell calculations. A new method to deal with self-shielding in the thermal energy region using the Equivalent Spherical Shell model is developed in Chapter 4. The results of the equivalent spherical shell model used in BOXER3 code for the HTR benchmark problems show satisfactory agreement with that of the reference results. The BOXER3 code with the equivalent shell method takes about 5sec per HTR lattice cell calculation for pre-computed outer shell radius of a given problem that gives acceptable results. However, the equivalent shell method is somewhat heuristic in nature and does not give a detailed variation of neutron flux in the fuel zone except a single mesh. Another shortcoming of this method is that the calculation of the equivalent radius of the spherical shell is not straightforward as it depends on fuel cross-section.

After this, Chapter 5 discussed the development of a new and rigorous theoretical model to solve the neutron transport equation in the random medium of the HTR lattice cell using the collision probability method. This includes the derivation of several collision probability formulae using two independent methods based on Poisson and coating corrected Poisson distribution of fuel particles in the graphite matrix. The lattice code BOXER3 is extended to implement the new formulae to solve the neutron transport equation in HTR lattice cells. Multigroup neutron transport equation solution using BOXER3 code with new collision probabilities is a major theoretical improvement and requires slightly more time (about 7sec

per HTR lattice cell calculation) as compared to the Equivalent Spherical Shell model. In addition, this method allows to compute flux in several radial meshes in random medium of HTR pebble. Results show that the new method can efficiently perform HTR analysis for any combination of fertile (Th^{232} , U^{238}) and fissile isotopes (U^{233} , U^{235} and Pu). This method is equally suitable with subgroup or ultrafine cross-section data libraries, as it does not require any free parameters such as the Bell factor. In fact, the proposed method presents a novel solution of the double heterogeneity effect involved in HTR lattice analysis. Hence, the equivalent spherical shell method and the one involving solution of transport equation in random medium using new collision probabilities are well suited for the scoping studies as the computational time is short compared to the MC methods.

These formulae laid the foundation of a very efficient new Monte Carlo approach for neutron transport in random medium, which was presented in Chapter 6. Further, we discussed the theoretical basis of the Monte Carlo algorithm and its implementation in **PebMC** code for the case of a lattice cell with a multigroup library. The proposed method has the statistical nature inherent in it and is faster than the methods requiring detailed neutron tracking through the millions of fuel particles randomly distributed in HTR. K-inf calculation using the PebMC code takes about 39min, 50min and 123min for HTR lattice benchmark problems, Phase1a-Uranium fuel, Phase2a- Plutonium fuel and Phase5a-Thorium/uranium fuel, respectively. The explicit modelling of fuel kernels and detailed neutron tracking is almost 4 to 5 times computationally more expensive as compared to the formulae-based tracking.

At the same time, the new method does not have any of the limitations of the delta algorithm. These features of the proposed method make it a better alternative to the traditional Monte Carlo neutron tracking in HTRs. While all studies in the thesis pertain to lattice cell calculations, the MC method described in the thesis is easily extendable to solve core problems

with continuous energy cross section data and full capability of the present method will be utilized with continuous data library and parallel computing.

1.2 Future Work

The collision probability method derived in Chapter 5 is applied to the HTR lattice cell in conjunction with the equivalence principle based WIMSD multigroup library. It will be very interesting to implement this method in the subgroup approach for resonance treatment. We have already obtained the expression for the collision probabilities based on the coating modified Poisson distributions. Implementation of these formulae to further improve the applicability in the higher packing range of TRISO particles is proposed to be carried out in future.

Another important aim for the future is to extend the Monte Carlo development to core calculations for HTR. This requires development of a method for stacking pebbles in the core under gravity. Another aim is to compare the results of our method with a Monte Carlo calculation based on detailed tracking within a fixed (random) configuration of fuel particles. The method will also include a study of the effect of explicit modelling of coatings. It is also proposed to evaluate the effect of packing density of fuel particles on HTR lattice cell results using the collision probability formulae for neutron tracking derived using the Poisson and modified Poisson statistics for random fuel particles dispersions. Since Monte Carlo is most effective together with continuous energy cross-section data, extension of the work to include this capability is envisaged in future.

SYNOPSIS

A nuclear fission reactor is a device in which self-sustained fission chain reactions take place in a controlled manner. The nuclear reactors can be designed to serve a specific purpose such as electricity generation, research application, production of isotopes for medical and industrial use, nuclear marine propulsion, and heat generation at high temperature etc. For the generation of electricity, several reactor types such as graphite-moderated reactors, light water reactors (pressurized water and boiling water reactors), heavy water reactors and sodium-cooled fast reactors have been designed, built and are under operation all over the world.

For industrial heat applications, along with co-generation of electricity, high temperature reactor (HTR) designs have been currently the subject of research worldwide. The HTR exhibits distinct advantages in terms of inherent safety, economic potential, high efficiency, and the potential to produce heat at a high temperature in the range of 700°C to 950°C for hydrogen production and the synthesis of carbon-neutral fuels. These attractive features make the HTR design as one of the candidates of the Generation IV nuclear energy initiative¹. However, the HTRs present unusual challenges with regard to performing physics design calculations compared to the traditional nuclear reactors. The primary reason for this is the geometry of the fuel elements in the form of spherical pebbles or cylindrical compacts that consist of a large number of tiny (~100µm-size) fuel lumps in the form of Tri Structural Isotropic (TRISO) particles having fuel kernel in their center surrounded with several coating layers and dispersed randomly in a graphite matrix. In the thesis, a number of novel solutions are presented for these problems associated with the deterministic as well as the Monte Carlo (MC) methods in HTR lattice cell analysis.

The physical behaviour of nuclear reactors is determined by the distribution of neutrons in space, energy and direction variables. Neutrons in the reactor interact with nuclides of the host medium and results in nuclear reactions such as scattering, capture and fission. These reactions are characterized by nuclide microscopic cross-section, which is measure of the probability of occurrence of a particular neutron-nuclide reaction at the specific energy and position. Accurate calculation of the neutron population density as a function of space, energy and direction variables is the main objective behind neutronics calculations of nuclear reactor. The linearized form of Boltzmann neutron transport equation is commonly used to model the average behaviour of neutrons in a nuclear reactor. The solution of this equation gives the flux distribution that enables us to calculate the neutron density/reaction rates. Since the analytical solution of the neutron transport equation is feasible only for a few very simple cases, numerical methods (deterministic or stochastic methods), are used to evaluate the neutron flux in reactors.

In the deterministic scheme of the solution of the transport equation, each of the variables of the phase space (r, Ω, E) is discretized (with the possible exception of the direction variable which is sometimes represented by expanding in the orthogonal polynomials). Due to the complicated distribution of materials in a reactor and the large range of neutron energies involved with a complex energy dependence of the cross sections on energy, it becomes necessary to introduce approximations in the computational methods. An accurate representation of the cross-section of nuclide requires several million data points and is almost impractical for routine reactor analysis. Instead of solving the transport equation for the full reactor core, deterministic reactor physics commonly uses a multi-level approach, namely the lattice level (assuming a periodic arrangement of fuel, moderator and coolant) and the full core level^{2,3}

Generally, the lattice cell is modeled by what is called the multigroup transport theory with detailed consideration of the heterogeneous distribution of materials. In the multigroup approach for energy discretization, the energy range of interest (typically from 10^{-5} eV to about 10 MeV) is divided into energy groups (about a few hundred at the lattice level). The cross section for a particular reaction with a specific nuclide is considered to be constant within the group and is obtained by averaging the variation within the group using a weighting function that is the expected neutron flux spectrum in that group^{4,5}. The lattice calculation is followed by the calculation of homogenized macroscopic cross-sections collapsed to a few energy groups using the detailed flux spectrum obtained from the lattice calculation. These homogenized few group cross sections are used for the whole core calculation generally employing the diffusion equation that is an approximate form the transport equation.

The heterogeneity of the distribution of materials in the HTR lattice cell described earlier namely, tiny TRISO fuel particles distributed randomly in the graphite matrix, followed by graphite and the coolant layers is referred to as the double heterogeneity effect. It might appear that such fine-particle dispersions may be treated as homogeneous for entire neutron spectrum but that is not the case for all energies. At certain energies, particularly around resonances, and to some extent in the thermal region, the neutron mean free path is comparable or shorter than the size of the fuel kernel, and the situation necessitates treatment of the dispersion as a heterogeneous medium⁶⁻¹¹.

The goal of the research described in the thesis is the development of new methodology as well as computational tools for HTR analysis. This includes the development of new theoretical models, algorithms and computer codes based on the models, and analysis of benchmark problems. The first of these is the development of new MC algorithm to realize the random distribution of fuel particles in the HTR lattice cell and pebbles in the HTR core and a

fast scheme to track neutrons to compute the Dancoff factors needed in the resonance self-shielding calculations¹². This is followed by the development of a rigorous theoretical method for solving the transport equation in the random fuel particle dispersion by an exact evaluation of the collision probabilities (CPs) in various regions of the HTR lattice cell¹³. The method is incorporated in the CP code BOXER3¹⁴. The method developed for exact evaluation of CPs is applied to the development of an algorithm for providing a solution by the MC method as well. To prove the validity of the proposed method, a multi-region, multigroup MC code (PebMC) is developed to simulate the spherical lattice cell of a pebble bed HTR¹⁵. These new methods and results of the computational tools so developed are presented in this thesis.

The thesis is organized in following chapters as briefly described below.

Chapter I gives a brief introduction to the nuclear energy, type of nuclear reactors in common use and more particularly a discussion on the general features of HTRs and an overview of the HTR designs available in the literature. It is followed by a general description of HTR components relevant to this thesis. A short overview of hydrogen production methods is presented as a feasible application of HTR along with electricity generation.

Chapter II presents brief introduction to the methods used in the neutronics calculation of the nuclear reactors. Use of the transport equation with multigroup library processing is discussed for the lattice level calculations. A brief description of the conventional methods for preparations of multi-group cross-sections using resonance integral table of multi-group library is presented. A brief description of the MC method in neutron transport problems is also included.

The chapter also presents a survey of the literature on the methods used in the physics design of HTRs. This includes algorithms used to generate randomly distributed spheres together with a discussion of their limitations such as slowing down or inability to generate

random media at high packing fractions. The methods developed by various authors for obtaining the Dancoff factor and calculation of the self-shielded resonance group cross sections are described for doubly heterogeneous pebble bed HTRs¹⁶⁻¹⁹. Methods for solving the double heterogeneity problem in lattice calculations in HTRs are also reviewed. Finally, a review of the MC approaches used to treat the random medium of HTRs is given. The chapter also describes the objective of this research and an outline of the work carried out.

Chapter III describes a new algorithm based on the MC method that has been proposed to realize the stochastic distribution of spherical fuel lumps, in the form of TRISO particles in a graphite matrix, and to overcome the limitations of the traditional algorithms as discussed in Chapter II¹⁹⁻²¹. The principal advantage of the method described in this chapter is that it can be used for the generation of low as well as high particle density random mediums. Further, it also presents the development of a fast scheme to track neutrons to compute the intra-fuel element Dancoff factor, which takes into account the heterogeneity at the level of TRISO particles and the inter-fuel element Dancoff factor, for taking into account heterogeneity at the level of the pebble lattice cell. These two Dancoff factors along with the Bell correction factor are required in the calculation of the self-shielded resonance group cross sections. The lattice level results of the analysis of benchmarks using the Dancoff factors so calculated are presented in the chapter.

Chapter IV presents a new method for treating the double heterogeneity effect in the thermal region (which arises due to the heterogeneity of the tiny fuel lumps itself together with the heterogeneous distribution of fuel lumps, graphite matrix, and coolant) for performing lattice calculations. The thermal region also presents significant heterogeneity on the scale of the TRISO particle for all nuclides and most significantly in high content plutonium (Pu) fuelled reactors, due to the low-lying resonances of Pu. While the method of resonance self-

shielding in the WIMS formalism takes care of the double heterogeneity in the epithermal region, the standard treatment of epithermal resonances is not available for resonances of the thermal energy.

A new method for self-shielding treatment of thermal resonances in TRISO particles having Pu fuel is developed. The self-shielding procedure is based on a heuristic method, using CPs, in which the random medium of TRISO particles and graphite is replaced with an equivalent spherical shell within the HTR lattice cell. The method is incorporated in the WIMS library-based lattice code BOXER3. An option for handling the spherical geometry of the lattice cell of a pebble bed reactor has been added in the code. It also presents the results of the analysis of a number of HTR benchmark problems.

Chapter V discusses another new CP approach for the solution of the transport equation in the random medium of HTR lattice cells. It includes the development of a more rigorous theoretical method for solving the transport equation in a random dispersion by an exact evaluation of the CPs in various regions of the lattice cell. This approach is presented for thermal neutron transport in the random heterogeneous lattice cells of HTRs, particularly those containing high-concentrations of Pu fuel. Exact expressions for CPs in the random heterogeneous medium have been obtained by two independent methods under realistic assumptions of the statistical distribution of fuel kernels in the graphite matrix. The primary assumption in the derivation of CPs is that the distribution of the fuel kernels along the length of the intercept follows renewal statistics, more specifically, Poisson statistics. The merit of Poisson statistics is that it corresponds fairly close to the actual situation and allows a simple analytical treatment. This method does not make use of any free parameters such as the Bell factor used in the equivalence principle approach for resonance treatment. This is a major advantage, and hence, for calculating resonance absorption in HTR lattice cells, the method

could be used in conjunction with the subgroup approach or ultra-fine-group approach. A correction to the Poisson statistics due to the small but finite size of the TRISO particle together with the coatings is also worked out. The method also suggests a new MC approach to solving transport problems in HTRs, which is a subject of the next chapter.

In chapter VI, another new approach to MC calculations in HTRs is presented. This new method avoids detailed tracking through the millions of TRISO particles distributed through the reactor. It also avoids the limitations of the delta algorithm that may be used in place of detailed tracking. While the method is based on certain assumptions that introduce approximation in the theory, the effects of these has been seen to be very small, being mostly of the order of typical statistical errors and is actually less than the errors in many standard MC calculations that make some approximations in describing the statistical distribution of TRISO particles. These new methods have been successfully implemented in the multigroup code PeBMC for the pebble bed reactor lattice cell to demonstrate its utility. Thus, it may be expected to serve as an important alternative formulation of MC in HTRs analysis.

Chapter VII gives a brief summary of the research work presented in the thesis. It also presents the main conclusions drawn and scope for future work, which is summarized as follows.

This research work had led to the new theoretical models, equally suitable to the two alternative methods of reactor physics, the deterministic and MC methods, are developed to address the challenges involved in the HTR lattice cell. This effort includes the derivation of CPs in random media to solve the integral transport equations for pebble-bed lattice cell. The conventional MC methods are not practical for routine analysis, in particular for HTR lattice cell, due to the high computational cost. To address this challenge, a new MC methodology

based on CP formulas derived for random medium, is developed and benchmarked to demonstrate its validity and efficiency.

Future Work

It is planned to extend the present development based on the new approach for MC simulations of the HTR reactor core. This requires development of a method for stacking pebbles in the core under gravity. It is also planned to compare the results of our method presented in the thesis work with a MC calculation based on detailed tracking within a fixed (random) configuration of fuel particles. The method will also include a study of the effect of explicit modeling of coatings. Further work in this direction would be the extension of the code to continuous energy treatment with detailed tracking and anisotropic scattering for full core calculation of HTRs.

References

1. GIF Annual Report. Annual Report 2017. *GIF* **21**, 430 (2017).
2. Smith, K. S. Assembly homogenization techniques for light water reactor analysis. *Prog. Nucl. Energy* (1986). doi:10.1016/0149-1970(86)90035-1
3. Sanchez, R. Assembly homogenization techniques for core calculations. *Progress in Nuclear Energy* (2009). doi:10.1016/j.pnucene.2008.01.009
4. Gibson, N. A. Nathan A. Novel Resonance Self-Shielding Methods for Nuclear Reactor Analysis. (2016).
5. Lim, C., Joo, H. G. & Yang, W. S. Development of a fast reactor multigroup cross section generation code EXUS-F capable of direct processing of evaluated nuclear data files. *Nucl. Eng. Technol.* (2018). doi:10.1016/j.net.2018.01.013
6. Tsuchihashi, K., Ishiguro, Y. & Kaneko, K. Double heterogeneity effect on resonance

- absorption in very high temperature gas-cooled reactor. *J. Nucl. Sci. Technol.* **22**, 16–27 (1985).
7. Hébert, A. A Collision Probability Analysis of the Double-Heterogeneity Problem. *Nucl. Sci. Eng.* **115**, 177–184 (1993).
 8. Sanchez, R. & Pomraning, G. C. A statistical analysis of the double heterogeneity problem. *Ann. Nucl. Energy* (1991). doi:10.1016/0306-4549(91)90073-7
 9. Sanchez, R. Renormalized treatment of the double heterogeneity with the method of characteristics. *Proc. PHYSOR 2004 Phys. Fuel Cycles Adv. Nucl. Syst. - Glob. Dev.* (2004). doi:10.1109/GLOCOM.2017.8253967
 10. Kim, H., Choi, S., Park, M., Lee, D. & Lee, H. C. Extension of double heterogeneity treatment method for coated TRISO fuel particles. *Ann. Nucl. Energy* **99**, 124–135 (2017).
 11. Williams, M. L. Resonance Self-Shielding Methodologies in SCALE 6. *Nucl. Technol.* **174**, 149–168 (2014).
 12. Singh, I., Degweker, S. B. & Gupta, A. Treatment of Double Heterogeneity in the Resonance and Thermal Energy Regions in High-Temperature Reactors. *Nucl. Sci. Eng.* **189**, 243–258 (2018).
 13. Singh, I., Degweker, S. B. & Gupta, A. A New Collision Probability Approach for Solution of the Transport Equation in the Random Medium of High-Plutonium-Content HTR Lattice Cells. *Nucl. Sci. Eng.* **189**, 101–119 (2018).
 14. Ray, S., Degweker, S. B., Rai, R. & Singh, K. P. A Collision Probability and MOC-Based Lattice and Burnup Code for Analysis of LWR Fuel Assemblies. *Nucl. Sci. Eng.* (2016). doi:10.13182/nse15-127
 15. Singh, I., Degweker, S. B., Mallick, A. K. & Gupta, A. A New Approach to Monte Carlo

- in High Temperature Reactors. *Nucl. Sci. Eng.* (2019).
doi:10.1080/00295639.2019.1576453
16. Bende, E. E. Plutonium Burning in a Pebble-Bed Type High Temperature Nuclear Reactor (Ph.D. thesis). *Delft Univ. Technol. Netherlands* (1999).
 17. Kloosterman, J. L., Ougouag, A. M. & Falls, I. Spatial effects in Dancoff factor calculations for pebble-bed HTRs. *M&C 2005, Avignon, Fr. Sept. 12-15, 2005, CD-ROM* (2005).
 18. Ji, W. & Martin, W. R. Application of Chord Length Sampling to VHTR Unit Cell Analysis. in *PHYSOR 2008* (2008).
 19. Ji, W., Liang, C. & Pusateri, E. N. Analytical Dancoff factor evaluations for reactor designs loaded with TRISO particle fuel. *Ann. Nucl. Energy* **63**, 665–673 (2014).
 20. Ji, W. & Martin, W. R. Application of the Chord Method to Obtain Analytical Expressions for Dancoff Factors in Stochastic Media. *Nucl. Sci. Eng.* **169**, 19–39 (2015).
 21. Kloosterman, J. L. & Ougouag, A. M. Computation of Dancoff Factors for TRISO-Fueled Prismatic HTRs. *Office* (2009).

Chapter 1 **INTRODUCTION: High Temperature Reactors**

This chapter outlines the general context of the problem addressed in the thesis. It gives a brief introduction to nuclear energy and the types of reactors presently in operation. It presents a description of HTRs and their importance for power and hydrogen production. Reactor physics design objectives of nuclear reactors are discussed in general.

1.1 Need of Nuclear Energy

In both developed and developing countries, energy is an essential factor for economic development. Globally, the energy demand is continuously growing not only because of the increasing world population but also due to the increase in average energy consumption per capita [1]. On the other hand, the current energy generation technologies have badly affected the environment by emitting carbon dioxide (CO₂) into the atmosphere. This has created two major challenges of the century, namely climate change and air pollution [2]. There is an immediate need for alternate energy resources that can reduce the concerns about climate change and the inevitable exhaustion of fossil fuel.

As all the energy sources have their pro and cons, the ideal energy mix for the future is not yet clear. Although the energy sources like wind and solar are CO₂ free and produce no waste, they need large amounts of land resources and the electricity production is intermittent and requires backup power plants. The experience with nuclear reactors in the past has proved that nuclear energy can be used in conjunction with such intermittent energy sources to achieve air-pollution-free and greenhouse-gas-free energy and to meet the globally growing demands

of energy. Nuclear energy produced around 10.3% of the world's electricity using 413 nuclear power reactors in 2017 [3]. This results in a significant reduction in fossil fuel usage for power generation. To continue with the benefits of nuclear energy, the design and deployment of the next generation of nuclear reactors with enhanced safety features is needed to replace the retiring power plants as well as to increase the share of nuclear energy in the total energy mix.

A nuclear fission reactor is a device in which self-sustained fission chain reactions take place in a controlled manner. A nuclear reactor is designed to serve a specific purpose such as electricity generation, research application, production of isotopes for medical and industrial use, nuclear marine propulsion, heat generation at high temperature etc. For the generation of electricity, a number of reactor types such as graphite-moderated reactors, light water reactors (LWRs) i.e., pressurized water reactors (PWRs) and boiling water reactors (BWRs), heavy water reactors and sodium-cooled fast reactors have been designed, built, and are under operation all over the world. The clean and safe energy generation using LWRs has increased impressively due to continuous research and development efforts since the beginning of the nuclear reactor's concept. However, these traditional reactors with a lower outlet temperature of the coolant impose a low thermal efficiency cause relatively higher fuel consumption and thermal pollution of the environment. For industrial heat applications, along with co-generation of electricity, high-temperature reactor (HTR) designs are currently the subject of research worldwide (See Section [1.5](#)). The HTR exhibits distinct advantages in terms of inherent safety, economic potential, high efficiency, and the potential to produce heat at a high temperature in the range of 700°C to 950°C for hydrogen production and the synthesis of [carbon-neutral](#) fuels.

This chapter explains the HTR concept, including a description of its design and main components to provide a comprehensive picture of the problems tackled in the thesis. Section

[1.2](#) gives a brief introduction to the need for high-temperature reactor technology. Section [1.3](#) gives an overview of HTRs built and operated in the world. Section [1.4](#) gives a summary of the conceptual designs being considered worldwide. In Section [1.5](#), various types of HTRs and a description of their components are presented. Section [1.6](#) describes some processes for hydrogen production using heat from HTRs. The general objectives of the reactor physics design are discussed in Section [1.7](#). The peculiar reactor physics design challenges owing to the rather unusual configuration of fuel and moderator in HTRs are addressed in Section [1.8](#) along with an outline of the contents of each chapter of the thesis.

1.2 Why High Temperature Reactors

The concept of HTRs aims to avoid the limitations of traditional nuclear reactors by using a refractory core composed exclusively of ceramic materials and employing an inert coolant to serve as a viable LWR alternative. It also offers an economical heat source at high temperature to the industries for hydrogen production, oil recovery, refineries, and biomass conversion [4]. In addition to the production of electricity and various industrial applications mentioned above, HTRs possess enhanced passive safety features, operational simplicity, a stable waste form and more efficient fuel utilization. The HTR differs from conventional LWRs because the fission product containment is assured at the level of the ceramic-coated tiny fuel particles, called Tri-Structural Isotropic (TRISO) with a diameter of one millimetre, distributed in graphite spheres or cylinders a few centimetres in size. The VHTR nuclear reactors concepts are characterised by the use of TRISO as fuel, helium as coolant, graphite as moderator and reflector with high outlet temperature in the range of 700 to 1000°C [5]. In response, to today's concerns of nuclear safety, energy security and climate change, the inherent safety characteristic of the VHTR make this a unique concept among the next-generation nuclear

energy systems. Because of these excellent characteristics, the GEN IV has identified the Very High-Temperature Reactor (VHTR) concept as one of the candidates among the next-generation nuclear energy systems that offer advantages in terms of sustainability, safety and reliability, economics, proliferation resistance and physical protection [6]. In addition to the gas-cooled HTRs, interest in HTR has resulted in an innovative concept in which liquid fluoride salt will be used as a coolant ([7]–[9]). This concept combines the neutronics features of gas-cooled high-temperature reactors and the heat removal feature of molten salt reactors.

1.3 Experience with HTRs

The present day High-Temperature Gas-cooled Reactors (HTGR) designs were derived from the graphite moderated, gas-cooled MAGNOX reactor built and operated with a coolant outlet temperature of 415°C, and its successor, the Advanced Gas-cooled Reactor (AGR) with a coolant outlet temperature of 675°C [10]. The first prototype high-temperature gas-cooled reactor was the experimental DRAGON reactor at Winfrith in the UK, which became critical in August 1964 and operated until 1975. The Dragon project introduced the HTR to the whole of Europe and triggered interest in the USA and Japan.

The USA developed an experimental helium-cooled and graphite-moderated reactor of 40MWe power, called the Peach Bottom reactor and operated it from 1966 to 1972. The coated particles of mixed ThO_2/UO_2 and ThC_2/UC_2 were used as fuel in hexagonal prismatic blocks. The experience gained during the operation of the Peach Bottom reactor led to the construction of a commercial high-temperature gas-cooled reactor by General Atomics at Fort St. Vrain (FSV) in the US. The 330MWe FSV reactor in Colorado was the second HTGR built and operated between 1974 and 1989 [11].

In Germany at Juelich, the first pebble-bed test reactor was AVR (Arbeitsgemeinschaft Versuch Reaktor), which achieved its first criticality in August 1966, and operated until December 1988. The AVR core contained about 100,000-fuel pebbles with a maximum power per pebble of 2.4 KW [12]–[14]. The total heavy metal of (U, Th) loading varied from 6 to 11 g per pebble while ^{235}U loading was 1gram per pebble [15]. Initially, the outlet temperature was 850°C in the AVR core, but this was subsequently raised to 950°C. The successful demonstration of AVR led to the deployment of its successor Thorium High Temperature Reactor (THTR-300) in Germany. It started operation in 1983 and was terminated in 1989. The THTR contained 675,000 fuel pebbles in a cylindrical core of 5.6m diameter and 6m in height. Each fuel pebble contained 0.96g of ^{235}U and 10.2g of ^{232}Th [16]. In the next section, currently operating and conceptual HTRs are described briefly.

1.4 Currently Operating and Future HTRs

As listed in previous section 1.3 that there have been five HTGRs built and operated in the past [1]. Experience with these reactors makes HTR technology reasonably mature enough to support preliminary design and licensing as either test or demonstration reactors within a decade [17]. This encourages the construction of two test reactors China's HTR-10 and Japan's HTTR-30. HTR-10 is a pebble-bed high-temperature helium-cooled test reactor design and built by INET and it achieved its first criticality in December 2000 and is running successfully. With the success of HTR-10, China is constructing the world's first prototype HTR-PM (High-Temperature Reactor Pebble-bed Module) which is scheduled to be synchronised to the grid and start electricity generation in the year 2018[6], [18].

In Japan, a 30MWth prismatic block design, High-Temperature engineering Test Reactor (HTTR), was constructed and attained the first criticality in November 1998, full

power operation in December 2001, high temperature operation at 950 °C in April 2004, After earthquake and tsunami on 11 March 2011, new regulation standard for the test and research reactors was issued by Nuclear Regulations Authority (NRA) on 18 December 2013. These regulations demand that the plants should be able to respond to a variety of natural phenomena and establish new measures to mitigate the effects of severe accidents, such as reactor core damage caused by beyond design basis events. JAEA has applied for the permission of changes in nuclear installation of the HTTR in 2014. After several review meeting of NRA and JAEA, NRA has granted permission on 3rd June 2020 and its safety review has confirmed that no fuel damage would occur even in the event of a beyond design basis accident such as multiple losses of reactor shutdown functions. Review of Design and construction methods and Operational Safety Program changes are going on and need approval [19].

Several start-ups, plant vendors and national laboratories in China, the United States, Korea, and Japan are currently working on near or medium-term projects of HTR designs such as HTR-PM, NGNP, GT-MHR, NHDD, IHTR and GTHTR300. Research activities are in progress for the molten salt cooled and TRISO particles fueled HTRs such as MARS, AHTR, SmAHTR, PB-FHR, TMSR-SF and IHTR in Russia, US, US, US, China and India, respectively [6].

1.5 HTR Types and Fuel Elements

Depending upon the fuel element configuration, HTRs are categorized as the pebble-bed type and the prismatic block type. Both HTR designs use fuel in the form of TRISO coated particles in a graphite matrix having spherical or prismatic block geometry.

1.5.1 Pebble-bed Type

In the pebble bed reactor (PBR) concept, spherical shaped fuel elements, called pebbles, are randomly stacked to form a pebble-bed in a graphite-reflected cylindrical core. The pebble-bed type HTRs offer a continuous refuelling scheme, low excess reactivity, lower control rod worth, continuous reactor operation and relatively better fuel utilization. The Once Through and Then Out (OTTO) and Multi-pass continuous refuelling schemes allow pebble-bed type HTRs to have low excess reactivity. The Multi-pass refuelling also results in higher fuel burn-up and lower fuel peak temperatures. Coolant flow paths are formed by the interstitial space available in the pebble-bed. A high-pressure drop of helium coolant across the core is a drawback of this type of reactors due to its relatively thin and long core design. However, cross-flow design or use of molten salt as coolant may eliminate this issue[20]. Production of dust from control rod insertions in pebble-bed, rubbing of fuel pebbles, and drag of fuel pebbles on the vessel shroud are some of the problems with this type of HTRs[21]. A schematic of the fuel elements used in pebble-bed reactors is shown in [Figure 1-1](#).

1.5.2 Prismatic Block Type

The HTRs with hexagonal block-type fuel elements are known as prismatic reactors and have fixed fuel assemblies. In this type of HTR design, the helium-coolant flow paths are well defined and relatively controllable because of the fixed coolant channels. The control rod locations are in the core because control rod channels can be drilled into the hexagonal graphite block. Larger excess reactivity, higher control rod worth and relatively high packing density of TRISO are required for attaining the targeted operating cycle length. The prismatic reactor must be shut down periodically to perform the refuelling operation just like in LWRs. A schematic of the fuel elements used in the prismatic block reactors is shown in [Figure 1-2](#).

1.5.3 TRISO

The fuel in oxide or carbide form is lumped in a tiny spherical shape, called the fuel kernel, with a typical diameter of 500 μm , surrounded by a low-density carbon layer (buffer) and three containment layers, namely, an Inner Pyrolytic dense Carbon (IPyC) layer, a Silicon Carbide (SiC) layer, and an Outermost Pyrolytic dense Carbon OPyC layer. TRISO particles are mixed with an approximately 50/50 mixture of graphite powder and binder material to form the fuel zone of the pebble fuel element for the pebble-bed design or fuel compacts for the prismatic design.

1.5.4 Fuel Pebble

A 6-cm-diameter fuel pebble consists of two regions as shown in Figure 1-2: a central fuel zone with a 2.5-cm radius and a 0.5-cm-thick protective layer of graphite. This is referred to as a standard fuel pebble. The packing fraction of TRISO particles in the pebble and the enrichment of fuel are design parameters that are to be decided based on the target burnup required. The fuel-free region of the pebble not only protects the fuel zone but also moderates the neutrons.

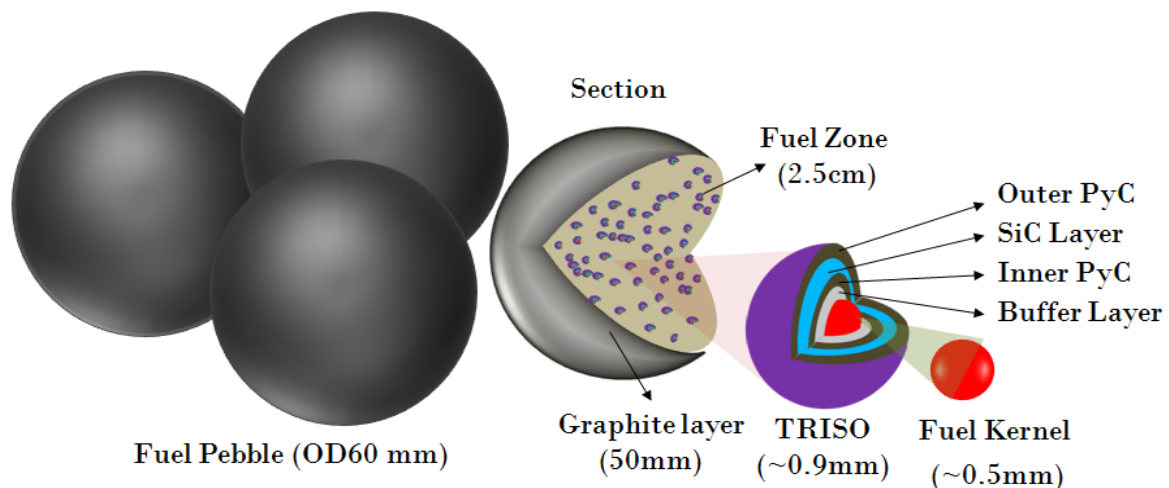


Figure 1-1: Schematic of TRISO and fuel pebbles in pebble-bed design

1.5.5 Fuel Compact

In the prismatic block type of HTRs, TRISO coated fuel particles are randomly distributed in graphite matrix of the fuel compact with a packing fraction of about 29%. The graphite layer of 1mm thickness coats the surface of fuel compacts to prevent the corrosion by exposure to the impurity gases in the primary helium. These fuel compacts are filled into hexagonal fuel blocks having coolant holes and fuel compact holes.

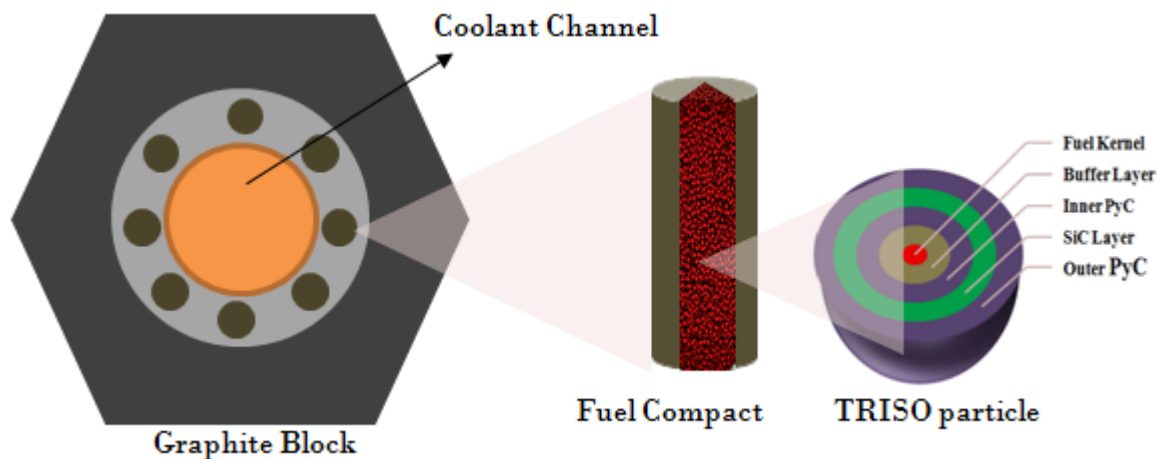


Figure 1-2: TRISO and Fuel Compact in the Prismatic HTR designs

1.6 Nuclear Hydrogen Production

Hydrogen is an energy carrier and considered as one of the future transport fuels because no greenhouse gas like CO₂ is emitted when hydrogen is burnt. Hydrogen exists abundantly on the earth in the form of its compounds but not in its free state. However, it can be separated from water, fossil fuels, or biomass using any one of the suitable methods like thermal processes, electrolysis or thermochemical cycles. Today's commercial scale hydrogen production is based on the steam reforming process in which hydrogen atoms are separated from carbon atoms in methane (CH₄). This results in the emission of carbon dioxide.

Electrolysis is a CO₂ free process (provided the primary energy source is CO₂ free as in the case of nuclear energy), but its overall efficiency is quite low, about 27% if the electricity generation efficiency (~30%) is also accounted for [efficiency of electrolytic process being~90%]. Nuclear reactors, HTRs in particular, can play a key role in efficient hydrogen production on a commercial scale without contributing any greenhouse gases to the environment. Hydrogen can be produced either by using the process heat alone as in the sulfur-iodine thermochemical cycle, as shown in Figure 1-3 or by using high-temperature steam electrolysis.

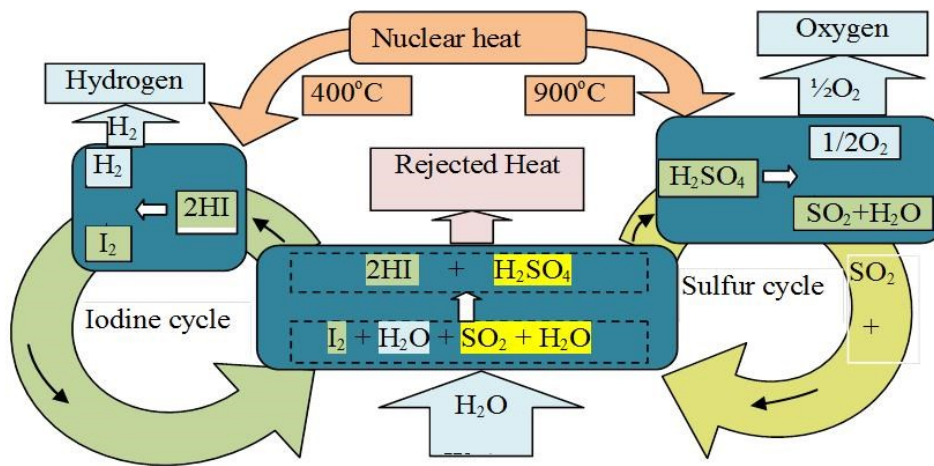


Figure 1-3: Sulphur–Iodine thermo-chemical cycle with HTR nuclear heat source

The former process of water-splitting is a chemical process that accomplishes the decomposition of water into hydrogen and oxygen using only heat. The latter process is known as high-temperature electrolysis in which a combination of heat and electrolysis is used for hydrogen separation. The efficiency of such processes increases with increasing the temperature of the process heat and it is in the range of 40-52% depending on the temperature (850°C-950°C)[22]. Recently, the hybrid copper-chloride process and the hybrid Sulphur cycle

have also been identified as alternative processes for efficient hydrogen production through the application of nuclear heat [6].

1.7 Reactor Physics Design Objectives

Nuclear reactor design is a multidisciplinary subject and requires iterative interaction among various nuclear engineering fields including fuel chemistry, reactor physics, thermal hydraulics, and material science and structural mechanics. The main objective behind a nuclear reactor design is to achieve the highest level of safety with a cost-effective operation of the reactor, prevent any accident, curtail the probability of accidents and mitigate the consequences of accidents [23]. A discussion of all these disciplines is beyond the scope of the thesis and we limit this section to cover only the reactor physics aspect.

The behaviour of a reactor is mainly governed by the reactivity that depends on the reactor size, relative amounts of fuel, moderator, coolant and structural materials, and their properties such as densities and neutron cross-sections. The material properties are affected by the temperature, pressure and fuel burn-up. Fission releases energy in the form of the kinetic energy of the fission fragments and other particles that ultimately appears in the form of heat. The heat produced must be removed efficiently using a coolant so that the temperatures and pressures of various components/materials remain within their design limits. Any imbalance in heat removal by coolant and production by fission results in changes in density and temperature of reactor materials and causes a change in the reactivity. This inter-dependence of reactivity on the material's temperature and pressure introduces a reactivity feedback mechanism in the system. It is always desirable that the reactor has an overall negative temperature coefficient of reactivity because this makes the reactor a self-regulating system.

The reactor physics design calculations start with some assumed configuration of fuel, moderator and coolant materials within the reactor. The physics behaviour of the reactor is then studied by evaluating the neutron flux distribution and the effective multiplication factor (k_{eff}), which is the most fundamental quantity, using the neutron transport equation. The reactor physics design includes the calculations for the steady and transient states of the reactor, using simple or detailed computational codes based on numerical methods. These codes require geometrical details of the reactor and nuclear cross-section data for material distributed in the reactor as input parameters to solve the neutron transport equation. The computational methods based on the solution of the neutron transport equation are called deterministic methods. The transport equation yields the neutron distribution and various derived parameters such as the core reactivity, reactor power, fuel burn-up, control rod worth and reactivity coefficient etc. Reactor design calculations are not only performed in steady state conditions, but also for various transients (including postulated accidental scenarios) due to reactivity insertions or loss of coolant etc. The studies include effects of burnup of fuel, refuelling, (including an interval of refuelling), and the action of control systems to ensure safe operation of the reactor. Safety is ensured by maintaining various parameters within their design limits throughout the designed life of the reactor.

An alternative approach to the deterministic method is known as the Monte Carlo method or the stochastic method that is now being increasingly used regularly in reactor physics. To determine the reactor behaviour, this method uses probabilistic theory and pseudo-random numbers to simulate all the possible physical process e.g., next collision distance, fission, scattering, capture, leakage and so on in the course of the history of a neutron starting from its birth to absorption or leakage. When a sufficiently large number of neutron histories are studied, various quantities of interest are obtained by averaging the corresponding tallies

over these histories. The capability to use the point nuclear data with an exact geometrical representation of the material distribution in the calculations results in very good accuracy. However, the accuracy comes at the cost of higher computation time as compared to the deterministic methods. The main source of uncertainty in the Monte Carlo method for a given set of nuclear data library is the statistical error that decreases as the inverse of the square root of neutron histories used as per the Central Limit theorem [24].

1.8 Special Problems of HTR Design and Thesis Outline

The use of TRISO particles as fuel and ceramic materials such as graphite and helium as coolant enables HTGRs to operate at high temperature. This is not possible with traditional reactors like LWRs or PHWRs due to the use of metal alloys for the cladding of fuel and other structural components. In TRISO particles, the IPyC layer protects the SiC layer from the hot kernel and OpyC layer can withstand the pressure of fission gases up to a very high burnup ($\sim 100\text{GWd/T}$). The role of SiC layer is the retention of the non-gaseous fission products in extremely severe conditions including temperatures of 1600°C for hundreds of hours. Work of Allelein, H.-J., et al., [25] shows that the failure fraction of modern TRISO particles are 4.7×10^{-5} during fuel manufacturing, 4.5×10^{-6} irradiation testing below 1200°C , and 3.7×10^{-5} during the accident testing below 1600°C . In this way, five layers of each coated TRISO particle is able to retain nearly complete fission products during the nominal and accidental conditions. Being tiny in size and presenting a large surface area, heat is quickly transferred to the surrounding graphite matrix that carries it away to the coolant. This fuel design enables HTRs to operate with coolant in the range of 750°C to 950°C temperature. Such high temperatures allow HTRs to have higher thermal efficiencies ($\sim 50\%$) for production of electricity [26] and for use in industrial processes that require heat at a high temperature.

This thesis deals with the unusual challenges that arise in the neutronics design of HTRs due to the peculiar design of fuel elements. The heterogeneous distribution of materials in the HTR lattice cell, tiny TRISO fuel particles dispersed randomly in the graphite matrix followed by graphite and the coolant layers, is referred to as the double heterogeneity effect. It might appear that such fine-particle dispersions may be treated as homogeneous for the entire neutron spectrum but that is not the case for all energies. At certain energies, particularly around resonances, and to some extent in the thermal region, the neutron mean free path is comparable or shorter than the size of the fuel kernel, and the situation necessitates treatment of the dispersion as a heterogeneous medium. This makes the treatment challenging using the deterministic methods based on the solution of transport equation as well as the stochastic methods (Monte Carlo methods).

The goal of the research described in the thesis is the development of new and improved methodology and computational tools for HTR analysis. This includes the development of new theoretical models, algorithms and computer codes based on the models, and the study of benchmark problems. The first of these is the development of a new MC algorithm to realize the random distribution of fuel particles in the HTR lattice cell and pebbles in the HTR core and a fast scheme to track neutrons to compute the Dancoff factor needed in the study of resonance self-shielding and its applications to lattice calculations of HTRs. This is discussed in [Chapter 3](#). [Chapter 4](#) discusses the development of a somewhat heuristic approach to addressing the double heterogeneity problem for the solution of the multigroup transport equation in lattice calculations of HTRs. This is followed by the development of a rigorous theoretical method for solving the transport equation in the random fuel particle dispersion by an exact evaluation of the collision probabilities (CPs) in various regions of the HTR lattice cell. The method is incorporated in the CP code BOXER3 and is described in [Chapter 5](#). The

method developed for the exact evaluation of CPs is extended to the development of an algorithm for providing a solution by the MC method as well. To prove the validity of the proposed method, a multi-region, multigroup MC code (PebMC) is developed to simulate the spherical lattice cell of a pebble bed HTR. This is described in [Chapter 6](#). [Chapter 7](#) gives a summary and the main conclusions of the research work presented in the thesis. It also presents the main conclusions drawn and the scope for future work.

Chapter 2 **REVIEW OF NEUTRONICS METHODS: currently used in traditional reactors and HTRs**

This chapter presents a brief introduction to deterministic and stochastic neutronic methods currently in use for performing reactor physics calculations. It also highlights the unusual challenges posed by HTRs and presents a survey of the existing literature on the methods developed for their solution.

2.1 Introduction

The discovery of the fission of a nucleus of a heavy isotope (e.g. uranium) and emission of secondary neutrons in the fission reaction led to the development of a device in which a sustained fission chain reaction can be maintained in a controlled way. Today, these devices are known as nuclear reactors, which usually consist of a periodic arrangement of fuel, moderator and coolant materials. Nuclear reactor design and analysis is a multi-disciplinary subject of science and engineering. In this context, reactor physics or neutronics has emerged as a distinct and mature discipline, which deals with the determination of the neutron density and reaction rates throughout the nuclear reactor for various states of the reactor.

The Chapter is organized as follows. In Section [2.2](#), a brief overview of the reactor physics methodology is given for traditional reactors. Section [2.3](#) introduces the neutron transport equation. The reactor physics calculations using the multi-step approach is explained in Section [2.4](#). The deterministic methods of reactor calculations are discussed in Section [2.5](#). This section also includes an overview of resonance self-shielding methods for the preparation

of multigroup cross-section. Section [2.6](#) gives a general description of the evolution of nuclear fuel composition during reactor operations. The Monte Carlo method for neutron transport in the reactor is discussed in Section [2.7](#). A survey of the literature on HTR-lattice reactor physics methods and Monte Carlo methods are presented in Section [2.8](#). Finally, Section [2.9](#) defines the objective of the thesis.

2.2 Neutronics Methodology

The physical behaviour of a nuclear reactor depends on the interaction of neutrons with the nuclides of the materials distributed inside the reactor. The linear form of the Boltzmann transport equation describes the transport of neutral particles (neutrons in this case) in the matter. Ludwig Boltzmann originally formulated the transport equation in the context of the kinetic theory of gases [22]. The neutron interactions with nuclides are described in terms of the microscopic cross-section, which is a measure of the probability of occurrence of a nuclear reaction. The reaction cross sections are energy-dependent quantities and often have a very complicated variation with energy. A resonant nuclide requires several hundreds of thousands of energy data points for an accurate representation of its variation with energy. As an example, the variation of U^{238} cross-section is as shown in [Figure 2-1](#). Nuclear-reaction theory codes are used to interpolate and extrapolate from the measured data to produce a complete set of evaluated cross-section data libraries from which it is possible to obtain various reactions cross-sections of the nuclides of interest at any energy in the energy range of interest (10^{-5} eV - 20 MeV) [23]. The nuclear theory is needed because the experimental nuclear data of various nuclides of interest of Reactor Physics have been measured only at a limited number of points

in the energy range of interest and also because the nuclide cross sections depend upon the temperature of the material and the chemical binding with other nuclides of the material.

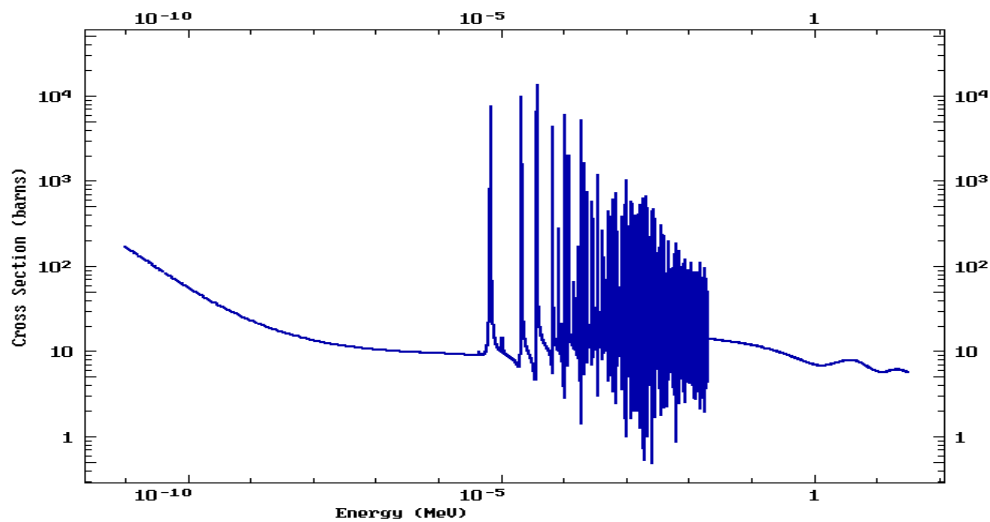


Figure 2-1: Variation of Total microscopic continuous cross-section of U238

In principle, the neutron transport equation should be solved to determine the neutron distribution to predict the physics behaviour and properties of the reactor. However, solving the transport equation for a highly heterogeneous three-dimensional reactor with wildly varying reaction cross-sections is so time-consuming as to be practically infeasible, even on the most powerful computers at present [27]. This naturally demands simplifications based on various approximations. A brief discussion of various methods applied to solve the neutron transport equation is presented in this chapter.

An alternative approach to solving neutron transport problems in Reactor Physics is a stochastic approach based on the Monte Carlo method. Its primary advantage is that it allows an exact treatment of the geometrical and cross-section details without any approximations. For this reason, it is becoming increasingly popular. However, its principal disadvantage is that it is computationally expensive for obtaining detailed flux/reaction rate distributions. This approach is also discussed in this chapter.

2.3 Neutron Transport Equation

The average behaviour of a large population of free neutrons can be described mathematically by the neutron transport equation in an integrodifferential form, characteristics form or integral equation form. This equation is based on the principle of particles balance in an arbitrary phase space volume element $d^3r d\Omega dE$. The transport equation is solved for the angular flux distribution $\psi(\mathbf{r}, E, \boldsymbol{\Omega})$ that is related to the distribution of the density of particles and is a function of seven independent variables (one in time, three in space, one in energy and two in angle). The integrodifferential form of the transport equation for the steady-state problem is given by Eq. (2.1) [since work in the thesis deals with the time-independent steady-state condition of the reactor].

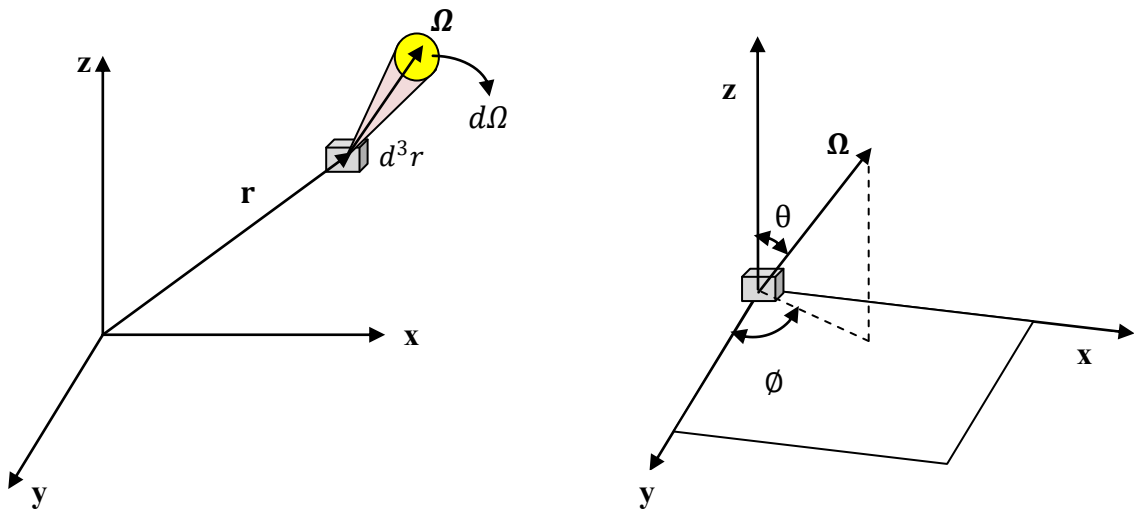


Figure 2-2: Neutrons location at r in d^3r volume element and motion in direction cone $d\boldsymbol{\Omega}$ around $\boldsymbol{\Omega}$.

$$\boldsymbol{\Omega} \cdot \nabla \psi(\mathbf{r}, E, \boldsymbol{\Omega}) + \Sigma_t(\mathbf{r}, E) \psi(\mathbf{r}, E, \boldsymbol{\Omega}) = Q(\mathbf{r}, E, \boldsymbol{\Omega}) \quad 2.1$$

Where, $\mathbf{r} = (x, y, z)$ and $\boldsymbol{\Omega} = (\Omega_x, \Omega_y, \Omega_z) = (\sqrt{(1 - \mu^2)} \cos \phi, \sqrt{(1 - \mu^2)} \sin \phi, \mu)$

The product of the number density of a nuclide with the microscopic cross-section is defined as the macroscopic cross-section (Σ) of that nuclei. The subscripts s, f, a and t are used to represent the total, scattering, fission and absorption cross-sections respectively. The first term in neutron transport equation describes the net removal of particles through the volume element at the point \mathbf{r} , with energy E in the direction $\boldsymbol{\Omega}$ of the phase space due to streaming (i.e. the motion of the particles) while the second term represents the removal due to collisions. Finally, the term on the right-hand side is the net number of particles added to the volume element due to the neutron source term $Q(\mathbf{r}, E, \boldsymbol{\Omega})$. This is given in Eq.(2.2) as the sum of the scattering source (Q_s) and the fission source (Q_f) with the eigenvalue, fission neutron spectrum, and the average number of neutrons released per fission at position r , represented by $K, \chi(E)$ and ν respectively.

$$Q(\mathbf{r}, E, \boldsymbol{\Omega}) = \int_{4\pi} \int_0^\infty \left[\Sigma_s(\mathbf{r}, E', \boldsymbol{\Omega}' \rightarrow E, \boldsymbol{\Omega}) + \frac{\chi(E)}{4\pi K} \nu \Sigma_f(\mathbf{r}, E', \boldsymbol{\Omega}') \right] \psi(\mathbf{r}, E', \boldsymbol{\Omega}') dE' d\boldsymbol{\Omega}' \quad 2.2$$

The steady state neutron transport Eq. (2.1) can also be written in the characteristic form by writing the partial derivatives of the streaming operator in terms of the total derivative with respect to the distance ($\boldsymbol{\Omega} \cdot \nabla = d/ds$) along the trajectory of the neutron motion in space, as shown in Figure 2-3. The equivalent total derivative can be obtained by change of variables $\mathbf{r} = \mathbf{r}_0 + s\boldsymbol{\Omega}$, where s is the distance measured along the direction $\boldsymbol{\Omega}$, from \mathbf{r}_0 which is an arbitrary starting point on the characteristic path[28].

$$\frac{d}{ds} \psi(\mathbf{r}_0 + s\boldsymbol{\Omega}, E, \boldsymbol{\Omega}) + \Sigma_t(\mathbf{r}_0 + s\boldsymbol{\Omega}, E) \psi(\mathbf{r}_0 + s\boldsymbol{\Omega}, E, \boldsymbol{\Omega}) = Q(\mathbf{r}_0 + s\boldsymbol{\Omega}, E, \boldsymbol{\Omega}) \quad 2.3$$

The characteristic form of the neutron transport equation is a linear first-order ordinary differential equation, which can be integrated along the neutron trajectory to obtain the integral form of the transport equation in an infinite medium, as given in Eq. (2.4)

$$\psi(\mathbf{r}, E, \boldsymbol{\Omega}) = \int_0^{\infty} Q(\mathbf{r}, \mathbf{r} - s'\boldsymbol{\Omega}, E, \boldsymbol{\Omega}) e^{-\int_0^s \Sigma_t(\mathbf{r}, \mathbf{r} - s'\boldsymbol{\Omega}, E) ds'} ds' \quad 2.4$$

Physically, the angular flux at location \mathbf{r} is contributed by neutrons having direction $\boldsymbol{\Omega}$ and energy E starting from all other possible locations (behind the point \mathbf{r}) $\mathbf{r} - s'\boldsymbol{\Omega}$, with all positive values of s' , reduced by the attenuation factor $\exp(-\int_0^s \Sigma_t(\mathbf{r}, \mathbf{r} - s'\boldsymbol{\Omega}, E) ds')$. The integral in the attenuation factor is defined as optical path $\tau(\mathbf{r}, \mathbf{r}', E) = \int_0^s \Sigma_t(\mathbf{r}, \mathbf{r} - s'\boldsymbol{\Omega}, E) ds'$ between the source point \mathbf{r}' and the target point \mathbf{r} .

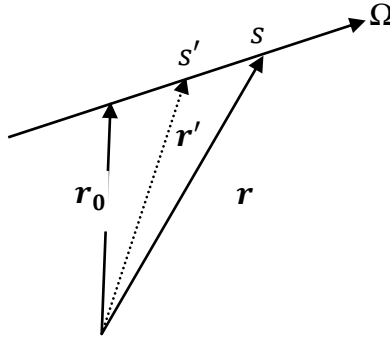


Figure 2-3: Spatial coordinate along the direction of trajectory.

The result of integration of the characteristics form of transport Eq. (2.2) over a finite medium is expressed by Eq. (2.5)

$$\begin{aligned} \psi(\mathbf{r}, E, \boldsymbol{\Omega}) = & \psi(\mathbf{r} - \mathbf{R}_s \boldsymbol{\Omega}, E, \boldsymbol{\Omega}) e^{-\int_0^{\mathbf{R}_s} \Sigma_t(\mathbf{r}, \mathbf{r} - s'\boldsymbol{\Omega}, E) ds'} \\ & + \int_0^{\mathbf{R}_s} ds' Q(\mathbf{r} - s'\boldsymbol{\Omega}, E, \boldsymbol{\Omega}) e^{-\int_0^s \Sigma_t(\mathbf{r}, \mathbf{r} - s'\boldsymbol{\Omega}, E) ds'} \end{aligned} \quad 2.5$$

The second term on RHS of Eq. (2.5) represents angular flux at point $(\mathbf{r}, E, \boldsymbol{\Omega})$ due to the neutron source distributed in finite volume (V) surrounded by boundary surface R_s . The first term represents the contribution of the incoming angular flux at surface R_s to the point $(\mathbf{r}, E, \boldsymbol{\Omega})$ with attenuation factor $e^{(-\int_0^{R_s} \Sigma_t(\mathbf{r}-s'\boldsymbol{\Omega}, E) ds')}$. The angular flux at a point $(\mathbf{r}, \boldsymbol{\Omega})$ in the multigroup approximation can be written as

$$\psi_g(\mathbf{r}, \boldsymbol{\Omega}) = \psi_g^{in}(\mathbf{r}_s, \boldsymbol{\Omega})e^{-\tau(\mathbf{r}, \mathbf{r}_s)} + \int_0^{R_s} ds' Q_g(\mathbf{r}', \boldsymbol{\Omega})e^{-\tau_g(\mathbf{r}, \mathbf{r}')} \quad 2.6$$

Where, $\mathbf{r}_s = \mathbf{r} - R_s\boldsymbol{\Omega}$ is a point on the line passing through the point \mathbf{r} along the neutron direction $\boldsymbol{\Omega}$ on the surface S and $\mathbf{r}' = \mathbf{r} - s'\boldsymbol{\Omega}$. The incoming flux is specified by the boundary conditions. Methods based on obtaining numerical solutions of the transport equation for the neutron distribution (generally using numerical methods) are known as deterministic methods. Section 2.5 presents a brief description of some of the commonly used deterministic methods. Simulation of sequences of physical events of numerous neutrons from their birth in fission to their loss either by leakage or by absorption using statistical theory is called the stochastic or Monte Carlo method and is discussed in Section 2.7.

2.4 Multi-Step Methodology

Most of the deterministic methods, involving the solution of the transport equation, for reactor calculations, are based on the multi-step procedure [27]. This methodology is developed to get the neutron flux distribution and reaction rates in a reasonable amount of computing time for routine reactor analysis. It is based on the principle of the conservation of reaction rates at each step. The results at one step serve as inputs to the next step. A schematic of reactor physics calculations using the multi-step approach is shown in Figure 2-4. The geometrical details and cross-sections of materials in the reactor are the input parameters for the solution of the

transport equation with any of the deterministic method discussed above. The computational efficiency and the demand for accuracy for the problem play an important role in the selection of an appropriate method of solution. However, the computational efficiency comes at the cost of accuracy. As previously discussed in Section 2.2 that the solution of the transport equation with a point data library is impractical with any of the deterministic method and it becomes indispensable to use the multi-group method of transport theory.

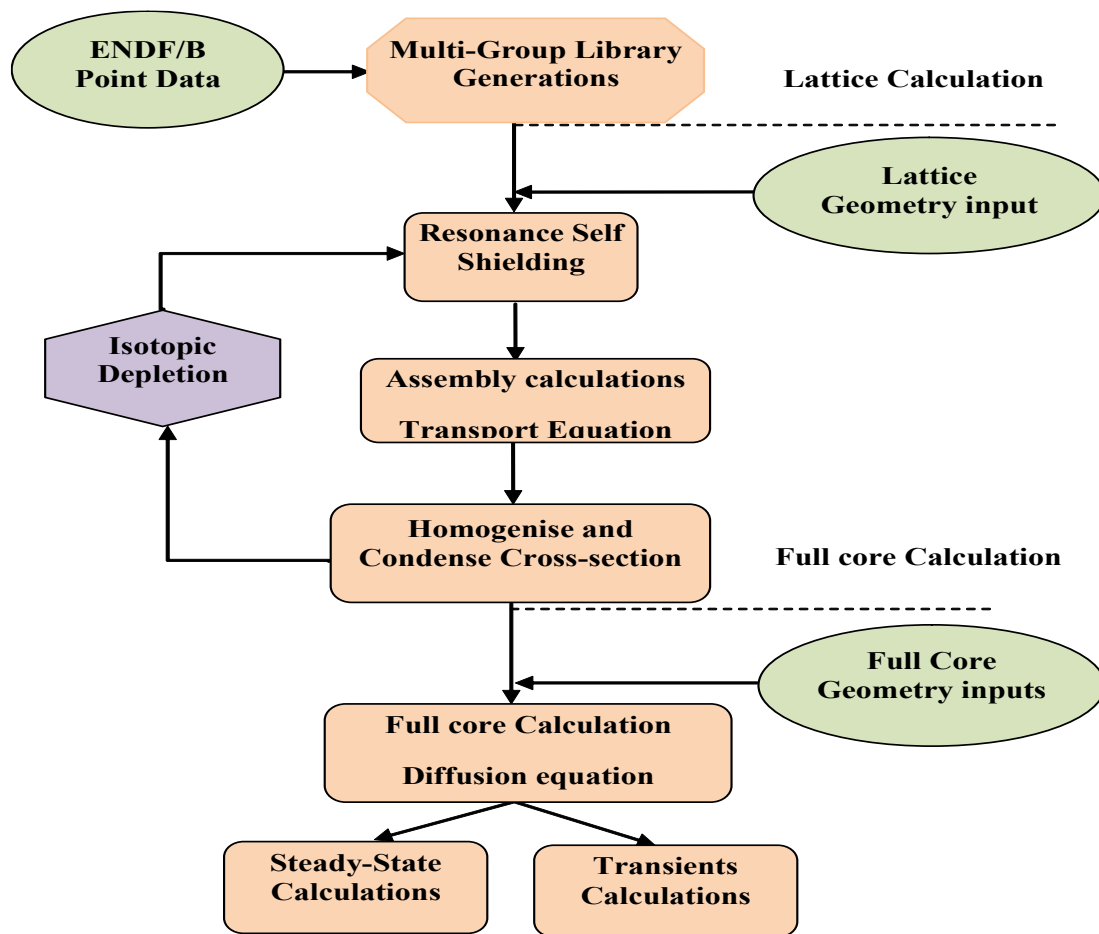


Figure 2-4: A multi-step reactor physics analysis procedure

2.4.1 Multi-group approximation

The first approximation in deterministic calculations is the generation of multigroup constants or cross-sections by processing the cross-sections of each isotope in the ENDF/B file. To generate the multigroup constants, the energy range of interest is discretized into G groups where the first group represents the highest energy group [upper boundary 20MeV] and the last group ($g = G$) is the lowest energy group [lower energy boundary 10^{-5} ev]. The group cross-section $\Sigma_{x,g}$ of reaction type x is defined in Eqs. (2.7)-(2.9) and it is a constant within the energy interval $[E_g, E_{g-1}]$.

$$\Sigma_{x,g}(\mathbf{r}, \boldsymbol{\Omega}) = \frac{\int_{E_g}^{E_{g-1}} \Sigma_{x,g}(\mathbf{r}, E) \psi(\mathbf{r}, E, \boldsymbol{\Omega}) dE}{\int_{E_g}^{E_{g-1}} \psi(\mathbf{r}, E, \boldsymbol{\Omega}) dE} \quad 2.7$$

$$\psi_g(\mathbf{r}, \boldsymbol{\Omega}) = \int_{E_g}^{E_{g-1}} \psi(\mathbf{r}, E, \boldsymbol{\Omega}) dE \quad 2.8$$

$$\chi_g = \int_{E_g}^{E_{g-1}} \chi(E) dE \quad 2.9$$

However, Eqs. (2.7)-(2.9) need continuous energy dependent angular flux $\psi(\mathbf{r}, E, \boldsymbol{\Omega})$, which is not known a priori. This also makes the total cross-section angular dependent. Therefore, it becomes necessary to make an approximation for the angular flux by separating the angular and energy variables as given in the Eq. (2.10).

$$\psi(\mathbf{r}, E, \boldsymbol{\Omega}) \approx \phi(E) \psi(\mathbf{r}, \boldsymbol{\Omega}) \quad 2.10$$

With this approximation for the angular flux, the multigroup cross sections can be defined in terms of the weighting spectrum $\phi(E)$, as shown in Eqs. (2.11)-(2.13) [29]–[33].

$$\Sigma_{x,g} = \frac{\int_{E_g}^{E_{g-1}} \Sigma_{x,g}(E) \phi(E) dE}{\int_{E_g}^{E_{g-1}} \phi(E) dE} \quad 2.11$$

$$\phi_g = \int_{E_g}^{E_{g-1}} \phi(E) dE \quad 2.12$$

$$\chi_g = \int_{E_g}^{E_{g-1}} \chi(E) dE \quad 2.13$$

The weighting spectrum $\phi(E)$ is also not known in advance for the system to be analyzed and some approximate forms have to be used. If the cross-section varies slowly with energy in a group, sufficient accuracy can be obtained with the fixed functional form of weighting spectrum $\phi(E)$. In the WIMS formalism for the light elements, the fixed form is the fission spectrum in the fast region, $\frac{1}{E}$ energy dependence in the resonance region and Maxwellian distribution in the thermal region [34]. This assumption is often valid, but cannot be used when the flux varies rapidly within a group, as it is the case where the cross-section exhibits resonances in the group.

For treating resonant isotopes, the neutron-weighting spectrum $\phi(E)$ can be obtained by solving the slowing down equation, as given in Eq. (2.14), using two approaches. The first approach is based on the analytical solutions (obtainable under the three approximations discussed below) of the slowing down equation for a homogeneous infinite medium formed by a mixture of resonant absorber and background moderator nuclides [35], [36]:

$$\begin{aligned} & \left(N_r \sigma_{t,r}(E) + \sum_{k \neq r} N_k \sigma_{p,k} \right) \phi(E) \\ & = \frac{1}{1 - \alpha_r} \int_E^{E/\alpha_r} N_r \sigma_{s,r}(E') \phi(E') \frac{dE'}{E'} + \sum_{k \neq r} \frac{1}{1 - \alpha_k} \int_E^{E/\alpha_k} N_k \sigma_{p,k} \phi(E') \frac{dE'}{E'} \end{aligned} \quad 2.14$$

Where N_r and N_k : is number density of resonant and non-resonant nuclides, respectively

$1 - \alpha_k$: is the maximum fractional energy loss per collision with nuclide k .

In Eq. (2.14), the cross-section of moderator nuclides is assumed to be constant with zero absorption cross-section ($\sigma_{a,k} = 0$) and their total cross-sections ($\sigma_{t,k}$) are equal to the potential scattering cross-sections ($\sigma_{p,k}$). In the resonance region, fission neutrons are ignored, and elastic scattering is the dominant mechanism for the slowing down of neutrons. The resonance width is assumed to be small as compared to the energy loss per elastic collision i.e. slowing down width. In the narrow resonance approximation (NR) it is assumed that the resonance width is small as compared to the energy loss per elastic collision with both the resonant nuclide and the background moderator nuclides and the slowing down equation becomes

$$\left[\Sigma_{t,r}(E) + \sum_{k \neq r} \Sigma_{p,k} \right] \phi_{NR}(E) = \frac{1}{E} \left[\Sigma_{p,r}(E) + \sum_{k \neq r} \Sigma_{p,k} \right] \quad 2.15$$

$$\phi_{NR}(E) = \frac{1}{E} \frac{\sigma_{p,r} + \sigma_b}{\sigma_{t,r}(E) + \sigma_b} \quad 2.16$$

Where, $\sigma_b = \frac{\sum_{k \neq r} N_k \sigma_{pk}}{N_r}$ is defined as background cross-section or the dilution cross-section

$\Sigma_{t,r}(E)$: Total macroscopic cross-section of resonant nuclide

$\Sigma_{p,r}(E)$: Potential macroscopic cross-section of resonant nuclide

$\Sigma_{p,k}$: Potential macroscopic cross-section of nuclide k

The background cross-section σ_b determines the depression of the neutron flux at resonance peak energy and acts like a fictitious microscopic cross-section. For large σ_b , flux variation with energy approaches to $\frac{1}{E}$ as if no absorber is present and the scattering of other non-resonant moderator nuclides dominates the spectrum. On the other hand, the neutron flux is inversely proportional to $\sigma_{t,r}(E)$ of the resonance nuclide for low background cross-section.

In thermal reactor analysis, the NR approximation is not valid for some of the most important low-energy resonances of fertile materials. The slowing down equation can also be solved by assuming that the resonant nuclide has infinite mass, which implies that the width of the resonance peak is wide compared to the average energy loss due to scattering with the resonant nuclide. It means the energy loss due to collisions with absorber atoms is neglected. The asymptotic flux variation using this approximation, called wide resonance (WR) approximation is given by Eq. (2.17)

$$\phi_{WR}(E) = \frac{1}{E} \frac{\sigma_b}{\sigma_{a,r}(E) + \sigma_b} \quad 2.17$$

It is obvious from Eqs. (2.16) and (2.17) that the scattering cross-section of a resonant nuclide is fully accounted for in the NR approximation, but it is completely ignored in the WR approximation. To deal with condition in which the resonances are neither narrow nor wide, an intermediate form of the spectrum can be deduced by considering the partial scattering cross-section of the resonant nuclide. The intermediate resonance approximation is obtained by defining a factor λ called the intermediate resonance (IR) or the hydrogen equivalent factor[37]. In order to apply the IR factor to all nuclides, the IR factors for resonance nuclide r and the non-resonance nuclide k are represented by λ_r and λ_k respectively. For hydrogen $\lambda_k = 1$ and for other nuclides it is less than one i.e., $\lambda_k < 1$. The analytical expression of the spectrum for the intermediate resonance width is given [27] in Eq. (2.18).

$$\phi_{IR}(E) = \frac{1}{E} \frac{\lambda_r \sigma_{p,r} + \sigma_b}{\sigma_{a,r}(E) + \lambda_r \sigma_{p,r} + \sigma_b}; \text{ where } \sigma_b = \frac{\sum_{k \neq r} \lambda_k N_k \sigma_{pk}}{N_r} \quad 2.18$$

With weighting flux $\phi(E)$ analytically or numerically evaluated, the continuous energy cross-section can now be collapsed to a few hundred groups [33]. The group constants so generated will preserve the reaction rate within each energy group as long as the guess flux $\phi(E)$ used in

collapsing the continuous cross-section accurately represents the neutrons spectrum for the system to be analyzed. According to Eq. (2.18), the weighting function depends upon the quantity σ_b that is called the background cross-section. It may therefore be expected that the weighted cross-section will depend upon this quantity. Due to the Doppler broadening of resonances, the group cross-sections also depend upon the temperature of the fuel. The cross-sections in the resonance groups are generally represented by the resonance integrals, which are tabulated as functions of the "background cross-section and the temperature. The spectrum weighted multigroup cross-sections in the resonance groups of the library are generated using infinite homogeneous media and thus they are called homogeneous data tables or effective multigroup cross-sections e.g. WIMS(69g, 172g) [38] or DRAGLIB(172g, 295g, 361g)[39][40]. However, such libraries can be used not only for homogeneous problems but also for heterogeneous problems by making use of equivalence theory, which will be discussed in Section [2.4.2](#).

In the second approach, called the *ultra-fine group method*, direct numerical solutions to the slowing down equation or transport equation for the given problem are obtained using very fine energy groups (CE). In this approach, the multigroup cross-section is evaluated with a very detailed neutron spectrum distribution. As this method is based on the first principle for energy dependence, it generates quite accurate multigroup cross-sections. However, it becomes impractical to use this approach even in the regular lattice cell problems due to high computational costs [41]–[45].

2.4.2 Self-Shielding Methods

The absorption rate is determined by the product of the macroscopic cross-section and neutron flux. Due to the inter-dependency of cross-section and the flux, a resonance peak with

high cross-section results in depression in the flux of neutrons around the resonance peak energy and result in the absorption rate reduction. This is referred to as *energy self-shielding* and it is treated using a direct numerical solution of slowing down equation or analytical approach by NR, WR or IR approximation [46]. Another component of self-shielding, called *spatial self-shielding* appears in heterogeneous geometry of resonant material and moderator material distribution. When neutrons around resonance peak flow from moderator to fuel lumped in a heterogeneous geometry, the absorption rate in the peripheral region is high and it reduces towards the centre of the lump. Thus, the depression in the neutron flux spatial distribution would be different for the surface and for the central part of the fuel near the resonance peak energy. The accurate estimation of self-shielding on the absorption rate becomes very crucial while calculating the group constants for a spatially homogeneous or a heterogeneous system. The use of expected flux as a weighting function for the continuous energy cross-section collapsing accounts for the self-shielding in the infinite homogeneous medium, but it does not account for the self-shielding in the heterogeneous medium.

2.4.3 Equivalence Principle

One of the most popular methods of self-shielding for the heterogeneous medium is the equivalence principle which permits the use of the group constants from a homogeneous data library to a heterogeneous system e.g., pin cell or fuel assembly. The equivalence principle states that a heterogeneous system, where fuel-to-moderator collision probability can be expressed in the form of a rational approximation, can be replaced with an equivalent homogeneous system in which the potential scattering cross-section is augmented with energy independent escape cross-section[34]. The rational approximation proposed by Wigner for the P_{esc} of an isolated fuel lump is given in Eq. (2.19) [47].

$$P_{fm} = P_{esc} = \frac{\Sigma_e}{\Sigma_{t,f}(E) + \Sigma_e} \quad 2.19$$

Where, $\Sigma_e := 4 * \frac{\text{fuel volume}}{\text{surface area}}$

The equivalence principle allows using a data table, which would be generated for a set of homogeneous problems, for solving heterogeneous problems via the table lookup with prior knowledge of problem specific Σ_e . For an isolated fuel element, the macroscopic escape cross-section (Σ_e) is equal to the inverse of the average chord length (\bar{l}_f). The Σ_e only depends on the fuel geometry if chord distribution is assumed to have an exponential. It allows us to apply homogeneous library data, in which resonance integrals are tabulated for several background cross-section and temperatures, directly to a heterogeneous problem provided Σ_e is known. By applying the IR and Wigner's approximation along with the equivalence principle, the neutron spectrum in the fuel region of the heterogeneous system can be written in a form that is similar to the homogeneous solution

$$\phi_{IR}(E) = \frac{1}{E} \frac{\lambda_r \sigma_{p,r} + \sigma_{b,f} + \Sigma_e/N_r}{\sigma_{a,r}(E) + \lambda_r \sigma_{p,r} + \sigma_{b,f} + \Sigma_e/N_r} \quad 2.20$$

Where, $\sigma_{b,f} = \frac{\sum_{k \neq r} \lambda_k N_k \sigma_{p,k}}{N_r}$: background cross-section for the resonance nuclide r (with the summation restricted to nuclides in the fuel region).

This implies that a heterogeneous system is equivalent to a homogeneous one having an effective background cross-section given by $\frac{\sum_{k \neq r} \lambda_k N_k \sigma_{p,k}}{N_r} + \frac{\Sigma_e}{N_r}$. For the intermediate value of the fuel cross-section, Wigner's approximation under predicts the escape probability which is improved by using the Bell factor (a_B). The rational form of escape probability with the Bell-Levine factor is referred to as Wigner-Bell's rational approximation. Fuel elements in a reactor are not isolated. Often, they are quite close to one another. The escape probability becomes

effectively smaller than that for the isolated fuel element due to the shadowing effect of neighboring fuel lumps present in the fuel assembly or lattice system. In this case, the equivalence principle for non-isolated fuel lumps can be established by making use of the Dancoff correction (C) to the escape cross-section as given below, by Eq. (2.21). [48], [49]

$$\Sigma_e(a_B, C) = \frac{a_B(1 - C)}{\bar{l}_f [1 + C(1 - a_B)]} \quad 2.21$$

The Dancoff correction takes into account the average probability that resonant neutrons escaping a fuel lump hit another fuel lump without any collision with moderator nuclei. The neutron spectrum using IR approximation with the Dancoff and Bell corrected escape cross-section can be written as

$$\phi_{IR}(E) = \frac{1}{E} \frac{\lambda_r \sigma_{p,r} + \sigma_{b,f} + \Sigma_e(a_B, C)/N_r}{\sigma_{a,r}(E) + \lambda_r \sigma_{p,r} + \sigma_{b,f} + \Sigma_e(a_B, C)/N_r} \quad 2.22$$

Where, N is the number density and the subscript r denotes the resonant isotope.

The self-shielded cross-sections σ_x for reaction type x can be obtained from the resonance integral (RI_x) as follows

$$\sigma_x(\sigma_b, T) \approx \frac{RI_x(\sigma_b, T)}{1 - \frac{RI_a(\sigma_b, T)}{\sigma_b}} \quad 2.23$$

where, the subscript a denotes absorption. The resonance integrals RI_x are tabulated in the cross-section data library as a function of the effective background cross-section (σ_b) and fuel temperature (T) and may be obtained for the specific values of these parameters by interpolation from these tabulations.

This background sets the classical resonance treatment in lattice cell calculation using the equivalence principle. However, further improvements to the equivalence theory have been

proposed by Carlvik [50], Stamm'ler [36] and later by Hebert and Marleau [51] to the rational approximation for the escape probability by increasing the number of terms.

2.4.4 Subgroup Method

The basic concept of the subgroup method, also known as the multiband method, is to use value of the cross-section, as the independent variable in integration to calculate the group constants, rather than the energy[52]–[54]. Such integral variable transformation can be applied because the spectrum $\phi(E)$ depends on energy only through the energy dependence of the cross-section. In this approach, the detailed energy-dependent cross-section behaviour in each coarse energy group is replaced by its probability density representation [55]. Unlike in equivalence principle, the subgroup method allows performing resonance self-shielding calculation on a heterogeneous geometry rather than on a homogeneous geometry and thereby permits the accurate evaluation of flux variation across the fuel rod in resonance-region.

2.5 Deterministic Methods: Solution of the Transport Equation

In the deterministic methods, the neutron transport equation is reduced to a solvable form by using discretization of independent variables. The energy variable is discretized by the use of energy groups (multi-group method discussed in greater detail in Section [2.4.2](#)). The neutron transport equation is solved over a discrete spatial mesh rather than for a continuous spatial function. The spherical harmonics method (P_N), and the discrete ordinates (DS_N) method are some of the methods commonly used to solve the integrodifferential form of the neutron transport equation. The method of characteristics (MOC) uses the characteristics equation [Eq. (2.3)] as the starting point for obtaining the angular flux. On the other hand, the

method of collision probability (CP) and interface current (IC) or some combination of these are used to solve the integral form of the transport equation.

2.5.1 Spherical Harmonics Method (P_N)

In the spherical harmonics method, angular flux and scattering cross-section are expressed in terms of infinite series of complete orthogonal set e.g. spherical harmonics. The expansion coefficients are determined by orthogonality properties of the polynomial set. The substitution of the expansions into the neutron transport equation results in an equivalent infinite system of ordinary differential equations. In-plane geometry, the spherical harmonics reduce to the Legendre polynomials. In order to develop a practical method of solution, a finite number of terms (up to order N) of the expansion are retained by setting the expansion coefficients of all other terms to 0. In particular, the P_1 equations with additional assumptions can be reformulated into the well-known neutron diffusion equations [56]. The higher-order expansion complicates the solution method and this limits the application of this method.

2.5.2 Discrete Ordinates Method (DS_N)

The DS_N method is most easily illustrated in the simple case of one group, one-dimensional plane geometry problems with isotropic scattering, wherein the transport equation takes the form

$$\mu \frac{\partial \Phi(x, \mu)}{\partial x} + \Sigma_t(x) \Phi(x, \mu) = \frac{1}{2} \int_{-1}^1 c(x) \Sigma_t(x) \Phi(x, \mu) d\mu \quad 2.24$$

where $c(x)$ is the mean number of secondaries per collision. In the DS_N method, the angular dependence of neutron flux is represented by its values along a set of discrete directions (μ_N) with associated weights (w_N). The integration on the right-hand side can then be written using a suitable quadrature formula and the equation becomes.

$$\mu_i \frac{\partial \Phi(x, \mu_i)}{\partial x} + \Sigma_t(x) \Phi(x, \mu_i) = \frac{1}{2} \sum_{j=1}^N w_j c(x) \Sigma_t(x) \Phi(x, \mu_j) \quad 2.25$$

Thus, the transport equation is replaced with a set of N coupled differential equations. The most commonly used quadratures set in DS_N method in plane geometry is the Gauss quadrature and in multidimension geometries, a specially developed quadrature called fully symmetric quadrature is used [57]. To solve the above system of equations numerically, the spatial domain is divided into meshes such that material properties are uniform within each mesh. Integration of Eq. (2.25) w.r.t. x over the k^{th} mesh, gives

$$\begin{aligned} \mu_i [\Phi(x_{k+1/2}, \mu_i) - \Phi(x_{k-1/2}, \mu_i)] + \Delta x_k \Sigma_t(x_k) \Phi(x_k, \mu_i) \\ = \frac{\Delta x_k}{2} \sum_{j=1}^N w_j c_k \Sigma_k \Phi(x_k, \mu_j) \end{aligned} \quad 2.26$$

where $\Phi(x_k, \mu_i)$ stands for the average flux in the k^{th} mesh whereas $\Phi(x_{k+1/2}, \mu_i)$ and $\Phi(x_{k-1/2}, \mu_i)$ stand for the angular fluxes at the right and left boundaries of the mesh respectively. Δx_k stands for the mesh width. The above equation has more variables than the number of equations. This is remedied by assuming the following relation between the average and boundary fluxes.

$$[\Phi(x_{k+1/2}, \mu_i) + \Phi(x_{k-1/2}, \mu_i)] = 2 \Phi(x_k, \mu_j) \quad 2.27$$

Eq. (2.27) is called the ‘diamond difference’ relation. Together with the boundary condition which specifies the incoming angular flux, there are as many equations as there are unknowns for solving the above set of linear algebraic equations. These are solved iteratively. The method is easily extendable to multi group and multidimensional problems. This method can treat the anisotropic neutron scattering because of the direct angular discretization. This method is computationally very efficient and has been implemented to solve the whole core neutron

transport equation. Such computer codes are DORT[58], TORT[59] and ATESS[60]. However, the complex geometries, especially with curved surfaces at the outer edge of the problem domain, are not represented accurately due to the use of finite difference for the spatial variable.

2.5.3 Method of Characteristics (MOC)

To deal with more complex geometries, a method called the method of characteristic (MOC) is devised to solve the neutron transport equation along the neutron flight path using Eq. (2.3). [61], [62]. Thus, the 3D neutron transport variable r is replaced with the 1D variable along the path of neutron motion. Similar to the DS_N , the method of MOC is also based on discrete ordinate approximation to the angular integral. The MOC method requires neutron tracking across the spatial domain for several paths along which the characteristics equation is solved for each direction of the quadrature set [63]. Like the DS_N method the MOC can also treat anisotropic scattering. For simplicity of the solution method, the constant flux approximation within a mesh is used. This requires rather small-sized meshes and hence longer computing times for obtaining good accuracy. Higher-order representations such as linear flux within a mesh have been successfully used to reduce computing time [64].

2.5.4 Integral Transport Theory Based Methods

The integral transport equation is written entirely in terms of the scalar neutron flux. This is its main advantage and introduces simplicity in problems where the anisotropy in the scattering cross-section is not important and can be handled with the use of the transport correction to the scattering cross-section. This method is suitable for treating the complex geometry but is generally limited to small sized problem domains (in terms of mean free paths) and where anisotropy through the simple transport correction to the isotropic scattering cross-

section is adequate. It is particularly suited for lattice cell codes particularly in simple one-dimensional pin cell problems [65]. A number of codes for two dimensional, lattice calculations have also been developed [66], [67]. The method has also been applied for some special three dimensional problems as well [61], [67]–[69]. We discuss this method in greater detail partly because of its widespread use in lattice calculations but mainly because the work discussed in the thesis largely makes use of this method.

The Collision Probability Method

The integral form of the neutron transport equation is usually solved using a method called the Collision Probability or P_{ij} method [50]. The spatial problem domain is discretized into small meshes such that the material properties are constant with respect to the spatial variable within each mesh. The neutron sources due to fission, scattering or external source are assumed to be constant across the mesh. This assumption is called the flat flux approximation. However, a difficulty arises in solving the dense non-zero collision probability matrix involved due to the coupling of all regions to all other region in large domains. To illustrate the collision probability method for solution of the integral form of the transport equation, we assume that use transport corrected cross-section adequately represents the anisotropy of the scattering and neutron sources. With this approximation, the scalar flux of neutrons at point (\mathbf{r}, E) due to the neutrons originating in all points \mathbf{r}' in space is calculated by integrating the Eq. (2.4) over the angular variable Ω .

$$\phi(\mathbf{r}, E) = \int_0^r d^3r' \int dE' \left[\Sigma_s(\mathbf{r}, E' \rightarrow E) \phi(\mathbf{r}', E') + Q_f(\mathbf{r}', E) \right] T(\mathbf{r}' \rightarrow \mathbf{r}, E) \quad 2.28$$

Where,

$\phi(\mathbf{r}, E)$ is scalar flux of neutrons with energy E at point \mathbf{r}

$\Sigma_s(\mathbf{r}, E' \rightarrow E)$ is scattering cross-section from energy E' to energy E at point \mathbf{r}

$Q_f(\mathbf{r}', E)$ is neutron source with energy E at point \mathbf{r}' due to fission

$T(\mathbf{r}' \rightarrow \mathbf{r}, E) = \frac{e^{-\tau(\mathbf{r}, \mathbf{r}', E)}}{4\pi|\mathbf{r}-\mathbf{r}'|^2}$ represents the transport kernel.

$d^3r' = 4\pi d\Omega s^2 ds$ is elemental volume around the point \mathbf{r}'

The integral transport equation [Eq. (2.28)] can be written in multigroup form as follows

$$\phi_g(\mathbf{r}) = \int_0^r d^3 r' \left[\sum_h \Sigma_{s0,i,g \leftarrow h} \phi_{i,h} + \frac{\chi_g}{K} \sum_h v \Sigma_{f,h} \phi_{i,h} \right] T_g(\mathbf{r}' \rightarrow \mathbf{r}) \quad 2.29$$

In the collision probability method for solution of the integral transport equation, we discretize the spatial domain into small regions ($i=1, 2, 3, \dots, N$). The CP form of the equations is obtained by integrating the integral transport equation [Eq. (2.29)] over the volume of the region j and multiplying both sides by the total cross section $\Sigma_{j,g}$ of region j . These are

$$V_j \Sigma_{j,g} \phi_{j,g} = \sum_i Q_{i,g} V_i P_{i,j,g} \quad 2.30$$

Where,

$$\phi_{j,g} = \frac{1}{V_j} \int_{V_j} \phi_g(\mathbf{r}) d^3 r \quad 2.31$$

$$Q_{i,g} = \sum_h \Sigma_{s0,i,g \leftarrow h} \phi_{i,h} + \frac{\chi_g}{K} \sum_h v \Sigma_{f,h} \phi_{i,h} \quad 2.32$$

$$P_{ij,g} = \frac{1}{4\pi V_i} \int_{V_i} d^3 r' \int_{V_j} d^3 r \Sigma_g(\mathbf{r}) \frac{e^{-\tau_g}}{|\mathbf{r}-\mathbf{r}'|^2} \quad 2.33$$

The collision probability $P_{ij,g}$ is the probability that a neutron born uniformly and isotropically in any of the regions V_i will have its first collision in region V_j . Eq. (2.33) is a six-dimensional

integration that must be carried out numerically. In practice, some of the integrations can be

carried out analytically which depends upon the symmetry of the problem. In the general three-dimensional case, four of the six variables require numerical integration and two can be obtained analytically. Calculation of different collision probability to solve neutron balance equation is discussed in Section [0](#).

The Interface Current Method (J^\pm)

Another method based on solution of the integral transport theory is referred to as the interface current or J^\pm method, which couples only adjacent regions through the interface currents. In this method, fuel assembly or problem domain is divided into a number of regions and equations are written for the flux and out currents of each region in terms of the flux and in currents into the region. This requires calculation of only a few collision probabilities (volume to volume and surface to volume) per region thereby simplifying the solution of the equations and storage requirement of a large number of collision probabilities [61], [70]–[72].

Often a combination of the collision probability and interface current methods is used [70], [73]. The region of interest is divided into a number of macro regions and each macro region is further sub divided into finer meshes. Within a macro region, the meshes are coupled to one another by the collision probabilities P_{ij} whereas the macro regions are coupled to their neighbours through interface currents. This improves the accuracy compared to the J^\pm method and at the same time uses less computing resources than the P_{ij} . The codes CLUB[66], LWRBOX, BOXER3[74] use the combined method.

Suppose a macro region is partitioned into V_i regions $i= 1,2 \dots N_v$ and the boundary surface S is divided into S_m surfaces elements $m = 1,2 \dots N_s$. The collision probability Eq. (2.30) get modified due to an additional term due to the in currents as follows

$$\phi_{i,g} \Sigma_{i,g} V_i = \sum_j Q_{j,g} V_j P_{ji,g} + \sum_m S_m J_{m,g}^{(in)} P_{mi,g} \quad 2.34$$

where,

$\phi_{i,g}$ is the flux in region i in group g

$J_{m,g}^{(in)}$ is the in current at surface m in group g

$$J_{m,g}^{(in)} = \int_{\Omega \cdot N^{(in)} > 0} \int_{S_m} \psi_g^{in}(\mathbf{r}_s, \boldsymbol{\Omega}) (\boldsymbol{\Omega} \cdot \mathbf{N}^{(in)}) d^2 \mathbf{r}_s d\boldsymbol{\Omega} \quad 2.35$$

$J_{m,g}^{(out)}$ is the out current at surface m in group g

$$J_{m,g}^{(out)} = \int_{\Omega \cdot N^{(out)} > 0} \int_{S_m} \psi_g^{out}(\mathbf{r}_s, \boldsymbol{\Omega}) (\boldsymbol{\Omega} \cdot \mathbf{N}^{(out)}) d^2 \mathbf{r}_s d\boldsymbol{\Omega} \quad 2.36$$

$P_{ji,g}$ is the region-to-region collision probabilities in group g

$P_{mi,g}$ is the surface-to-region collision probabilities in group g

$P_{jm,g}$ is the region-to-surface collision probabilities in group g

$P_{m'm,g}$ is the surface-to-surface (escape) collision probabilities in group g

S_m is the area of surface m

$S_{m'}$ is the area of surface m'

Σ_i^g is the transport cross-section in region i in group g

To close the system of equations, another equation is written giving the out currents from the macro region

$$S_m J_{m,g}^{(out)} = \sum_j Q_{j,g} P_{jm,g} + \sum_{m'} S_{m'} J_{m',g}^{(in)} P_{m'm,g} \quad 2.37$$

Eqs. (2.34) and (2.37) are the closed system (since $J_g^{(out)}$ and $J_g^{(in)}$ are essentially the same set of variables for adjacent macro regions) of neutron balance equations in terms of collision probabilities and interface currents. To solve these equations, we require prior knowledge of

the incoming angular flux (current) at both sides of the interface of the cells for the computation of the surface to region and surface-to-surface collision probabilities. A fairly widely used approximation is to assume the angular distribution is constant in the solid angle 2π . This is called the cosine current approximation [62].

More generally, the incoming angular flux can be expanded at each point \mathbf{r}_s of the surface of a macro region in terms of a basis set of functions of the direction variable $\boldsymbol{\Omega}$ in a range of $\boldsymbol{\Omega}$ given by $\boldsymbol{\Omega} \cdot \mathbf{N}^{(in)} > 0$, (where $\mathbf{N}^{(in)}$ is a unit inward normal vector)

$$\psi_g^{in}(\mathbf{r}_s, \boldsymbol{\Omega}) = \frac{1}{4\pi} \sum_n a^{n(in)}(\mathbf{r}_s) \varphi_g^{n(in)}(\boldsymbol{\Omega}, \mathbf{N}^{(in)}) \quad 2.38$$

where, $a^{n(in)}$ are the expansion coefficients and $\varphi_g^{n(in)}(\boldsymbol{\Omega}, \mathbf{N}^{(in)})$ are the linearly independent basis functions satisfying the orthonormality relation as given in Eq. (2.39)

$$\int_{\boldsymbol{\Omega} \cdot \mathbf{N} > 0} \varphi_g^{m(in)}(\boldsymbol{\Omega}, \mathbf{N}) \varphi_g^{n(in)}(\boldsymbol{\Omega}, \mathbf{N}^{(in)}) (\boldsymbol{\Omega} \cdot \mathbf{N}^{(in)}) d\boldsymbol{\Omega} = \pi \delta_{mn} \quad 2.39$$

The expansion coefficients become additional variables and accordingly the set of Eqs. (2.34) and (2.37) get modified. There are as many equations for the outgoing values of $a^{n(out)}$ of the form (2.37) as are the number of terms in the expansion and each of these equations as well as the equation for the flux (2.34) has extra terms corresponding to the coefficients $a^{n(in)}$. The equations form a closed system since, as noted earlier, $a^{n(out)}$ and $a^{n(in)}$ are essentially the same set of variables for adjacent macro regions. The expansion coefficients are commonly assumed to have uniform distribution on along each side of the cell[27]. This assumption reduces the accuracy in comparison to the P_{ij} method.

Calculation of Collision Probabilities

For one-dimensional slab geometry (plate type fuels) no numerical integration is necessary and the collision probabilities can be written in terms of the E_3 (exponential integral

functions[39]. For example, the calculation of various probabilities for slab geometry can be done by the following analytical expressions[75]

$$P_{ii} = \left\{ 1 - \frac{\frac{1}{2} - E_3[-\tau_i]}{\tau_i} \right\} \quad 2.40$$

$$P_{ij} = \frac{1}{2\tau_i} \{ E_3[-\tau_{ij}] - E_3[-(\tau_{ij} + \tau_i)] - E_3[-(\tau_{ij} + \tau_j)] + E_3[-(\tau_{ij} + \tau_i + \tau_j)] \} \quad 2.41$$

$$P_{is} = \frac{1}{2\tau_i} \{ E_3[-\tau_{ij}] - E_3[-(\tau_{ij} + \tau_i)] \} \quad 2.42$$

$$P_{si} = 2 \{ E_3[-\tau_{ij}] - E_3[-(\tau_{ij} + \tau_i)] \} \quad 2.43$$

$$P_{S_1 S_2} = 2E_3[-\tau_{S_1 S_2}] \quad 2.44$$

Most reactors have fuel in the form of long rods. Lattice calculations are therefore carried out in two-dimensional geometries (in which it is assumed that the reactor composition and flux etc. are uniform along a direction parallel to the length of rods fuel rods). For the general two-dimensional geometry that has uniformity in the z direction (along the fuel rod length), integration over the polar angle (or z variable) can be carried out analytically and two-dimensional integrals have to be solved numerically. The expressions for collision probabilities [Eqs. (2.45)- (2.49)] can be obtained by numerical integration over one or two variables with the integrands being written in terms of (Ki_3) Bickley functions

$$Ki_3(x) = \int_0^{\pi/2} \sin^2 \theta \exp(-x/\sin \theta) d\theta$$

$$P_{ii} = \frac{1}{2\pi\Sigma_i V_i} \int dy d\theta \{ \tau_i - Ki_3(0) + Ki_3(-\tau_i) \} \quad 2.45$$

$$P_{ij} = \frac{1}{2\pi\Sigma_i V_i} \int dyd\theta \{Ki_3[-\tau_{ij}] - Ki_3[-(\tau_{ij} + \tau_i)] - Ki_3[-(\tau_{ij} + \tau_j)]\} \quad 2.46$$

$$+ Ki_3[-(\tau_{ij} + \tau_i + \tau_j)]\}$$

$$P_{iS} = \frac{1}{2\pi\Sigma_i V_i} \int dyd\theta \{Ki_3[-\tau_{iS}] - Ki_3[-(\tau_{iS} + \tau_i)]\} \quad 2.47$$

$$P_{Si} = \frac{1}{\pi S} \int dyd\theta \{Ki_3[-\tau_{iS}] - Ki_3[-(\tau_{iS} + \tau_i)]\} \quad 2.48$$

$$P_{S_1 S_2} = \frac{1}{\pi S_1} \int dyd\theta Ki_3[-\tau_{S_1 S_2}] \quad 2.49$$

The lattice calculations are generally performed in one- or two-dimensional lattice cells with full heterogeneity of material distribution at a specific elevation of a reactor assembly. Some examples of two-dimensional codes based on the collision probability method are CLUP77[76] and THERMOGENE[77] while CLUB and LWRBOX are based on a combined collision probability and interface current method.

For the general three-dimensional problem, four types of collision probabilities are required to solve the neutron balance Eqs. (2.34) and (2.37) and they take the following form[61]

$$P_{ii} = \frac{1}{4\pi\Sigma_i V_i} \int dAd\Omega \{\tau_i - 1 + \exp[-\tau_i]\} \quad 2.50$$

$$P_{ij} = \frac{1}{4\pi\Sigma_i V_i} \int dAd\Omega \{\exp[-\tau_{ij}] - \exp[-(\tau_{ij} + \tau_i)] - \exp[-(\tau_{ij} + \tau_j)] + \exp[-(\tau_{ij} + \tau_i + \tau_j)]\} \quad 2.51$$

$$P_{iS} = \frac{1}{4\pi\Sigma_i V_i} \int dAd\Omega \{\exp[-\tau_{iS}] - \exp[-(\tau_{iS} + \tau_i)]\} \quad 2.52$$

$$P_{Si} = \frac{1}{\pi S} \int dAd\Omega \{ \exp[-\tau_{iS}] - \exp[-(\tau_{iS} + \tau_i)] \} \quad 2.53$$

$$P_{S_1 S_2} = \frac{1}{\pi S_1} \int dAd\Omega \exp[-\tau_{S_1 S_2}] \quad 2.54$$

where τ_{ij} , τ_i and τ_j are the optical path lengths between i and j , in i and in j respectively, τ_{iS} is the optical path length between i and S and $\tau_{S_1 S_2}$ is the optical path length between the surfaces S_1 and S_2 . A set of discrete directions and associated weights are chosen (quadrature set) for integration over the angle variables. For each direction corresponding to the angular quadrature, the integration over the area is obtained by constructing a rectangular area grid in a plane perpendicular to the direction and starting a ray from the centre of each such grid element. The area of the grid element (distance in two dimensions) is associated with each ray for the integration over area. The rays are traced across the problem geometry. Intercepts of each of the rays in the meshes, encountered by them, are obtained, which are used to compute the optical path lengths that go into computation of the integrand. The integration is performed by multiplying each of the integrands by the area associated with the ray and the angular quadrature weight and summing over all rays. The integrals are obtained by choosing an angular quadrature set such as the fully symmetric quadrature used in the DS_N method. For two dimensions, there is a single angle and equally spaced or Gaussian quadrature may be used.

Properties of Collision Probabilities

To satisfy the neutron balance equation, calculated region-to-region, region-to-surface, surface-to-region and surface-to-surface collision probabilities must follow the conservation theorem given by [Eq. (2.55)-(2.56)]

$$\sum_j P_{ij} + \sum_m P_{iS_m} = 1 \quad \text{for all } i \quad 2.55$$

$$\sum_j P_{S_m j} + \sum_n P_{S_m S_n} = 1 \quad \text{for all } m \quad 2.56$$

In addition, the collision probabilities follow the reciprocity relation due to symmetry in optical path i.e. $\tau(r, r') = \tau(r', r)$.

$$\Sigma_i V_i P_{ij} = \Sigma_j V_j P_{ji} \quad 2.57$$

$$4\Sigma_i V_i P_{mi} = S_m P_{im} \quad 2.58$$

$$S_m P_{nm} = S_n P_{mn} \quad 2.59$$

2.5.5 Solution of Collision Probability Equations

The solution of multigroup integral transport equation for a lattice cell reduces to evaluation of collision probabilities by numerical integrations, which in turn requires neutron tracking through the system geometry for calculation of neutron track lengths within each of the regions. Next, the problem-specific neutron distribution i.e. multigroup flux and partial currents across the surfaces and fluxes in each region are obtained by solving the set of the algebraic Eqs. (2.34) and (2.37) using the inner-outer power iteration technique [78]. The above procedure yields the flux distribution and eigenvalue. The energy and space dependent flux obtained in the lattice calculations is used as a weighting function to collapse the multi-group cross-sections into a fewer (2-10) energy groups averaged (homogenized cross sections) over the entire lattice cell.

2.6 Fuel Burn-up

The final step of the lattice calculation is to determine the change in fuel composition with time. This is calculated by using the burnup equations, which can be derived by considering the following phenomena during the fuel depletion in a reactor.

1. Depletion of Fissile Nuclides
2. Conversion from Fertile Nuclide to Fissile Nuclide
3. Production of Fission Products
4. Decay
5. Transmutation due to neutron capture

Based on the formation and the destruction processes of the nuclei as given above, the rate of change of concentration of nuclei is given by the following equation [27].

$$\frac{dN_i}{dt} = \sum_j \gamma_{ji} \sigma_{f,j} N_j \phi + \sigma_{c,i-1} N_{i-1} \phi + \sum_k \lambda_{ki} N_k - \sigma_{a,i} N_i \phi - N_i \lambda_i \quad 2.60$$

While the decay constants are inherent properties of the corresponding nuclide, the reaction cross-sections are obtained by averaging them over energy and space using the flux distribution obtained in the lattice calculation. Eq. (2.60) forms a set of the first order differential called decay and transmutation equations or depletion equations. The large and stiff system of coupled depletion equations can be solved using numerical solution methods based on assumption of time independent flux and spectrum distribution throughout the burn-up step and (consequently) constant reaction cross-sections. The burnup time step must be such that this assumption holds good. The one-group cross-sections for different reactions are evaluated by a steady-state neutron transport calculation at the beginning of each step. In literature, there exists several numerical methods to solve the depletion equation e.g. the Euler Method[79], the

Runge–Kutta Method, the Matrix Exponential Method[80], [81], the Matrix Decomposition Method and Bateman Method[82]. The method used in BOXER3 is based on Gear’s method[83]. When the first burnup step is completed, a new set of average cross-sections is computed for the changed flux distribution corresponding to the altered material composition by solving the steady state transport equation (lattice calculation) and this process is repeated for the upcoming burn-up step.

2.7 Monte Carlo Methods for Neutron Transport

Unlike the deterministic methods as discussed in previous Section [2.5](#), the Monte Carlo methods are able to model the exact three-dimensional geometry and use almost no approximations to the actual physics of the system. The only uncertainties are those associated with statistics and errors in user controlled nuclear data input itself. The Monte Carlo methods are numerical ways to solve a deterministic problem by a stochastic approach using random numbers. Therefore, In contrast to the deterministic method for neutron transport, the Monte Carlo methods do not directly deal with any governing physical equation of a macroscopic system rather they infer the results through simulation of all the microscopic interactions in the system [84]. The continuously growing computing power has not only allowed applying the Monte Carlo method to simple problems but also to actual 3D nuclear systems.

In this section, a background detail of different Monte Carlo techniques within the scope of this thesis is discussed. It includes the sampling methods, random number generator, probability density functions, standard deviations, Russian roulette and splitting techniques.

2.7.1 Pseudo Random Numbers and Generators

Random numbers or more precisely pseudo random numbers are real numbers between zero and one representing samples generated independently from a uniform probability distribution function, which is defined below.

$$U(\xi) = \begin{cases} 1, & \text{if } 0 \leq \xi \leq 1; \\ 0, & \text{otherwise.} \end{cases} \quad 2.61$$

The random numbers based on computer algorithms are reproducible sequences of finite size. Therefore, these numbers are not truly random and are referred to as pseudo random numbers. Nevertheless, numbers generated by good generators should appear to be statistically independent, that is not correlated with one another; the sequence of generated numbers should be fast to generate and be indistinguishable from a real random sequence, and should have long period of repetition [85]. The most commonly used random number generators are the linear congruential generators (LCRNG). The LCRNG employs a large integer, M called the modulus, to generate a sequence of integers X_n by recursion relation

$$X_{n+1} = \text{mod}(aX_n + c, M) \quad 2.62$$

In this equation a is a “magic” multiplier and c is an odd number. This sequence of random numbers is normalised to generate the sequence ξ_n between $[0, 1]$ as follows

$$\xi_n = X_n/M \quad 2.63$$

To start the sequence, the quantity X_0 is required to be set by the user. The maximum cycle length of the LCRNG depends on the computer word length. For example, the largest period for a 32-bit machine in single precision is $2^{32} - 1 = 2147483647$. The actual cycle length depends upon the choice of the parameters and could be much smaller and hence the parameters

need to be chosen carefully. The choice of $a = 2^7 = 16801$ and $c = 0$ for a 32-bit machine is recommended by Park and Miller [85].

2.7.2 Sampling Methods

The challenging task in the Monte Carlo calculations is to generate realizations of random variables X_j that are distributed according to a given probability density function $f(x)$. For a probability distribution function $f(x)$ defined on the interval $a \leq x < b$, the Eq. (2.64), given below, determines x uniquely as a function of ξ , which is uniformly distributed on $0 < \xi < 1$.

$$\xi = F(x) = \int_0^x f(x') dx' \quad 2.64$$

It is then easy to show that the random variable x , takes a value in between x and $x + dx$ with probability $f(x)dx$ [86]. Thus, all that is needed to obtain a random variable that is distributed with a probability distribution function $f(x)$ is to draw a random number ξ from the uniform distribution between 0 and 1 and to solve Eq. (2.64) for x . The basic principles of CDF inversion are described using simple examples relevant to the particle transport. The distance to the next collision of a particle in a homogeneous medium having total macroscopic cross-section Σ_t is governed by the well-known exponential distribution function. The probability that a particle makes its first collision between x and $x + dx$ along the direction of flight is written as

$$f(x)dx = \Sigma_t e^{-x\Sigma_t} dx \quad 2.65$$

The PDF is given by

$$f(x) = \Sigma_t e^{-x\Sigma_t} \quad 2.66$$

The corresponding CDF of $f(x)$ is given by

$$F(x) = \int_0^x \Sigma_t e^{-x' \Sigma_t} dx' = (1 - e^{-x \Sigma_t}) \quad 2.67$$

The particle distance to the next collision point can be sampled by equating a random number ξ to the CDF given in Eq. (2.67) and solving for x i.e.

$$x = \frac{-\ln(1 - \xi)}{\Sigma_t} = \frac{-\ln(\xi)}{\Sigma_t} \quad 2.68$$

The identity result in Eq. (2.68) is because both $(1 - \xi)$ and ξ have uniform distribution over $[0, 1]$. This is how exactly the inversion method of sampling for a given PDF works to compute the samples. There exist alternative methods of sampling, such as the rejection technique and numerical evaluation, beneficial particularly in the cases where direct inversion of $F(x)$ is difficult to obtain by integration or PDF is given in form of numerical data [57].

In second example, let us sample the direction of particles emitted isotropically from the point of emission. This is best represented in the spherical geometry and the probability distribution function is given as

$$f(\theta, \phi) d\theta d\phi = \frac{d\Omega}{4\pi} \quad 2.69$$

$$f(\theta, \phi) d\theta d\phi = \frac{\sin \theta d\theta d\phi}{4\pi} = \frac{\sin \theta d\theta * d\phi}{2 * 2\pi} = f_1(\theta) d\theta * f_2(\phi) d\phi \quad 2.70$$

Where, θ is the polar angle and ϕ is the azimuthal angle

Here, the independent variables θ and ϕ can be sampled independently using CDF of respective distributions functions $f_1(\theta)$ and $f_2(\phi)$ as follows.

$$f_1(\theta) d\theta = \frac{\sin \theta d\theta}{2} \quad 2.71$$

Thus, CDF of $f_1(\theta)$ to sample θ is

$$\xi_1 = \int_0^\theta f_1(\theta) d\theta = \int_0^\theta \frac{\sin \theta}{2} d\theta = \frac{(\cos \theta + 1)}{2} \quad 2.72$$

$$\theta = \cos^{-1}(2\xi_1 - 1) \quad \text{or} \quad \mu = 2\xi_1 - 1 \quad 2.73$$

Similarly, the CDF of $f_2(\phi)$ to sample ϕ is

$$\phi = 2\pi\xi_2 \quad 2.74$$

The direction cosines of particles can easily be obtained using simple relations as follows- where, [$\mu = \cos(\theta)$]

$$u = \frac{x}{r} = \frac{r \sin\theta \cos\phi}{r} = \sqrt{1 - \mu^2} \cos\phi \quad 2.75$$

$$v = \frac{y}{r} = \frac{r \sin\theta \sin\phi}{r} = \sqrt{1 - \mu^2} \sin\phi \quad 2.76$$

$$w = \frac{z}{r} = \frac{r \cos\theta}{r} = \mu \quad 2.77$$

2.7.3 Neutron Tracking in Finite Geometry

In Monte Carlo calculations, neutrons are followed from points of birth to death either by way of absorption or escape out of system. This is termed as a neutron history.

All possible physical processes need to be precisely modeled throughout the neutron's life. In fact, a neutron life begins with its emission from the source. Thus, Monte Carlo simulation starts with random sampling of position co-ordinates (x_o, y_o, z_o) , direction cosines (u, v, w) and energy (E) of particles emitted from the source. In case of fission source, we prepare and store a cumulative distribution of the fission spectrum. For $c_{g-1} < \xi < c_g$, the sampled energy group is g . The next step is to calculate the distance to the next collision in the direction of its flight using Eq. (2.). This is compared with the distance to the surface of the region to determine whether the neutron collides in the region or crosses the surface. Two possibilities arise. In the first case, if the collision site is in the same region as the starting point, the particle position is

moved to the point of collision. Suppose, if λ is the distance to the point of collision, then co-ordinates of the collision point are obtained using Eqs. (2.78)-(2.80) given below

$$x = x_o + \lambda u \quad 2.78$$

$$y = y_o + \lambda v \quad 2.79$$

$$z = z_o + \lambda w \quad 2.80$$

The second case is that the particle crosses the boundary of starting region. The particle position is moved to the crossing point at the boundary surface. The macroscopic cross-section of the new region is selected to sample the distance to the next collision and the procedure is repeated until the particle collides somewhere within the bounding surface of the system or leaks out from the system. If the neutron leaks from the system, neutron history is simply terminated.

At the point of collision, the physics of interaction between the particle and constituent nuclide of the material are processed to identify the nuclear reaction type. The total cross-section is simply a sum of fission, capture and scattering cross-sections.

$$\Sigma_t = \Sigma_c + \Sigma_f + \Sigma_s \quad 2.81$$

The probability of reaction types i is the ratio of cross-section of reaction i to total cross-section i.e. $P_i = \frac{\Sigma_i}{\Sigma_t}$. Discrete sampling procedure is adopted to know the reaction type in a collision by comparing a random number ξ with P_i . For example, if $\frac{\Sigma_c}{\Sigma_t} > \xi$, then collision results in capture else if $\frac{\Sigma_f + \Sigma_c}{\Sigma_t} > \xi > \frac{\Sigma_c}{\Sigma_t}$ then it results in fission else it results in scattering reaction. Neutron capture or fission simply leads to the termination of the neutron history in case of **analog** Monte Carlo approach. The direction and energy after scattering reaction are sampled using the appropriate scattering law. In case of fission, the co-ordinates of the fission site and number of

neutrons produced in fission are recorded and are used as starting points for the source neutrons to be tracked in the next generation.

In **non-analog** Monte Carlo approach, a statistical weight is assigned to each neutron. If the assigned statistical weight of a neutron is greater than unity, then this neutron represents the contribution of several particles. At a collision site for the scattering reaction, the weight of a particle is reduced to $W' = W(1 - \frac{\Sigma_a}{\Sigma_t})$ and treated as having been scattered with this reduced weight. Here W and W' represents the neutron weights before and after the collision. If the weight W' of the particle is below a preset value W_l , the particle is killed (Russian Roulette) with probability $1 - W'/W_u$ or continued with a higher weight W_u with probability W'/W_u , where W_u is a preset higher weight. Typically, $W_u = 0.5$, and $W_l = 0.25$. On scattering, the particle may go to another group. The probability to which group it goes depends upon its scattering cross-section into that group. $P_{g \rightarrow g'} = \Sigma_{g \rightarrow g'} / \sum_{g'} \Sigma_{g'}$. Like in the case of the fission spectrum, the group to which the particle goes is sample by creating a cumulative distribution. The direction of the scattered particle is sampled as per the scattering law. The history is terminated if the particle leaves the system volume (in case of lattice cell calculations this is not possible) or by Russian roulette.

2.7.4 Statistical Estimators

The parameter of interest has to be recorded during the neuron history to calculate the results for a physical event. The process of scoring for a parameter of interest is referred to as tallying or scoring. The tallies can be combined in different ways to form statistical estimates of the physical quantities, generally called an estimator. For example, the collision, the absorption and the track length estimators are commonly used to estimate the reactor multiplication factor (k_{eff}). The power iteration procedure is adopted in all Monte Carlo

codes for criticality calculations. To apply power iteration method, the successive neutron generations are simulated, where each generation (also called cycle) contains a certain number of neutrons (N) and this is called a batch. To obtain the collision estimator $k_{eff}^{(c)}$, during the course of a cycle, at each collision in a fuel, we tally this quantity using Eq. (2.82). This results in the k_{eff} of a single cycle.

$$k_{eff}^{(c)} = k_{eff}^{(c)} + \frac{Wv\Sigma_f}{N\Sigma_t} \quad 2.82$$

The number of active neutron generations (i.e. those for which tallying is carried out) becomes equal to the number of batches M . Thus, the final k_{eff} is calculated by taking mean of k_{eff} obtained in each cycle. The absorption estimate can be obtained by tallying as follows

$$k_{eff}^{(a)} = k_{eff}^{(a)} + \frac{(W - W')v\Sigma_{fg}}{N\Sigma_{ag}} \quad 2.83$$

To obtain the track estimator $k_{eff}^{(t)}$, during the course of a cycle, for each track length (L) between consecutive collisions in the fuel, we tally the quantity

$$k_{eff}^{(TL)} = k_{eff}^{(TL)} + \frac{WLv\Sigma_{fg}}{N} \quad 2.84$$

The quantities of interest, like k_{eff} , neutron flux, reaction rates, etc., must be tallied with a converged fission source. Fission source can be converged by performing Monte Carlo simulations over few inactive cycles before starting the active cycles.

2.7.5 Statistical Error

The results in MC are obtained by averaging the scored values of physical quantity of interest for many particle histories. Therefore, it becomes important to study the variation of statistical error, associated with estimated expectation value of random variable corresponding to a physical event, as function of neutron histories. Suppose X is a random variable and the true mean value $\mu = E[X]$ is approximated with mean (using Eq. (2.85)) of N

samples $x_1, x_2, x_3, \dots, x_N$ obtained independently and randomly from identical probability distribution function during the course neutron history.

$$\tilde{x} = \frac{1}{N} \sum_{i=1}^N x_i \quad 2.85$$

Where x_i is the value of X selected from $f(x)$ representing the contribution of the i th history and N is the number of histories used. Thus, in the Monte Carlo calculation, the contribution x_i to the physical quantity, e.g. number of collisions or track length for flux, is scored due to each history in order to calculate the estimated or sample mean \hat{x} at the end of each calculation [57]. The law of large numbers suggests that as number of histories N tends to infinity, then the sample mean approaches the true mean in probabilistic sense. To measure the spread of x about its mean μ , expectation value of the second moment of x is introduced and it is called variance σ of x . The population variance associated with the distribution of the x_i is approximated by the sample estimate as given by Eq. (2.86)[87].

$$\sigma^2 = \frac{1}{(N-1)} \sum_{i=1}^N (x_i - \tilde{x})^2 = \frac{N}{(N-1)} \left(\frac{1}{N} \sum_{i=1}^N x_i^2 - \tilde{x}^2 \right) \quad 2.86$$

The variance of the sample mean is then estimated by Eq. (2.87)

$$\sigma_{\tilde{x}}^2 = \frac{\sigma^2}{N} \quad 2.87$$

The square root of the variance $\sigma_{\tilde{x}}$ is called the standard deviation of the population of scores. The mean value of some random variable is referred to as the result of the simulation and the standard deviation is a measure of statistical accuracy, or precision.

2.8 Review of Existing Methods Used in HTRs Calculations

The unusual design of fuel elements poses additional challenges with regard to studying neutron transport in HTRs compared to that in traditional reactors. The primary reason for this is the nature of the fuel in HTRs, which consists of a large number of tiny fuel particles dispersed randomly in a graphite matrix. It might appear that such a dispersion of fine particles may be treated as homogeneous, but that is not the case for all energies. For most of the neutron energies where cross-section is not very high, the neutron mean free path is much longer than the particle size. In this case, the random TRISO dispersion in graphite may be treated as a homogeneous medium. However, at the resonances of the major nuclides, namely, ^{238}U or ^{232}Th , the neutron mean free path is comparable to the size of the fuel kernel. This necessitates treatment of the dispersion as a heterogeneous medium around the resonance energies.

In addition to the treatment of resonances for obtaining group cross-sections in the resonance groups, the double-heterogeneity problem can occur in the subsequent multigroup calculations, particularly in the thermal region under certain situations. When the fuel is a few percent enriched uranium or Th mixed with some low enriched uranium or ^{233}U , the thermal macroscopic cross-section of the fuel is not large and hence the mean free path is long compared to the fuel kernel size and the dispersion may be considered to be a homogeneous medium. However, in reactors designed to burn Pu, the fuel contains only PuO_2 . Such a fuel has a large macroscopic cross-section in the thermal groups, particularly around the 1.0 and 0.3 eV resonances of Pu, and hence the mean free path in thermal groups around the low-lying resonances is shorter than or comparable to the size of the fuel kernel. For such fuels, homogenization of the fuel zone is not permissible. It is necessary to solve the multigroup

transport equation for lattice calculations in a doubly heterogeneous random medium in such situations.

There have been many attempts made to resolve these two issues in the doubly heterogeneous (micro and macro levels in this case) HTR medium, namely, that of calculating the Dancoff factor for obtaining resonance group cross-sections and for subsequent solution of the multigroup transport equation. In the following paragraphs, we briefly review these efforts.

2.8.1 Calculation of Dancoff Factors in HTR

One of the earliest attempts at obtaining the analytical expression for the Dancoff factor in HTRs is due to Lane et al. [88], Bende et al.[89] and Kloosterman and Ougouag [90]. They used simple arguments to calculate the Dancoff factor based on analytical expressions for the first flight escape probability from spheres. Another approach to the problem is through an estimation of the chord length distribution based on analytical or numerical considerations[91]. A third approach involves a detailed Monte Carlo simulation of a random dispersion of fuel particles in the graphite matrix followed by tracking neutron trajectories beginning at the surface of a fuel kernel up to the point of its entry in another kernel[92]. The Monte Carlo method based computer codes Dancoff-MC[93], PEBDAN and INTRAPEB[94] can simulate the random distribution of TRISO particles in the fuel zone of a pebble to calculate average Dancoff factors. The Monte Carlo approaches are important as they help in validating the simpler analytical models based on escape probabilities or chord length distributions.

2.8.2 Deterministic Approach to HTRs

With regard to the solution of the multigroup transport equation for lattice calculations in the doubly heterogeneous medium, one of the earliest approaches is based upon calculating equivalent cross-sections for the stochastic medium formed by distribution of the fuel lumps in

the graphite matrix. This method computes the spatial self-shielding factor using conservation of collision probabilities[95]–[97]. Hebert developed another type of method by obtaining the expressions of the collision probabilities at lattice cell level using the collision probabilities defined at micro- and macro-level geometries[98], [99]. These collision probabilities are based on the assumption that the neutron angular flux entering or escaping the fuel lump is uniform and isotropic. Sanchez and Pomraning developed the method of renewal theory for solution of the transport equation in a random medium [100], [101]. These two models are successfully implemented in the lattice codes DRAGON[102], APOLLO-1 and APOLLO-2[98]. The code SCALE [103] follows a different method for double-heterogeneity treatment and resembles the pin cell and assembly-level calculations used in earlier days for LWRs [41]. The calculation is first performed at the micro (TRISO particle surrounded by graphite layer) level followed by another calculation at the macro level (pebble cell). In the micro-level calculation, resonance shielding calculation is performed based upon an externally calculated Dancoff factor, and it is followed by a solution of the transport equation for obtaining flux disadvantage factors using a white boundary condition. These fluxes are then used to compute the flux-weighted cross-sections, i.e., shielded cross-sections. These weighted cross-sections are passed on to the CENTRM transport solution for the macro-level geometry formed by fuel zone (having weighted cross- sections), graphite layer, and coolant. Similar to the SCALE code, WIMS9 also generates homogenized total cross-sections that have the same escape probability as the heterogeneous particle by solving the collision probabilities for the micro region (TRISO particle surrounded by graphite layer) [104], [105]. Subsequently, collision probabilities are derived for the various macro regions of the pebble using the homogenized cross-sections in the fuel zone. Then the micro and macro-region collision probabilities are combined to form a

full set of collision probabilities for the complete pebble to obtain lattice cell fluxes and reaction rates.

2.8.3 Monte Carlo Approach to HTRs

Monte Carlo based computer codes, with general geometry modelling capability, can handle very complex geometries that may arise in a reactor. MCNP[106], TRIPOLI[107] and MONK[108] are examples of such computer codes developed over many decades to perform the neutronics simulations of various reactor types including HTRs. These codes use the repeated lattice features to approximate the stochastic media formed by random distribution of pebble bed in core and TRISO in pebble. Use of repeated lattice results in clipping of kernels at fuel zone and graphite layer interface and this is a source of error as fuel mass and number of TRISO may not be preserved in this model [109]. However, these codes are continuously being improved to include geometries that are more complex. For example, latter versions of MCNP allow jiggling of the TRISO particles within the cubical cell of the lattice structure to replicate the randomness. Another approach is to employ explicit packing of randomly distributed TRISO particles. Examples of recently developed codes having such a feature are SERPENT[110], RMC[111] and OpenMC[112]. However, treatment of heterogeneous system with randomly distributed TRISO particles using the direct Monte Carlo method poses difficulties both in modeling billions of TRISO particles and in the resulting computing cost. In addition, this method uses a single realization of a random distribution of spheres in a region. This approach is computationally very costly exercise due to calculation of distance to next region interface in stochastic mixture containing a large number of surfaces of TRISO particles. The computational efficiency can be improved by adopting Monte Carlo method based on stochastic sampling of fuel particles locations using a spatial probability distribution.

Analytical distribution or packing simulation code generated distribution can be used to sample the random positions[113], [114]. Another class of Monte Carlo approaches rely on defining equivalent homogenized medium obtained during a random walk process for the heterogeneous random media[95], [115].

2.9 Thesis Objective

The goal of the research described in the thesis is the development of a new methodology as well as computational tools for HTR analysis. This includes the development of new theoretical models, algorithms and computer codes based on the models, and analysis of benchmark problems.

The first of these is the development of a new MC algorithm to realize the random distribution of fuel particles in the HTR lattice cell and pebbles in the HTR core and a fast scheme to track neutrons to compute the Dancoff factors needed in the resonance self-shielding calculations. This part of the work is discussed in [Chapter 3](#).

Application of the Dancoff factors, generated by the method developed in [Chapter 3](#), to the HTR lattice cell calculations is discussed in [Chapter 4](#). The results suggest that a more detailed treatment of the double heterogeneity in the solution of the transport equation during the lattice calculations, particularly in the thermal region of high Pu content fuels, is also necessary. A simple heuristic procedure for this is developed in [Chapter 4](#).

This is followed by the development of a rigorous theoretical method for solving the neutron transport equation in the random fuel particle dispersion by an exact evaluation of the collision probabilities (CPs) in various regions of the HTR lattice cell. The method is incorporated in the CP code BOXER3. This is discussed in [Chapter 5](#).

The method developed for exact evaluation of CPs is applied to the development of an algorithm for providing a solution by the MC method as well. To prove the validity of the proposed method, a multi-region, multigroup MC code (PebMC) is developed to simulate the spherical lattice cell of a pebble bed HTR. This is discussed in [Chapter 6](#).

In [Chapter 7](#), we present our conclusions and scope for further work.

Chapter 3 **STOCHASTIC LOADING IN THE HTR FUEL ELEMENTS: Dancoff factor calculation in the fuel pebble and compact**

In this chapter, a new method for generating a random distribution of TRISO particles in the fuel zone of a pebble or fuel compact is discussed. Dancoff factor calculations, in the random dispersion so generated, are carried out using the Monte Carlo method. The results of these calculations are compared with reference values.

3.1 Introduction

For the self-shielded resonance group cross-section calculations, the WIMS formalism uses the equivalence principle approach as discussed in [Chapter 2](#). The equivalence principle is deducible whenever the escape probability can be approximated in the form of a rational expression. For isolated lumps, Wigner's rational approximation or one of the improved approximations for P_{esc} proposed by Bell et al.[116], Kelber et.al [117], or Levine [118] may be used. For non-isolated fuel lumps such as fuel rod clusters, closely spaced fuel rods arranged in a lattice, or TRISO particle dispersions used in high temperature reactors (HTRs), the rational approximation needs to be corrected by applying the Dancoff factor[119]. In the context of HTRs, the Dancoff factor is defined as the probability that a neutron escaping a fuel kernel will enter another fuel kernel, without any collision in the moderator. An accurate estimation of the Dancoff factor is an important part of any lattice calculation.

The spacing between different units of the fuel (i.e. pebbles and compacts) is also such that neutrons from one unit easily travel to another unit. Hence, the Dancoff factor in HTRs is usually split into two factors. One factor, called the intra-pebble or intra-compact Dancoff factor, accounts for the probability that a neutron leaving a fuel kernel enters another kernel in same fuel element (pebble or compact), without having any collision in the moderator. The second factor, called the inter-pebble or inter-compact Dancoff factor, accounts for the probability that a neutron emerging from a fuel kernel enters a fuel kernel located in another fuel element (pebble or compact), without any collision in the moderator [89], [90], [120], [121]. These two factors together account for the double heterogeneity and constitute a significant correction to the escape probability P_{esc} from a fuel kernel [122].

There have been many attempts made to resolve the issue of the doubly heterogeneous (micro and macro levels in this case) HTR medium viz. that of calculating the Dancoff factor for obtaining resonance group cross-sections and for subsequent solution of the multigroup transport equation. In the following paragraphs we briefly review these efforts.

One of the earliest attempt at obtaining the analytical expressions for the Dancoff factor in HTRs is due to Lane et al. [88], Bende *et al* [89] and Kloosterman and Ougouag[90]. They used simple arguments to calculate the Dancoff factor based on analytical expressions for the first flight escape probability from spheres. Another approach to the problem is through an estimation of the chord length distribution, based on analytical or numerical considerations [91], [120]. A third approach involves a detailed Monte Carlo simulation of a random dispersion of fuel particles in the graphite matrix [92] followed by tracking neutron trajectories beginning at the surface of a fuel kernel up to the point of entry in another kernel. The Monte Carlo approaches are important as they help in validating the simpler analytical models based on escape probabilities or chord length distributions. However, the Monte Carlo method

requires realization of random distribution of the fuel kernels in the fuel zone followed by neutron tracking to compute the Dancoff factors.

A number of different algorithms have been used to generate randomly distributed spheres. These may be classified as geometry based models [123] (also called synthetic techniques) or dynamics-based models [124]–[126]. In the geometry-based models, spheres are randomly distributed in a region with the condition that there is no overlap between two spheres. The Random Sequential Addition (RSA) [127], modified Fast RSA method [128], Monte Carlo rejection method [94] and method of removing overlaps [129] are examples of geometry based methods. Since the RSA method is based on a sequential addition and rejection technique, the maximum volume packing fraction that can be produced with this algorithm is only 38% [130]. On the other hand, the dynamics-based models move the spheres around in the medium under realistic contact forces. This motion causes relocation of the spheres and removes any overlap between two spheres that may have been initially present. The recently developed quasi-dynamics method (QDM) [124], [126] is an example of dynamics-based models and these methods are mostly not used to pack the TRISO in pebbles.

In this chapter, a new method, called the cyclic randomization method (CLR), for generating a random distribution of TRISO particles in the fuel zone of a pebble or fuel compact is discussed. Dancoff factor calculations in the random dispersion so generated are carried out using the Monte Carlo method. The results of these calculations are compared with reference values. The chapter is organized as follows: In Section [3.2](#), we discuss methods to generate the randomly distributed particles in different geometries. It includes development of the fast RSA and the CLR methods. Section [3.3](#) presents a Monte Carlo method to calculate Dancoff factors in the random media realised by the fast RSA or CLR methods. In Section [3.4](#), the Dancoff factors, so computed, are compared with reference results at several packing fraction of TRISO

in finite and infinite geometries. Section [3.5](#) summarizes the chapter and presents the main conclusions.

3.2 Stochastic Loading Schemes

In this section, we briefly describe the CLR algorithm, developed in the present work, for simulating a random distribution of TRISO fuel particles in graphite. The CLR method is found to be computationally efficient for higher volume packing fractions of TRISO particles than the fast RSA method. The latter is based on a sequential addition and rejection process and becomes very slow above 35% packing which therefore also is the practical limit on the maximum packing fraction that can be achieved using this algorithm.

3.2.1 The RSA and modified (fast) RSA methods and its limitations

The original Random Sequential Addition (RSA) method [127] consists of adding spheres randomly in the region of interest and checking whether the added sphere overlaps any of the other spheres. This has two problems. The first is that as the number of spheres added increases, the number of checks that are required to be performed also increases and hence the program becomes rather slow. The second is that since spheres are added at random, a large amount of vacant space is left in between that cannot accommodate new spheres and hence beyond a packing fraction of about 38%, further addition of spheres is not possible.

The first problem was resolved with the development of a faster algorithm by Brown[128]. This algorithm checks for overlap with neighboring spheres, since only such spheres are likely to overlap. This is done by introducing a rectangular mesh and recording the three mesh indices in which the coordinates of the centre of the added sphere fall. The neighboring meshes are easily located and the only checks that are required are: (a) whether

any sphere is present in the neighboring meshes and (b) whether it overlaps the newly introduced sphere. This cuts the computing time from being $\mathcal{O}(N^2)$ to $\mathcal{O}(N)$.

The second problem is however inherent to the method and constitutes a major limitation. This is easily seen in one dimension. As the spheres are added, some of them may be spaced from their neighbors by less than a sphere diameter. This precludes the possibility of another sphere coming in between. In one dimension, the maximum random packing fraction is about 74%. The situation is worse in two and three dimensions as the amount of space, in the form of gaps that cannot be occupied by newly added spheres, becomes larger and the packing fraction falls to 54% and 38% respectively. This problem is avoided in the CLR method described in the following Section [3.2.2](#).

3.2.2 The Cyclic Lattice Randomization Method

To overcome the limitations of the RSA and fast RSA method, a new geometrical packing method based on Monte Carlo is developed which is named as cyclic lattice randomization method. In this method, a number (N) of spherical TRISO particles are first arranged in a lattice structure, (like Body Centered Cubic and Face Centered Cubic etc.), covering the region of interest. The lattice arrangement is then randomized by the following procedure.

All the particles placed in the region of interest are labeled in some serial order by means of a positive integer i ($i = 1, N$). The randomization operation is carried out on each of the spheres according to this serial ordering i.e. the spheres are selected one by one in this order and the randomization operation carried out on each one of them. Each randomization trial involves the following two steps.

(i) In the first step, the coordinates (x, y, z) of the centre of the selected sphere are updated using Eq. (3.1)

$$\begin{aligned}x_{new} &= x + d(2\zeta_1 - 1) \\y_{new} &= y + d(2\zeta_2 - 1) \\z_{new} &= z + d(2\zeta_3 - 1)\end{aligned}\tag{3.1}$$

Where,

$$d = D_t \left[\frac{1}{\sqrt{2}} \left(\sqrt[3]{\frac{16\pi}{3p_f}} \right) - 2 \right]\tag{3.2}$$

is the nearest neighbor separation between spheres in the lattice and is chosen as the maximum distance by which a sphere may be moved in one operation, and D_t is the diameter of a TRISO particle. p_f is the (targeted) volumetric packing fraction, and $\zeta_1, \zeta_2, \zeta_3$ are three independent random numbers.

(ii) In the second step, a check is performed on the sphere so moved, with its centre now located at $(x_{new}, y_{new}, z_{new})$, for any overlap with its neighboring spheres. If there is an overlap, the new coordinates are rejected and the particle continues to remain at the old position (x, y, z) . Else (if it does not overlap), the new co-ordinates of the centre $(x_{new}, y_{new}, z_{new})$ are accepted and the old co-ordinates of the centre (x, y, z) are replaced by the new ones.

We refer to the above two steps as a trial. Once these two steps have been repeated for all the spheres in the region of interest, we say that one cycle of randomization is completed. Several such cycles may have to be carried out to generate the required stochastic distribution of TRISO particles in the region of interest. The Face Centered Cubic (FCC) lattice structure of TRISO particles is shown in [Figure 3-1\(a\)](#) and corresponding randomized distribution

obtained by using the CLR method is shown in [Figure 3-1\(b\)](#). It may be mentioned that the method is very similar to the Metropolis algorithm [131] used in equilibrium statistical mechanics for generating the Gibbs ensemble. Since overlap is not permitted the method is equivalent to treating a hard sphere gas.

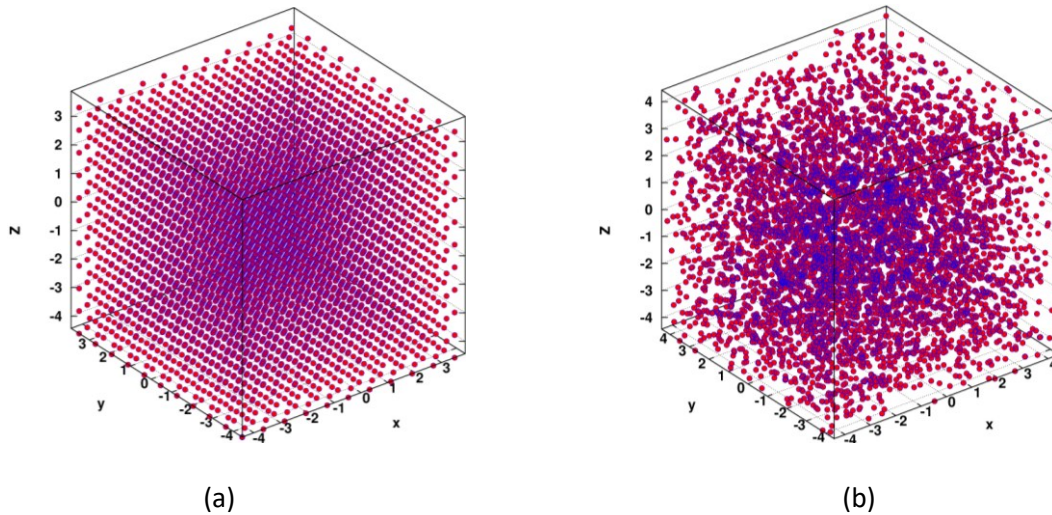


Figure 3-1 TRISO particles arranged in a FCC lattice (a) and (b) after randomisation of the lattice structure using the CLR method.

The maximum packing density that can be achieved using the CLR method is only limited by the theoretical packing density of the initial lattice structure considered (for subsequent randomization). Therefore, if the FCC lattice structure is considered for randomisation, the CLR method would be able to generate the stochastic medium with packing density up to 74% of the space filled with spheres.

3.3 Dancoff Factor Calculation

The Dancoff factor C that represents the probability of neutrons leaving the surface of a fuel particle reaching successfully another fuel kernel without colliding in the moderator contributes to intra-pebble or compact Dancoff factor and it is calculated by using Eq. (3.3).

$$C = \frac{\sum_{N_C} \exp(-\Sigma_M d)}{N} \quad 3.3$$

Where,

d – Track length of the neutron from emission to entering another kernel

Σ_M – Total macroscopic cross-section of the moderator

N – Total number of neutrons tracked

N_C – Total number of neutrons that successfully reach another fuel kernel without colliding with the moderator nuclei

If the neutron path does not intersect any other kernel within the same finite stochastic region, but intersects with a kernel of a neighboring finite stochastic region, then it contributes to the inter-pebble or inter compact Dancoff factor.

3.3.1 Monte Carlo Tracking

To compute the distance between the point of origin and the first point of intersection of the neutron path with another fuel kernel (d), the neutron is tracked using the Monte Carlo sampling methods. The point of emission (x, y, z) is uniformly sampled on the surface of randomly selected fuel kernel of radius r and its co-ordinates are obtained using Eq. (3.4)

$$\begin{aligned} x &= x_0 + r \sin \theta \cos \varphi \\ y &= y_0 + r \sin \theta \sin \varphi \end{aligned} \quad 3.4$$

$$z = z_0 + r \cos \theta$$

where, (x_0, y_0, z_0) is the centre of the selected sphere and $\varphi = 2\pi\zeta_1$ and $\theta = \cos^{-1}(2\zeta_2 - 1)$ are the azimuthal and polar angles respectively, and ζ_1 and ζ_2 are random numbers uniformly distributed over interval $[0, 1]$.

After the point of emission of the neutron on the surface of a fuel kernel has been selected, the direction is determined by sampling for outgoing directions from a cosine current distribution [91], [94], [120]. C is determined by obtaining the average of the quantity $\exp(-\tau)$ where τ is the optical path length of the track in the moderator. A sufficiently large number of neutron histories are considered to obtain an accurate estimate of the Dancoff factor (with small standard deviation). The tracking is rather time consuming as it requires checking for the intersection of each neutron trajectory with a very large number of spherical surfaces corresponding to each of the fuel kernels. A nearest neighbor search procedure has been devised to determine the next possible fuel particle likely to be intersected that reduces the computing effort by a large factor [92]. This is achieved by introducing a rectangular mesh of cells and advancing the neutron position from one cell to the neighboring cell and checking for intersection with spheres lying within a close neighborhood of the cell.

For calculating the infinite medium Dancoff factor, one must consider a finite region such as a cube and impose boundary conditions like periodic or reflective. For a finite medium, such as a pebble or compact, the tracking is discontinued once the track leaves the region of interest. For a distribution of pebbles or compacts as in a reactor, in case the neutron path does not intersect any other kernel within the same pebble or compact, but intersects with a kernel of a neighboring pebble or compact, it contributes to the inter-pebble (or inter-compact) Dancoff factor.

3.4 Comparison with Reference Results

In this section, results of Dancoff factor calculations for infinite and finite media made up of a stochastic distribution of TRISO particles, as realized by the CLR and RSA methods, are discussed. We also present comparisons of our results with the reference Monte Carlo results [91], [120]. For the benchmarking purpose, the TRISO particle geometry used here is identical to that of NGNP Point Design[131] and the macroscopic cross-section of graphite is taken to be the same as the one used by Liang *et. al*[92], (obtained from the BNL website, <http://www.nndc.bnl.gov/exfor/endl.htm>). The fuel kernel radius is 0.0175cm and the coating thickness is 0.039cm. The total macroscopic cross-section of graphite is 0.4137cm^{-1} . This choice of values of the parameters is decided by the fact that the reference Monte Carlo results, against which our results are compared, are available for this set of parameters.

3.4.1 Infinite Medium Dancoff Factor

To mimic an infinite medium, a finite cubical region is used together with periodic boundary conditions. A comparison of our results with the reference Monte Carlo values can be seen in [Figure 3-2](#) . The average relative deviations of the CLR and RSA from the reference values are 0.17% and 0.34% respectively.

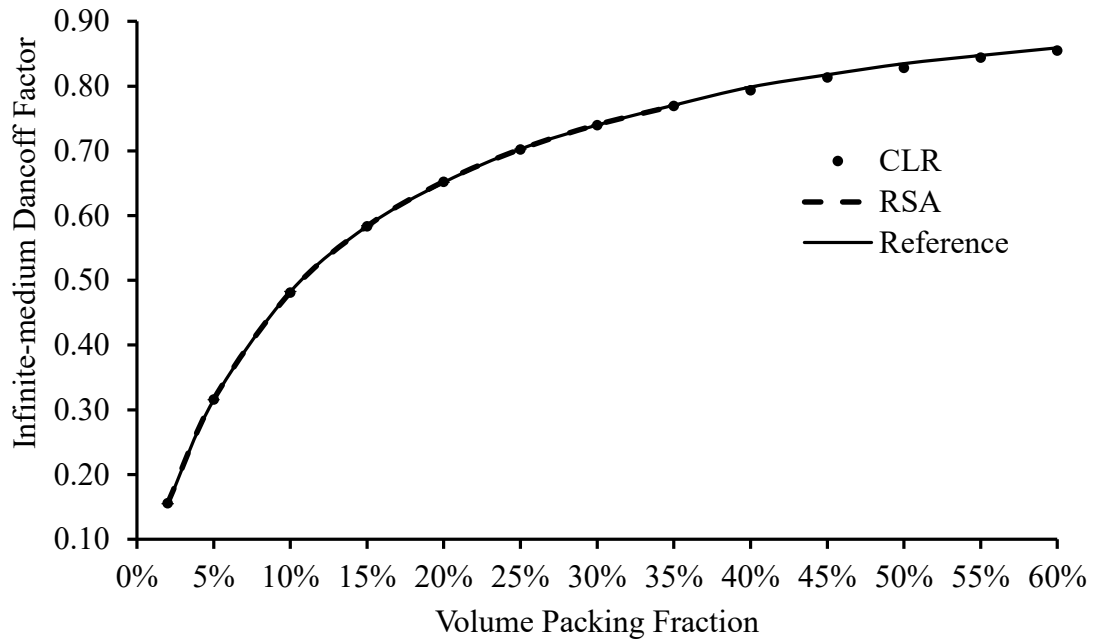


Figure 3-2 Variation of the infinite-medium Dancoff Factor with packing fraction:
comparison between various methods

To compute the intra-compact Dancoff factor, for an infinite cylindrical pin of radius R_c 0.6225cm we have taken the height to diameter ratio H/D equal to 200. The results of Dancoff factors obtained by the CLR and RSA methods for an infinite cylinder are compared with the reference Monte Carlo results in [Figure 3-2](#). The average relative deviations of the CLR and RSA from the reference values for infinite cylinder are 0.38%, 0.51% respectively.

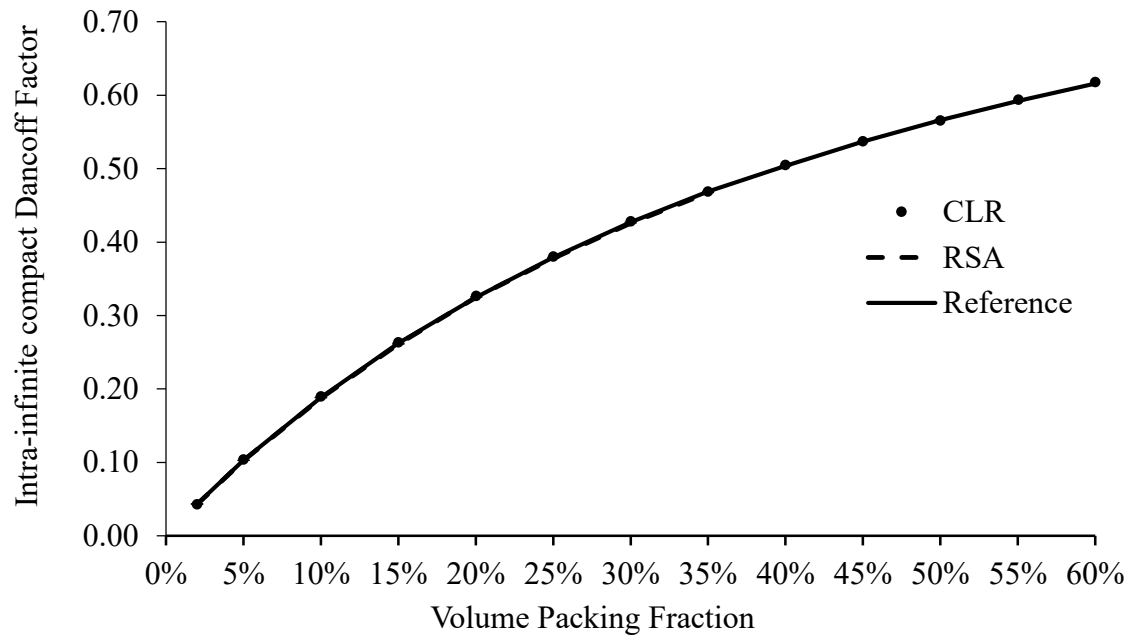


Figure 3-3 Variation of the intra-infinite compact Dancoff Factor with packing fraction: comparison between various methods

3.4.2 Finite Medium Dancoff Factor

In the finite medium Dancoff factor calculations, the actual geometry has been considered. For example, in the case of a pebble bed reactor, the intra-pebble Dancoff factors are tallied in the actual geometry of the fuel pebble consisting of two concentric spheres. The inner sphere of radius 2.5 cm, called fuel zone which embodies a stochastic distribution of TRISO fuel particles. The outer spherical shell of radius 3.0 cm forms the TRISO free moderator layer. The modelled geometry of the pebble with fuel kernel distribution is shown in Figure 3-4a. In case of prismatic type HTRs, the intra-compact Dancoff factors are estimated for a cylindrical pin of radius R_c 0.6225cm and its height to diameter (H/D) ratio is varied from 2 to 100. The modelled geometry of the compact with fuel kernel distribution is shown in

Figure 3-4b. The spatial distribution of the starting points is assumed to be uniform within the finite region.

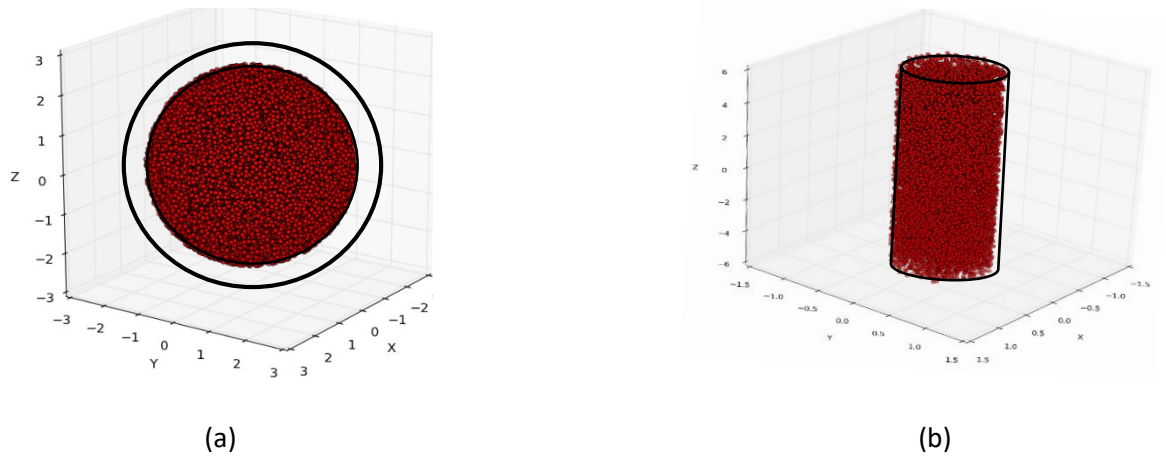


Figure 3-4: Random packing of TRISO in the fuel pebble (a) and fuel compact (b) for finite medium Dancoff factor calculation.

Intra-Pebble Dancoff factor

In the intra pebble Dancoff factor calculation, neutrons are emitted from the surface of uniformly sampled fuel kernels inside the fuel zone of a pebble and tracked until they collide with any other fuel kernel or escape from the fuel zone. The stochastic medium in the fuel zone of the pebble has been generated with the CLR and RSA methods with all possible ranges of packing fractions that can be realized by the respective methods and the average Dancoff factors are computed at each packing fraction. A comparison of the intra pebble Dancoff factor by our method and the reference Monte Carlo values is shown in Figure 3-5. The average relative deviations of CLR and RSA from the reference values are found to be about 0.21%

and 0.32% respectively.

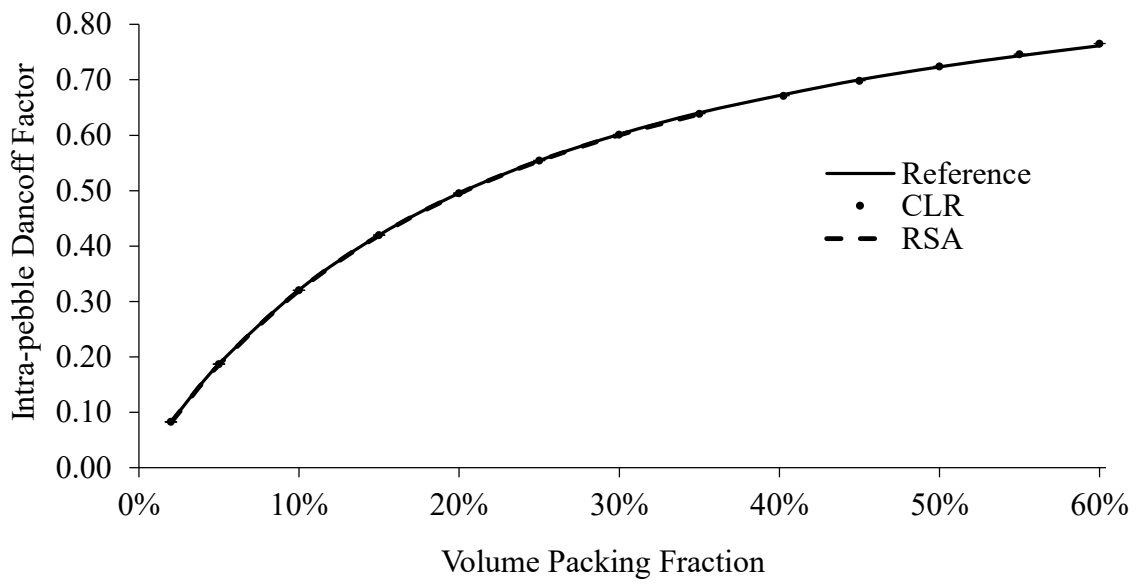


Figure 3-5: Variation of the intra-pebble Dancoff factor with packing fraction: comparison between various methods.

Intra-compact Dancoff factor

The intra-finite compact Dancoff factors are evaluated by tracking neutrons emitted from the surface of uniformly sampled fuel kernels in the fuel zone of the compact. The compact H/D ratio is varied from 2 to 100 and the Dancoff factor is computed for the stochastic finite compact fuel zone generated by the CLR and RSA methods, with all possible range of packing fractions that can be realized by the respective methods. At each H/D ratio, the Dancoff factors are compared with reference Monte Carlo values in (Figure 3-6) - (Figure 3-11).

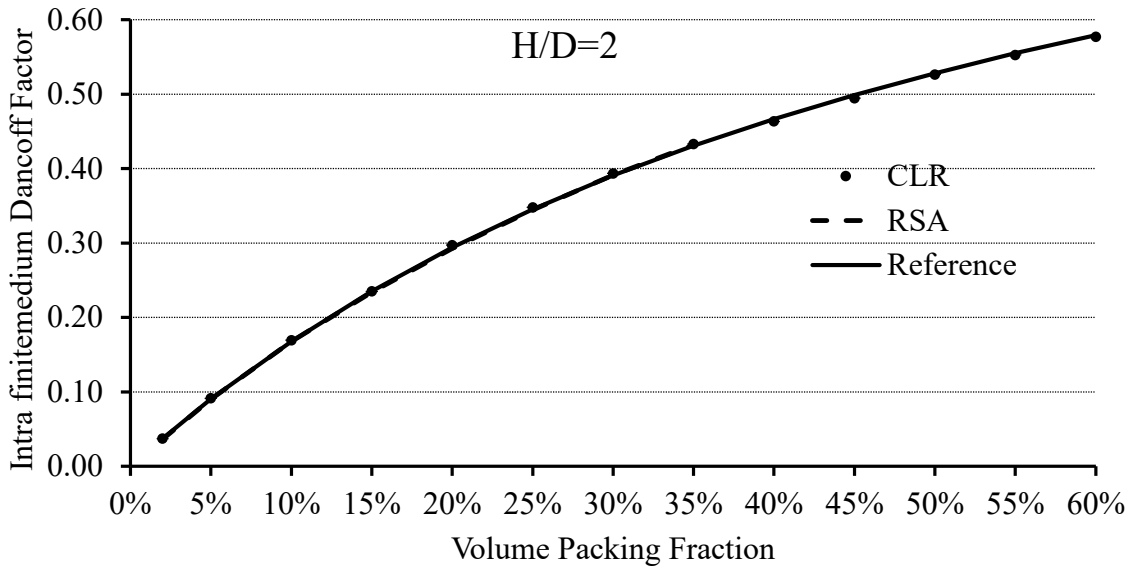


Figure 3-6: Intra-finite compact Dancoff factor with volume packing fraction of TRISO particles at H/D ratio equal to 2

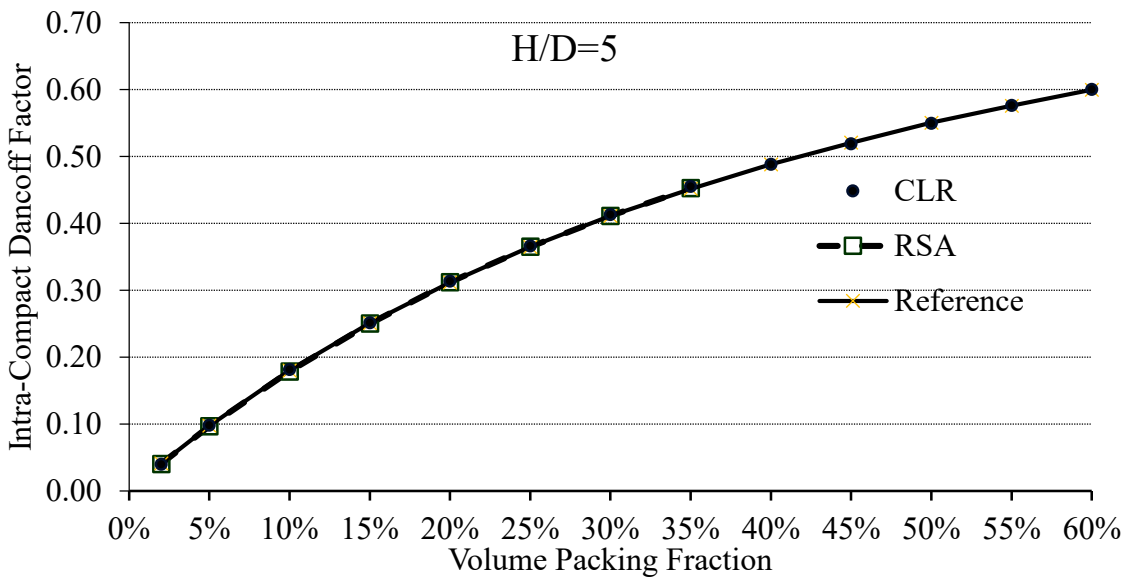


Figure 3-7: Intra-finite compact Dancoff factor with volume packing fraction of TRISO particles at H/D ratio equal to 5.

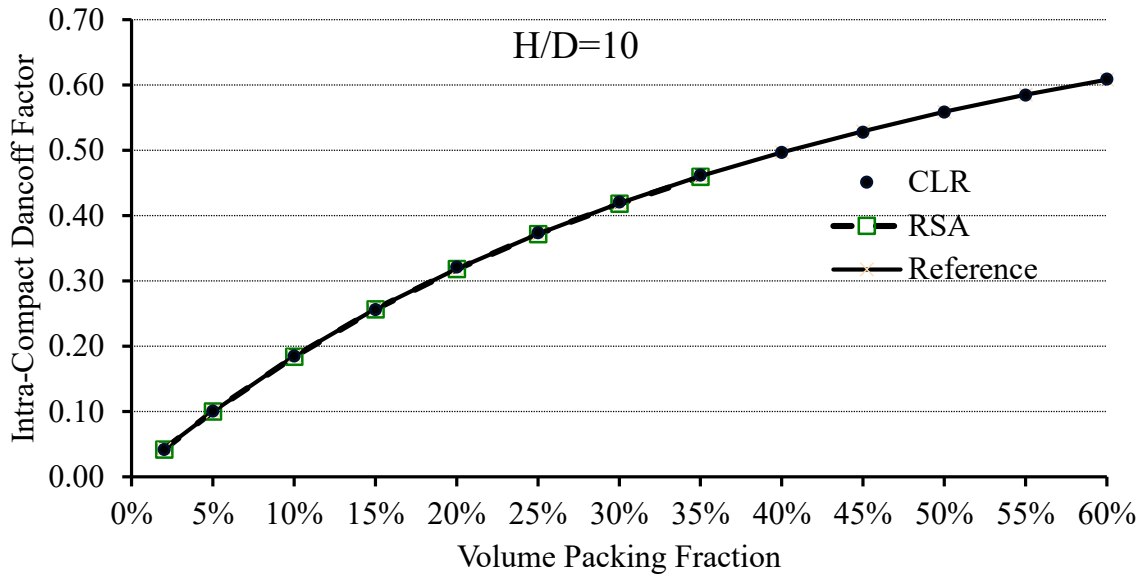


Figure 3-8: Intra-finite compact Dancoff factor with volume packing fraction of TRISO particles at H/D ratio equal to 10.

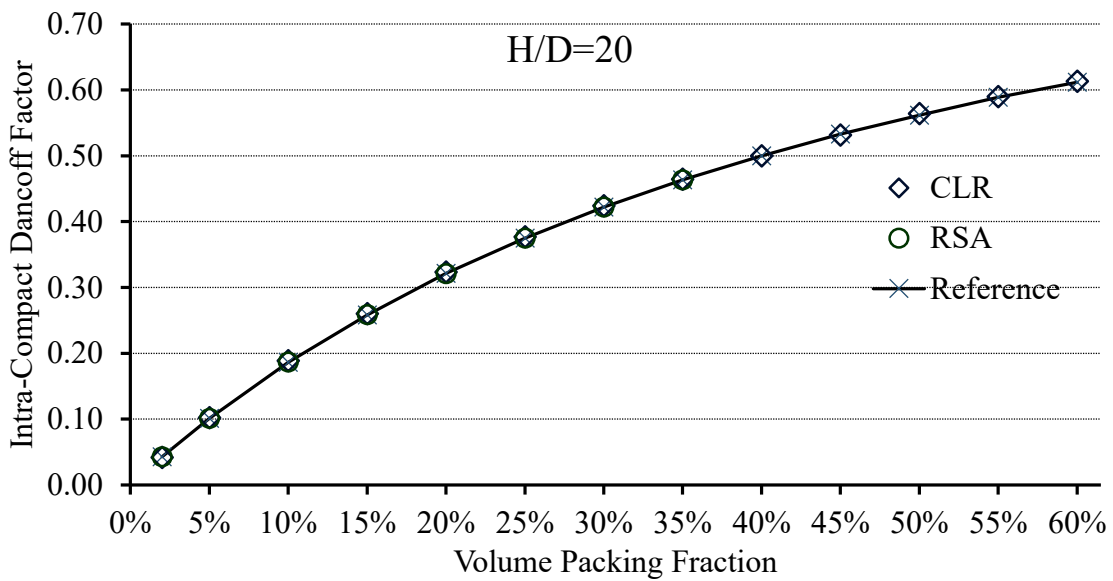


Figure 3-9: Intra-finite compact Dancoff factor with volume packing fraction of TRISO particles at H/D ratio equal to 20.

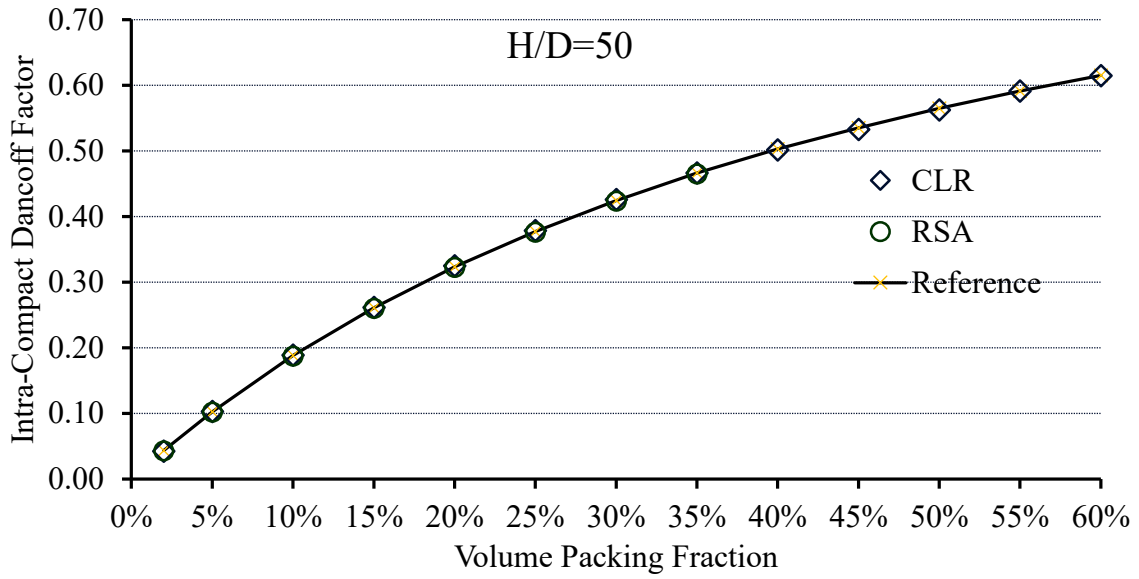


Figure 3-10: Intra-finite compact Dancoff factor with volume packing fraction of TRISO particles at H/D ratio equal to 50.

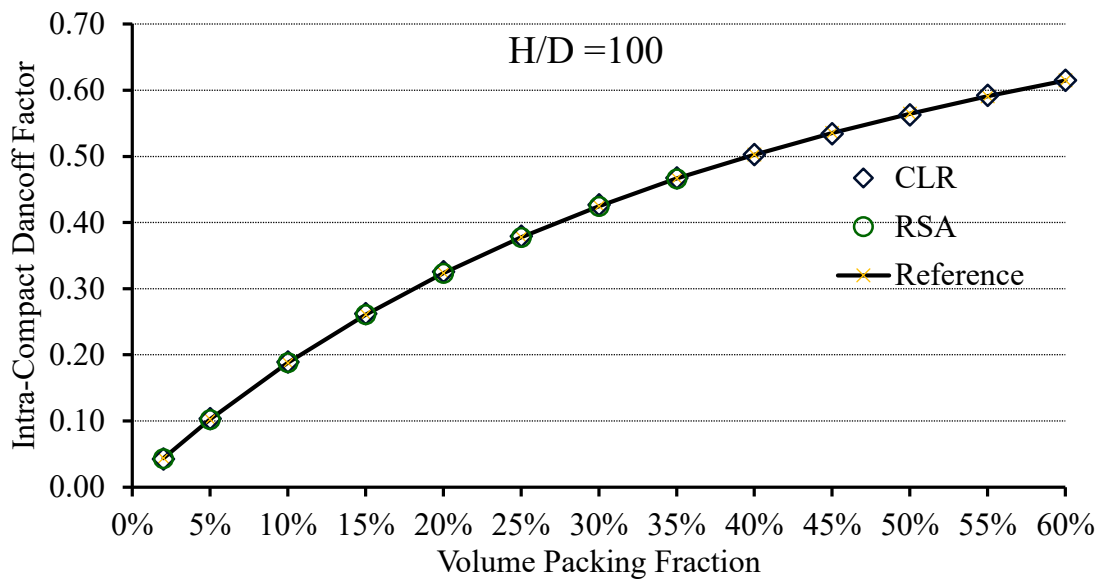


Figure 3-11: Intra-finite compact Dancoff factor with volume packing fraction of TRISO particles at H/D ratio equal to 100.

In this study, an important observation is found that the Dancoff factors computed for various geometries with entirely different packing schemes result in accurate values having average relative deviation less than 0.7% as given in [Table 3-1](#).

Table 3-1 Average relative deviations for CLR and RSA schemes from the reference results

H/D ratio	2	5	10	20	50	100
CLR (%)	0.65	0.52	0.49	0.59	0.38	0.58
RSA (%)	0.58	0.51	0.43	0.15	0.38	0.31

3.5 Conclusions

In this chapter, we have described the development of a new scheme (CLR) to generate the randomly distributed TRISO particles in the fuel zones of the pebble and the compact. This scheme is based on the Monte Carlo methods. The principal advantage of the method described here is that it can be used for low as well as high particle densities. Other methods tend to slow down at high particle densities and some of the methods (RSA) are unusable above a certain packing fraction. Thereafter, development of a fast neutron tracking algorithm to compute the Dancoff factors for randomly distributed fuel particles in finite and infinite media is described. Our results compare well with reference values. The Dancoff factors are required to estimate the accurate background cross-section that is in turn used in the calculation of the self-shielded cross-sections in the resonance region. The generation of self-shielded cross-sections and solution of the multi-group transport equation for the HTR lattice cells using these self-shielded cross-sections is the subject of the next chapter.

Chapter 4 **BOXER3 MODEL OF HTR LATTICE CELL: treatment of double heterogeneity in the resonance and thermal energy regions**

Here we discuss the development of a new methodology to solve the double heterogeneity problem at the stage of the multigroup transport theory solution. These features have been incorporated in the WIMS library-based lattice code BOXER3. Results of analysis of several HTR-lattice cell benchmark problems are presented.

4.1 Introduction

High temperature reactors present unusual challenges with regard to the neutron transport compared to traditional reactors. The primary reason for this is the geometry of the fuel elements in the form of spherical pebbles or cylindrical compacts which consist of a large number of tiny ($\sim 100 \mu\text{m}$ sized) fuel lumps in the form of TRISO particles, having a fuel kernel in the center surrounded with several coating layers, dispersed randomly in a graphite matrix. It might appear that such fine particle dispersions may be treated as homogeneous but that is not the case for all energies. For much of the neutron energy range the dispersion may be treated as a homogeneous medium. However, at certain energies, particularly around resonances, the neutron mean free path is comparable or shorter than the size of the fuel kernel and the situation necessitates treatment of the dispersion as a heterogeneous medium. The heterogeneity of the fuel region together with the heterogeneous distribution of the fuel region, graphite moderator, and the coolant is referred to as the double heterogeneity of HTRs. As

discussed in [Chapter 2](#), the resonance treatment in heterogeneous systems in the WIMS library is carried out through the equivalence principle. The calculation of the Dancoff factor in HTRs that is required for this purpose was discussed in the previous chapter. In this Chapter we study a number of HTR lattice benchmark problems using the lattice code BOXER3. The self-shielded multigroup cross-sections (in the epithermal resonance groups) required for this purpose are obtained using the Dancoff factors obtained by the methods described in [Chapter 2](#).

HTRs containing only plutonium as fuel (as may be the case in reactors designed for burning plutonium) have high concentrations of the isotopes ^{239}Pu and ^{240}Pu in the kernels. This fact together with their rather large resonance cross-section in the thermal groups results in a very short neutron mean free path in the fuel that is comparable to the kernel dimensions. In such cases, the fuel zone must be treated as a heterogeneous medium in the thermal energy region as well. However, the resonance treatment method in libraries such as the WIMS library does not cover the two large resonances of plutonium lying in the thermal region. Instead, a large number of groups are provided to cover the details of cross-section variation in this region. For this reason, it becomes necessary to develop a method for solving the multigroup transport equation for HTR lattice cells (with the doubly heterogeneity). This problem is also discussed in the present chapter.

In order to solve the multigroup transport equation for HTR lattices with double heterogeneity, one of the earliest approaches is based upon calculating equivalent cross-sections for the stochastic medium formed by the distribution of the fuel lumps in the graphite matrix. In this approach, the spatial self-shielding factor is computed based on conservation of collision probabilities [95]–[97]. Another class of method is based on obtaining the collision probabilities at the lattice cell level using the collision probabilities defined at micro- and

macro-level geometries [98], [99]. These collision probabilities are based on the assumption that the neutron angular flux entering or escaping the fuel lump is uniform and isotropic. A renewal theory based solution method of the transport equation in the random medium was developed by Sanchez and Pomraning [100], [101]. The lattice code DRAGON and APPOLO uses these two double heterogeneity treatment models in the HTR lattice cells analysis. The code SCALE follows a different method for double-heterogeneity treatment and resembles the pin cell and assembly-level calculations adopted in early days for LWRs [41]. The procedure used by the SCALE system for HTR lattice cell is a two-steps calculation: In the first step, the micro level calculation is performed for the TRISO particle surrounded by a graphite layer of appropriate thickness depending on the packing fraction. The macro level calculation is used in the second step for the pebble cell. In the micro-level calculation, resonance shielding calculation is performed based upon an externally calculated Dancoff factor, and it is followed by a solution of the transport equation for obtaining flux disadvantage factors using a white boundary condition. These fluxes are then used to compute the flux-weighted cross-sections, i.e., shielded cross-sections. These weighted cross-sections are passed on to the CENTRM transport solution for the macro-level geometry formed by fuel zone (having weighted cross-sections), graphite layer, and coolant. Similar to the SCALE code, WIMS9 also generates homogenized total cross-sections that have the same escape probability as the heterogeneous medium by solving the collision probabilities for the micro region (TRISO particle surrounded by graphite layer)[104], [105]. Subsequently, collision probabilities are derived for the various macro regions of the pebble using the homogenized cross-section in the fuel zone. Then the micro and macro region collision probabilities are combined to form a full set of collision probabilities for the complete pebble system and used in the solution for obtaining the system fluxes.

4.2 The Problem of High Pu Content Fuel

The WIMS-D library has a thermal cut off at 4.0 eV and the variation of cross-section around the resonances at 0.3 eV and 1.0 eV of Pu is represented using a large number of groups. The maximum cross-section of the Pu²⁴⁰ resonance is ~ 115Kilo barns which gives a mean free path much shorter than the radius of a fuel kernel. It is clear that spatial self-shielding of this resonance lying in the thermal energy region cannot be ignored and a simple volume homogenization is not permissible. The standard treatment of epithermal resonances, based on tables of resonance integral together with the use of equivalence theory as discussed in section [2.4.3](#), is not available for resonances of the thermal energy. Instead, the detailed cross-section variation due to resonances of the Pu isotopes in the thermal region is represented by having a large number of groups. Hence self-shielding due to these resonances must be accounted for at the stage of solution of the multigroup transport equation for the lattice calculation. We discuss a simple heuristic approach to this problem here. A more rigorous solution is developed in [Chapter 5](#).

4.3 Self-Shielding by Equivalent Spherical Shell: Theory

In Section [2.4.3](#), we discussed methods of obtaining the escape cross-section from the fuel which goes as input in the computation (interpolation) of the resonance integral and for obtaining cross-sections in the (epithermal) resonance groups. There are no resonance tables as a function of background cross-section and temperature for the resonances in the thermal region (in the WIMS-D library) and the self-shielding in this region is treated explicitly with several groups representing the cross-section variation in the resonances. The task of self-shielding is therefore transferred to the multigroup transport equation solution. As explained in

greater detail in Section 4.4, BOXER3 solves the transport equation by the collision probability method in which the collision probabilities are obtained by tracing rays through the geometry consisting of piecewise homogeneous regions. For the one-dimensional geometry of a macro cell of a pebble, we have a division into homogeneous spherical annuli. To ensure that self-shielding is correctly accounted for as well as to confirm to this geometrical description, we use the following device. We create a fuel region which has the required spherical symmetry and also has the same escape cross-section as the one computed by the methods of Section 2.4.3 (i.e. for the epi-thermal resonances). The uniformly distributed fuel kernels (Figure 4-1, left) are replaced by a thin spherical shell, as shown on the right in Figure 4-1, with the same volume as the total kernel volume and the same escape probability as the randomly dispersed kernels. Thus, from the point of self-shielding, the two problems are identical and the geometry is the same one dimensional spherical which the code can handle. In the following paragraphs we show how this is accomplished.

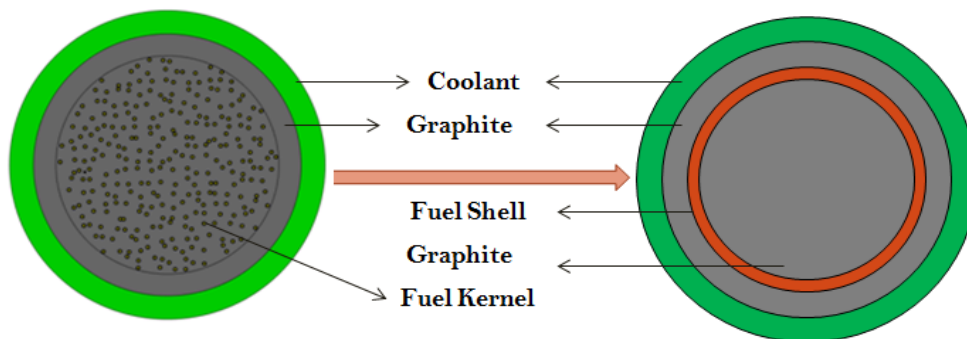


Figure 4-1: Double heterogeneous fuel pebble and equivalent spherical shell model.

The escape probability from a thin spherical shell is almost the same as that from a slab [132] viz. Eq. (4.1)

$$P_{esc} = \frac{\frac{1}{2} - E_3(-\tau_f)}{\tau_f} \quad 4.1$$

Where, E_3 is the exponential-integral function[133] of third order.

Half of these neutrons escape into the interior of the shell, and after crossing the inner graphite, are incident once again on the shell. If we assume that the neutrons escaping from the inner surface of the shell are distributed isotropically on the surface, the probability of neutrons crossing the inner moderator region and re-entering the shell can be expressed by

$$P_{in} = \frac{2\pi}{\pi} \int_0^{\pi/2} \exp(-\Sigma_m D \cos\theta) \sin\theta \cos\theta \, d\theta = 2 \int_0^1 \exp(-\Sigma_m D \mu) \mu \, d\mu \quad 4.2$$

$$= \frac{2}{\Sigma_m D} \left[\frac{1 - \exp(-\Sigma_m D)}{\Sigma_m D} - \exp(-\Sigma_m D) \right]$$

Where, D is the diameter of the shell. The fuel-to-fuel collision probability now consists of two contributions: one due to those neutrons that did not escape the fuel and the other due to those that escaped from the inner surface and reentered the shell. Thus, we write

$$P_0 = (1 - P_{esc}) + \frac{1}{2} P_{esc} P_{in} P_{Sfc} \quad 4.3$$

Where, P_{Sfc} , the probability of a neutron incident on the surface of the fuel colliding with it, may be written (using reciprocity relations) [116] as $P_{Sfc} = \frac{4\Sigma_f V_f P_{esc}}{S_f}$.

Now we consider those neutrons that escaped from the outer surface of the shell. This again consists of two parts. One is the half neutrons that escape from the outer surface of the shell. The other consists of those that escape collision in the fuel after escaping from the inner surface of the shell, crossing the graphite and reentering the fuel shell. This can be written as

$$f_0 = \frac{1}{2} P_{esc} \left(1 + P_{in} (1 - P_{S_{fc}}) \right) \quad 4.4$$

Assuming an isotropic angular distribution for both these components, the probability that they reach the cell boundary is

$$P_{out} = \frac{2\pi}{\pi} \int_0^{\pi/2} \exp\left(-\Sigma_m \sqrt{R^2 - r^2 \sin^2 \theta} - r \cos \theta\right) \sin \theta \cos \theta \, d\theta \quad 4.5$$

Where R is the radius of the outer graphite portion of the cell [for He coolant, attenuation in the coolant portion can be ignored] and $r=D/2$ is the radius of the shell. Assuming that they are reflected isotropically from the cell boundary, the probability of return to the fuel surface is $(S_f/S_c)P_{out}$, where S_f and S_c are the surface areas of the fuel layer and the cell outer boundary respectively. Of these, a fraction $\{P_{S_{fc}} + (1 - P_{S_{fc}})P_{in}P_{S_{fc}}\}$ will collide in the fuel and $\{(1 - P_{S_{fc}})P_{in}(1 - P_{S_{fc}})\}$ will once again leave the outer side of the fuel. Thus, the fraction of neutrons leaving the outer boundary that on a second pass collide in the fuel is given by Eq. (4.6)

$$f_1 = \frac{S_f}{S_c} (P_{out})^2 \left[P_{S_{fc}} + (1 - P_{S_{fc}})P_{in}P_{S_{fc}} \right] \quad 4.6$$

Moreover, the fraction that leaves the outer surface of the fuel once again is given by Eq. (4.7)

$$f_2 = \frac{S_f}{S_c} (P_{out})^2 \left[P_{S_{fc}} + (1 - P_{S_{fc}})^2 P_{in} \right] \quad 4.7$$

Summing over all passes through the cell we obtain

$$P_{ff} = P_0 + f_0 f_1 + f_0 f_2 f_1 + f_0 f_2^2 f_1 + f_0 f_2^3 f_1 + \dots = P_0 + \frac{f_0 f_1}{1 - f_2} \quad 4.8$$

In addition, the overall escape probability from the fuel (or the fuel to moderator collision probability) is $1 - P_{ff}$.

$$1 - P_{ff} = 1 - P_0 - \frac{f_0 f_1}{1 - f_2} \quad 4.9$$

This is compared with the Dancoff corrected escape probability from the fuel kernel. The escape probability from a single kernel is given by[35]

$$P_{esc} = \frac{3}{8(a\Sigma)^3} [2(a\Sigma)^2 - 1 + (1 + 2a\Sigma)\exp(-2a\Sigma)] \quad 4.10$$

In addition, the Dancoff corrected escape probability[35] is given by Eq. (4.11).

$$P_{fm} = P_{esc} \frac{1 - C}{1 - C(1 - \bar{l}_{fk}\Sigma_f P_{esc})} \quad 4.11$$

By equating the fuel to moderator collision probabilities for the spherical shell [Eq. (4.9)] and the distributed fuel kernels [Eq. (4.11)] we can obtain the radius of the fuel shell. The shell thickness is obtained by conservation of the fuel volume. The shell radius has a dependence on the fuel cross-sections which is group dependent. This may appear to be a problem. However, this variation is not very large. We choose an average thermal value of the fuel cross-section obtained by averaging over the spectrum in the thermal region so that the shell radius is the same for all groups. We note in passing that this is the equivalent of the dependence of the Bell factor on the fuel cross-section.

4.4 The Lattice Code BOXER3 and Its Modification for HTR Cells

The code BOXER3 is a three-dimensional code for treating PHWR supercells, that was recently modified for light water reactor assembly level lattice and burnup calculations. The code has been discussed in detail in Refs. [74], [75]. Here we restrict ourselves to the description necessary for understanding its extension to HTR cell calculations.

4.4.1 Geometry and Cross-Section Data

The program has the capability of treating three dimensional problems, two dimensional problems such as fuel assemblies and one-dimensional cylindrical pin-cell and slab geometries (as in plate type fuels). It is capable of treating the complex geometrical arrangements of fuel, clad, coolant and moderator commonly occurring in reactor lattices. The geometry that can be represented consists of cylinders imbedded in a rectangular mesh. For large domain problems in two- or three-dimensional systems, a mixed method involving a detailed collision probability treatment within smaller sub domains and coupling these sub domains using interface currents is used. However, one dimensional and smaller sized two problems can be handled using the exact P_{ij} method.

Treatment of spherical surfaces required in the lattice cell calculations of pebble bed HTRs, was not available in the code. This option has been added as described below. The lattice cell (as modeled in BOXER3) of a pebble bed reactor is illustrated in [Figure 4-2](#).

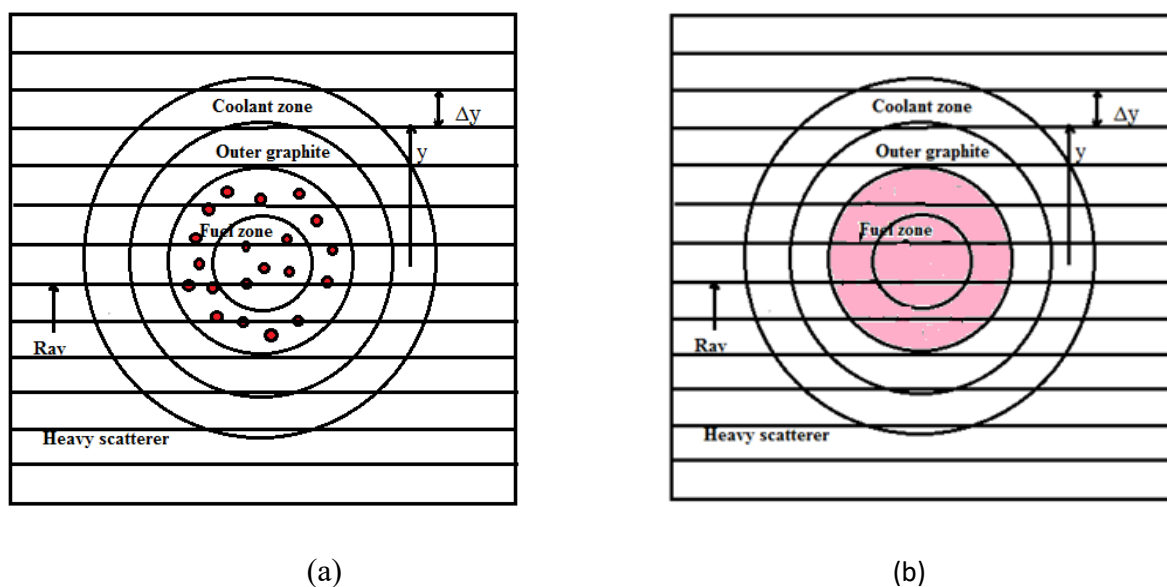


Figure 4-2: Schematic of fuel pebble (a) as it exists; (b) as modeled in BOXER3 code.

Multigroup cross-sections are obtained from the WIMS-D library. Self-shielded cross-sections in resonance groups are obtained from the resonance tables of the library using the Dancoff factor calculated in the manner described in Section [2.4.3](#). The group cross-sections of the fuel (including the self-shielded group cross-sections for the resonance groups) are not so large that the mean free path in the tiny fuel kernel will be shorter than its dimensions. Hence, we may homogenize the fuel and the coating and matrix materials into a homogeneous fuel zone and we make this assumption in the present sub section. However, in exceptional situations mentioned in the introduction, with large concentrations of plutonium in plutonium burning reactors, the thermal group cross-section of the fuel (particularly around the resonances) becomes so large that the mean free path is smaller than the kernel dimensions and homogenization is not permissible. This problem was discussed in Section [2.8](#) where the randomly dispersed fuel is replaced by a spherical shell as shown in [Figure 4-1](#).

Either way, we have a simple one-dimensional spherical geometry problem for the lattice cell calculations of HTRs. Since the resulting projected figure in this plane is the same as the corresponding projected figure in cylindrical geometry, the tracing routine for cylindrical geometry projection can be used. However, for calculating the collision probability integrals, it is necessary to carry out a modification in the area element, as described in Section 2.5.4 An additional optically thick heavy scatterer is included in the space between the outer boundary of the spherical cell and the cubical cell used in BOXER3. This artifice changes the reflective boundary condition at the spherical outer surface of the cell to white. It also allows the use of a cubical outer boundary instead of the spherical cell boundary.

The lattice cell of a pebble bed reactor is illustrated in [Figure 4-2](#). For the lattice cell calculations of HTRs we have a simple one-dimensional spherical geometry problem. Since the number of meshes is not large, we make use of the pure P_{ij} option. The integration over the angular variable in Eqns. (2.50)-(2.54) is not necessary due to the symmetry of the problem. The integration over the perpendicular area reduces to a single integral as described below. The integrals are obtained by constructing rays of the kind shown in [Figure 4-2](#), in any plane passing through the center. The area element associated with each ray in spherical geometry is given by $\Delta A = 2\pi y \Delta y$. Where, y is the distance from the center and Δy is the distance between the rays as shown in [Figure 4-2](#).

4.5 Analysis of HTR Benchmarks

The BOXER3 code, described above in [Section 4.4](#), was used for testing the validity of the methods discussed in this chapter for treating double heterogeneity of HTRs. The testing has been carried out by studying the benchmarks provided by the Organization for Economic Cooperation and Development, Nuclear Energy Agency (OECD NEA), Nuclear Science Committee, Working Party on the Physics of Plutonium Fuels and Innovative Fuel Cycles [105]. The computational benchmark has five phases that are concerned with high-temperature reactors (HTRs) and is defined for UO_2 , PuO_2 and ThO_2 - $^{233}\text{UO}_2$ fuel types. The specifications of fuel pebbles and coated particles of these benchmarks used in the present study are reproduced in [APPENDIX-A](#). The benchmarks defined in phases 1a, 2a and 3a with pebble cell having spherical outer boundary are used to calculate the infinite multiplication factor (k_∞) using BOXER3. Based on the evaluated nuclear data files recommended by WLUP participants, 69-group WIMS-D formatted library IAEA is used in the calculations [38]. The

k_{∞} for the infinite array problems are reported for cold condition and compared with results reported in the Ref. [105].

4.5.1 Results with Self-Shielding Treatment in Epithermal Groups

For each benchmark problem, the escape cross-section, as mentioned in Section 2.4.3, is calculated using Dancoff factor with a suitable Bell correction factor and supplied to the BOXER3 code to treat the double heterogeneity effect under the rational approximation. Dancoff factors corresponding to the benchmark problems are computed using the CLR method and listed in Table 4-1. The Dancoff factors in the two columns are the intra pebble and inter pebble Dancoff factors. The total Dancoff factor is obtained by adding these two.

Table 4-1 Finite medium Dancoff using CLR method and Bell Factors for Benchmark Problems [40], [65]

Fuel Type	TRISO Packing Fraction	C-intra	C-inter	Bell Factor
UO ₂ - fuelled pebbles	9.043E-02	0.3574	0.0433	1.73
²³³ UO ₂ /ThO ₂ or PuO ₂ fuelled pebbles	3.45E-02	0.1082	0.0210	1.75

Table 4-2 Comparison of BOXER Results with the Reference Values [40], [65]

Benchmark phase	Definition	k_{∞} at T=293.6K					
		BOXER		MCNP4B	SCALE	WIMS9	APPOLO
		Hom.	Hete.				

1a	Infinite array of UO ₂ fuelled pebbles	1.4282	1.5129	1.5108 ± 0.001	1.50748	1.51759	1.52232
2a	Infinite array of PuO ₂ fuelled pebbles	1.2323	1.2332	1.4573 ± 0.001	1.47656	1.46154	1.46369
5a	Infinite array of ThO ₂ -UO ₂ fuelled pebbles	1.4605	1.4664	1.46841 ± 0.0005	1.4645	1.46068	1.46269

The Bell factors were obtained by comparing the exact escape probability from a sphere with the Bell corrected rational approximation. The factor obtained by us is fairly close to that reported in Ref. [48]. In [Table 4-2](#), we have compared the BOXER3 results with other codes including the MCNP4B results. We have also included the BOXER3 results based on the assumption of a homogenized fuel zone without including the intra pebble heterogeneity. The results show that this has a very large effect for uranium fuel whereas for Th the effect, though smaller, is not altogether insignificant. After including the intra pebble heterogeneity, we find fairly good agreement for UO₂ and ThO₂-UO₂ fuelled pebbles. The BOXER3 result for uranium is somewhat on the lower side but only about as much as is the dispersion between various results of the benchmark exercise. More pertinently, it is small compared to the change seen from the homogenized result. For Th fuel, all codes predict very close to one another and so does BOXER3. However, for Pu fuel the BOXER3 prediction is rather poor. In fact, the results obtained using BOXER3 together with WIMS-D library shows that there is practically no effect

of the double heterogeneity correction, i.e. Dancoff and Bell corrections, on k_{∞} for Pu fueled pebble. This problem is addressed in the next Section [4.5.2](#).

4.5.2 Results with the Equivalent Spherical Shell Model

The method of the equivalent spherical shell is used to revisit the 2a phase benchmark plutonium fuel problem. The epithermal (resonance) group cross-sections were prepared as in the previous section. Using the equivalent shell model as described in Section [4.3](#), the outer shell radius of the shell was estimated to be 1.424 cm. The following procedure is employed for this purpose. First the lattice cell is modeled with an arbitrarily chosen shell radius, to estimate the flux weighted one group fuel total cross-section. Using this cross-section, the escape probability from the shell is equated to the Dancoff corrected escape probability from a fuel kernel and the resulting equation is solved to obtain a new shell radius. Iteration may be carried out if the difference between the assumed shell radius and the new shell radius is large. The spherical shell with this radius represents the ‘equivalent spherical shell’ model of the problem, which conserves the self-shielding of the resonances of plutonium below 4ev. The equivalent spherical shell model for PuO₂ benchmark gives a k_{∞} of 1.4528 which is in reasonably good agreement with the reference results of [Table 4-2](#).

4.5.3 Results of the Equivalent Spherical Shell Model for the Bende’s HTR problems

To study the uncertainty involved, we took up Bende’s 1st HTR problem of 2gram Pu loading in a pebble with 51659 fuel particles of 0.01cm radius[134]. We started with an arbitrarily chosen outer shell radius 1.5cm. We get spectrum averaged 1 group cross-section of the fuel shell (see the first row of Table 4-3) 12.67664cm⁻¹. In the first iteration of calculation, the outer radius of shell is determined using 1 group fuel cross section and used in BOXER3D code to calculate spectrum and K-inf. Table 4-3 shows that K-inf achieves its accuracy of 1pcm

within 3 iterations. This K-inf from spherical shell model shows very good agreement with the reference results obtained from MCNP, SCALE and WIMS7b within 0.072%, 0.15% and 0.23%, respectively.

Table 4-3 Iteration scheme used for Equivalent spherical model to study Bende's PuO₂ fueled pebble with 0.01cm kernel radius[134]

Number of Iteration	BOXER3D K-inf	R _{out} of Shell	R _{in} of Shell	Spectrum avg. Σ_f	Rel. error in Escape Probability	Rel. error in K-inf
Guess	1.304603	1.5	1.492307432	12.67664		
1	1.231012	1.7942797	1.78890014	12.67664	-2.33E-07	0.1612
2	1.232115	1.7893417	1.78393240	13.22499	-5.86E-07	0.0727
3	1.232113	1.78931534	1.78390588	13.22797	-1.17E-07	0.0712
4	1.232114	1.78931764	1.78390819	13.22771	-2.35E-07	0.0719
5	1.232114	1.7892703	1.78386060	13.22774	0.00E+00	0.07185

Similarly, we took up Bende's 2nd benchmark problem of 2gram Pu loading in a pebble with 38812 fuel particles of 0.011cm radius.

Table 4-4 Iteration scheme used for Equivalent spherical model to study Bende's PuO₂ fueled pebble with 0.011cm kernel radius[134]

Number of Iteration	BOXER3D K-inf	R _{out} of Shell	R _{in} of Shell	Spectrum avg. Σ_f	%Rel. error in Escape Probability	%Rel. error in K-inf
---------------------	---------------	---------------------------	--------------------------	--------------------------	-----------------------------------	----------------------

Guess	1.30229	1.5	1.492307466	12.60695		
1	1.240718	1.7410221	1.7353082	12.60695	-1.17E-05	0.5038
2	1.241662	1.7370172	1.7312768	13.05583	-1.18E-05	0.4281
3	1.241675	1.7370844	1.7313445	13.04901	0.00E+00	0.4270
4	1.241677	1.7370881	1.7313482	13.04859	0.00E+00	0.4269
5	1.241678	1.73708814	1.73134827	13.04858	-2.36E-07	0.4268

Again, the spherical shell model needs 3 iterations to result in K-inf with uncertainty no more than 1pcm. It can be seen from the Table 4-4 that K-inf for this problem also shows very good agreement with the reference results obtained from MCNP, SCALE and WIMS7b within 0.43%, 0.51% and 0.51%, respectively. It should be noted that the MCNP reference K-inf has ± 0.002 standard deviation. While the agreement appears satisfactory, the replacement of the large number of fuel particles by a shell is drastic approximation, and hence we have developed the more exact analysis in the next Chapter 5.

4.6 Conclusions

We have described the development of methods for lattice cell calculations in high temperature reactors of the pebble bed type. The other development is an ‘equivalent shell method’ for treating self-shielding in the thermal groups of the doubly heterogeneous cell. This is particularly important in Pu fueled reactors as the low-lying resonances of Pu which fall in the thermal region are not treated by the shielding methods used in the WIMS-D library. At the same time, the cross-section of Pu is so high that a homogeneous treatment in the thermal region is not permissible.

These developments have been incorporated in the computer code BOXER3 for performing lattice calculations in both spherical and cylindrical cells based on the WIMS-D library formalism and the collision probability method for solving the transport equation. Results of analysis of benchmarks clearly bring about the need for treating the micro-level as well as macro-level heterogeneity prevalent in HTRs. While our results for Th and U fuels show good agreement with benchmark values, after including double heterogeneity effects in the epithermal resonance groups, fuels containing high concentrations of Pu (as are expected to be used in Pu burning strategies) give poor results. However, this problem is resolved once the thermal double heterogeneity is also accounted for.

The ‘equivalent shell method’ described in this chapter is a simple heuristic approach for accounting for self-shielding in the thermal resonances of Pu by solving the multigroup transport equation in the doubly heterogeneous medium. Several approximations are involved at various stages such as the ‘cosine current approximation’ both at the stage of obtaining escape probabilities from the fuel kernel as well as from the shell. Moreover, it involves the replacement of the statistically distributed fuel kernels by a shell. While the method gives fairly good results for the Pu problem, it is important that a more rigorous treatment of transport in a random medium be carried out. We have developed such a rigorous method in the exact collision probability formalism and it is subject matter of [Chapter 5](#).

Chapter 5 **NEUTRON TRANSPORT IN STOCHASTIC MEDIA: collision probability method for pebble with random fuel distribution**

In this chapter, we describe the evaluation of the exact collision probabilities (CPs) to solve the transport equation in the random medium of an HTR lattice cell. This chapter also presents the implementation of the new method of calculating CPs in the code BOXER3 and results of analyses of HTR benchmarks problems.

5.1 Introduction

We saw in the previous chapter that when the fuel is a few percent enriched uranium or Thorium mixed with some LEU or ^{233}U , the thermal macroscopic cross-sections of the fuel and for that matter the epithermal group cross-sections obtained after accounting for the resonance self-shielding, are not so large that the mean free path is comparable to or shorter than the fuel kernel radius. However, in reactors designed to burn Pu, the fuel contains only PuO_2 . Such fuel has a large cross-section in the thermal groups around the 1 eV and 0.3 eV resonances of Pu and hence, for such fuels, homogenization of the fuel zone is not permissible. Since the resonance treatment method in the WIMS library, described above, is neither available nor applicable for thermal energies, a different method is clearly necessary as also described in [Chapter 4](#).

HTR lattice codes such as DRAGON [67] and WIMS [104] use some variants of the following collision probability method, discussed by Herbert [98] (and also by Bende [89] in a context of Dancoff factor calculations) for treating this problem. In this method, collision probabilities are calculated between the fuel and coating layers as well as the graphite matrix associated with a single TRISO particle, which we refer to as a micro cell. By assuming a cosine current on the boundary of this micro cell, collision probabilities of neutrons escaping the micro cell into neighboring cells and transmission probability across these cells are obtained. These are then used to obtain the total collision probabilities between the different material regions (fuel, coatings, graphite matrix) of the fuel zone. These probabilities go as input into the multi-group transport calculations within the HTR lattice cell.

In [Chapter 4](#), we had described a different (though somewhat heuristic) approach for solving this problem [135]. In this chapter, we present a more systematic approach involving solution of the neutron transport in a heterogeneous random medium for the lattice calculation. While the solution is based on the calculation of collision probabilities between different material regions of the fuel zone, the method of calculation of these probabilities is radically different from the above approaches. The method is based on exact expressions of collision probabilities along an integration ray and is therefore a more accurate approach.

There have been several studies on neutron transport in random media particularly for binary mixtures [100], [136]–[141]. Most of these attempt [136], [137] to obtain an equivalent transport equation for the average flux and are exact only for non-scattering media. In the context of HTRs, Sanchez and Pomraning [100] Sanchez and Masiello [141] and Sanchez [101] have made similar attempts at solving this problem by an approximate collision probability method and by the MOC. In this, chapter we described a new method developed for treating

the thermal neutron transport in a random heterogeneous medium (which in the WIMS-D formalism contains the two large resonances of Pu that are not part of the resonance treatment method of this library). The method attempts to obtain exact expressions for the collision probabilities from one macroscopic mesh to another taking into account the random heterogeneous distribution of TRISO particles. Other than the statistical assumptions used to describe the medium (which fairly accurately describe the situations at hand), the method is exact. The necessary modifications in the expressions for the integrands in the collision probability integrals taking into account the random heterogeneous structure of this medium are discussed in Sections [5.3](#) and [5.4](#). We present two independent derivations of the basic formulae of collision probabilities to solve the integral form of the neutron transport equation in random media. These are discussed in Sections [5.5](#) and [5.6](#). Both the methods give identical expressions for the collision probabilities, which gives us confidence in the formulae so derived. The method has been incorporated in the collision probability code BOXER3 [61], [74], [135] which was extended for application to HTRs [135]. Comparison with benchmarks of Pu based HTR fuels have been described in Section [5.8](#) and this show very good agreement thus validating the new approach. Lastly, Section [5.9](#) presents the main conclusions drawn from the work described in this chapter.

5.2 Application of BOXER3 Code to the HTR Lattice Cell

Details of the collision probability method and the BOXER3 code along with the extension to treat spherical geometry required in pebble-bed reactor cell have already been discussed in Sections [2.5.4](#) and [4.4](#). The discussion includes computation of the Dancoff factor for the doubly heterogeneous random medium of HTRs and the escape cross-section that goes into the computation of self-shielded cross-sections in the resonance groups. For the pebble

bed reactor, the cell has a spherical geometry that is divided into (homogeneous) spherical annuli. The collision probabilities are evaluated as described in Section 4.4. The primary difference in the method described in the present chapter is that the spherical annuli are no longer considered as being homogeneous but are treated as heterogeneous random fuel graphite mixtures in the evaluation of collision probabilities.

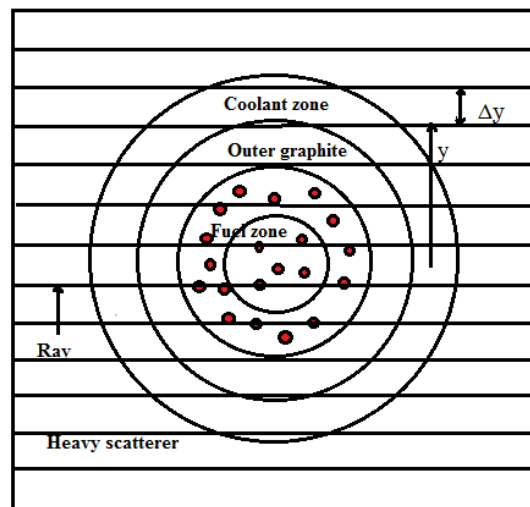


Figure 5-1: Schematic of fuel pebble used in BOXER3 code.

The lattice cell of a pebble bed reactor is illustrated in Figure 5-1. [Each mesh is not homogeneous in its composition and we will see shortly the necessary modifications to take this fact into account.] The aim is to obtain the detailed multi-group flux distribution across the cell (including separately for the fuel component and the graphite component in the fuel meshes). The spherical geometry permits a number of simplifications in the calculation of the probabilities. A single direction is enough due to spherical symmetry. Moreover, it is necessary to trace rays in any plane passing through the centre. Since the resulting projected figure in this plane is the same as the corresponding projected figure in cylindrical geometry, the tracing

routine for cylindrical geometry projection can be used. However, it is necessary to carry out a modification in the area element. Each area element is now given by

$$\Delta A = 2\pi y \Delta y$$

Where, Δy is the spacing between rays and y is the distance of the ray from the centre of the sphere, as shown in [Figure 5-1](#). Thus, the integrals in Eqs. (2.50) - (2.54) reduce to one-dimensional quadratures.

5.3 Modification for Calculation of Various Probabilities for a Heterogeneous Fuel Zone

The expressions for the integrands in Eqs. (2.50) - (2.54) are applicable for homogeneous meshes such as the coolant, the outer graphite coating of a pebble and the heavy scatterer. However, for our problem, the expressions for the integrands need to be modified for taking into account the random heterogeneous structure of this medium. We rewrite Eq. (2.50) for collision probability between two distinct meshes in a slightly modified form as follows

$$\begin{aligned} P_{ij} &= \frac{1}{4\pi V_i} \int l_i dA d\Omega \left\{ \frac{1 - \exp[-(\tau_i)]}{\Sigma_i l_i} \right\} \exp[-\tau_{ij}] \{1 - \exp[-(\tau_j)]\} \\ &= \frac{1}{4\pi V_i} \int dA d\Omega P_{iB_{2i}} P_{B_{2i}B_{1j}} P_{B_{1j}j} \end{aligned} \tag{5.1}$$

Where, $P_{iB_{2i}}$, $P_{B_{2i}B_{1j}}$, $P_{B_{1j}j}$ stand for the probability that a neutron in mesh i along the ray reaches the (second) boundary, the probability that having reached the boundary this neutron further reaches the first boundary of mesh j and finally that having reached the boundary of mesh j it collides in mesh j respectively. The probability $P_{B_{2i}B_{1j}}$ can be written as the product

of the probabilities $\prod_k P_{B_{k1}B_{k2}}$ of the various meshes k that lie between i and j . For homogeneous meshes, the expressions contained in Eq. (5.1) are directly usable for these probabilities. For heterogeneous meshes we derive the necessary expressions for P_{ii} , $P_{B_{k1}B_{k2}}$, $P_{iB_{i2}}$, and $P_{B_{j1}j}$ in the following sections. Instead of these four quantities we need 9 quantities since each mesh has a fuel and a moderator region.

Note that we have divided the first factor in the integrand by the chord length l_i and included Σ_i in its denominator so that we can interpret as a probability of escape of the neutron born in region i along the ray (the factor is then dimensionless). Of course, we have to multiply the integrand by l_i for maintaining consistency.

5.4 Collision Probability Integrands for Heterogeneous Random Fuel Graphite Mixture

We assume that the various layers of coatings around a TRISO particle have been homogenized with the graphite matrix in which these particles are embedded. The assumption has no material impact on the results as the various layers are small in size ($< 1\text{mm}$) compared to the mean free path in the medium ($\sim 25\text{mm}$) and the coating is made of Carbon and Silicon. With this assumption, each mesh of the fuel zone contains two parts the fuel kernel and the moderator. With the assumption of a flat average flux in the mesh, we can say that a mesh has the same flux in all the fuel kernels of the mesh while the graphite matrix of the mesh has a different flux. Thus, each mesh is split into two sub regions viz. fuel and matrix. The problem is to obtain collision probabilities between these two types of regions within a mesh and across different meshes.

In Section [5.2](#), we have seen that rays are drawn across the problem geometry and the program calculates the intercepts in each of the (macro) meshes. We are interested in calculating the contributions of a ray to collision probabilities of interest viz., $P_{fi \rightarrow fj}$, $P_{fi \rightarrow mj}$, $P_{mi \rightarrow fj}$, $P_{mi \rightarrow mj}$. As discussed in a previous section it is clear that it is enough if we obtain these quantities within the same mesh i.e. $P_{fi \rightarrow fi}$, $P_{fi \rightarrow mi}$, $P_{mi \rightarrow fi}$, $P_{mi \rightarrow mi}$ and the auxiliary quantities $P_{fi \rightarrow Bi}$, $P_{Bi \rightarrow fi}$, $P_{mi \rightarrow Bi}$, $P_{Bi \rightarrow mi}$, $P_{Bi \rightarrow Bi}$. Note that we have used the letter B for the boundary without specifying whether it is first or second. This is acceptable because within a given mesh these quantities are symmetrical with respect to a reversal in the direction of the ray.

The contribution of the ray to the mesh-to-mesh collision probabilities (for example $P_{fi \rightarrow fj}$) can be obtained from these using the product as in an earlier section

$$P_{fi \rightarrow fj} = P_{fi \rightarrow Bi} P_{Bi \rightarrow Bi+1} \dots P_{Bj \rightarrow fj} \quad 5.2$$

Of the nine quantities listed above, we need to calculate only three since they obey three reciprocity relations given by Eqs. (5.3) – (5.5)

$$\Sigma_{fi} \lambda L \langle \bar{l} \rangle P_{fi \rightarrow mi} = \Sigma_{mi} L P_{mi \rightarrow fi} \quad 5.3$$

$$\Sigma_{fi} \lambda L \langle \bar{l} \rangle P_{fi \rightarrow Si} = P_{Si \rightarrow fi} \quad 5.4$$

$$\Sigma_{mi} L P_{mi \rightarrow Si} = P_{Si \rightarrow mi} \quad 5.5$$

and three sum rules are given by Eqs. (5.6) – (5.8)

$$P_{fi \rightarrow fi} + P_{fi \rightarrow mi} + P_{fi \rightarrow Bi} = 1 \quad 5.6$$

$$P_{mi \rightarrow fi} + P_{mi \rightarrow mi} + P_{mi \rightarrow Bi} = 1 \quad 5.7$$

$$P_{Bi \rightarrow fi} + P_{Bi \rightarrow mi} + P_{Bi \rightarrow Bi} = 1 \quad 5.8$$

In view of this reduction in the number of quantities required, we obtain explicit expressions for the following three contributions $P_{fi \rightarrow fi}$, $P_{fi \rightarrow Bi}$, and $P_{Bi \rightarrow Bi}$ in the following Sections [5.5](#) and [5.6](#).

5.5 First Method for Calculating Integrands in the CP Calculations

5.5.1 Contribution to Fuel Kernel to Kernel Probability $P_{FF}(L)$

Let us assume that a length L_i of a ray is intercepted by some mesh i as shown in [Figure 5-1](#). The quantity L_i of course is different for different rays traced for carrying out the integration over the cell, but the number of fuel kernels intercepted by a given ray of length L_i is statistically distributed owing to the random character of the medium. For a given realization of this distribution let us assume that n_i fuel kernels lie along the ray in mesh i . We assume that the distribution of the fuel kernels along the length of the intercept follows renewal statistics. More specifically, we may assume Poisson statistics. The merit of Poisson statistics is that it corresponds fairly closely to the actual situation and allows us analytical treatment. The coating layers do not permit the centres of two kernels to be within a diameter of the TRISO particle (typically 1-2 mm) and this causes some deviation from Poisson statistics. While at low packing fractions, the deviation from Poisson is very slight and may be ignored, at intermediate packing fractions, this has the effect that instead of an exponential chord length distribution corresponding to Poisson statistics, we have a distribution that is zero up to a particle diameter and an exponential beyond this distance. From a practical point of view, since most HTR fuels have packing densities in the low and intermediate range, these two cases are the most interesting. The Poisson case (corresponding to low packing fraction) is discussed in

the present sub section and Section [5.6](#), and the non-Poisson case is discussed in some detail in Section [5.7](#) and represents a small correction to the theory developed in Sections [5.5](#) and [5.6](#) at intermediate packing fractions. At very high packing densities (close to the theoretical limit) of the TRISO particles, their arrangement is more like a lattice and this produces spikes at distances of a diameter of the TRISO particle and integral multiples thereof up to a few diameters before becoming a continuous exponential density. This case is difficult to treat analytically and is also not very interesting from a practical point of view and we do not consider it further. Having said this, we also note that the Poisson distribution is a fair approximation for all these situations as the mean chord length (several cms) and the mean free path in graphite (~ 2.5 cm) are long and hence the undulations on the scale of a TRISO particle diameter (<1 mm) have little impact on the results.

We make a number of other simplifying assumptions; the sum of the segments intercepted by the kernels in a mesh is small compared to the total length of the ray in that mesh. This follows from the fact that the volume fraction of kernels is typically 1% or less. The medium at the beginning and end of a segment is the graphite matrix and whole kernels lie in between with no partial kernels. This also follows from the small volume fraction of the fuel due to which the probability that any point is in a fuel kernel is expected to be 1 % or less. For this particular realization of the number of intercepts, we must write down all terms that contribute to the fuel-to-fuel collision probability. We then average over the distribution of the fuel kernels in the medium, finally over the number of kernels intercepted, and add the contributions from all these terms. There are basically two types of terms. The first are those in which the kernel in which the neutron undergoes collision is different from the one in which the neutron is born ($P_{FF1}(L)$). The second are those in which the kernel in which the neutron undergoes collision is the same as the one in which the neutron is born ($P_{FF2}(L)$). While there

will be a distinct contribution from each of the former types, all contributions from the latter type are essentially the same. We first consider a term of the former type in which there are k kernels ($k = 0, 1, \dots, n_i - 2$) between the birth kernel and the collision kernel. We then write down the following expression for such a term denoted by $P_{FF1}(n_i, k, L)$ of the fuel-to-fuel collision probability $P_{fi \rightarrow fi}$ (within mesh i) [written simply as $P_{FF1}(L)$ on dropping the mesh index].

$$\begin{aligned}
& P_{FF1}(n_i, k, L) \\
&= \int_0^L dx_1 \int_0^{L-x_1} dx_2 \int_0^{L-x_1-x_2} dx_3 \dots \int_0^{L-x_1-x_2-\dots-x_{n_i-1}} dx_{n_i} P_m(x_1) \dots P_m(x_{n_i}) C(L-x_1 \\
&\quad -x_2 - \dots - x_{n_i}) \langle \exp(-\tau_f) \rangle_A^k \prod_{l=i+1}^{i+k+1} \exp(-\Sigma_m x_l) [1 \\
&\quad - \langle \exp(-\tau_f) \rangle_A] \left\langle \left(\frac{1 - \exp(-\tau_f)}{\tau_f} \right) \right\rangle_V
\end{aligned} \tag{5.9}$$

where, the averaging symbol $\langle f(\tau_f) \rangle$ [of an arbitrary function $f(\tau_f)$] used in Eq. (5.9) is defined by Eqs. (5.10) and (5.11)

$$\langle f(\tau_f) \rangle_V = \frac{1}{\left(\frac{4}{3}\pi R^3\right)} \int_0^R f(\tau_f) 2\pi r l dr \tag{5.10}$$

$$\langle f(\tau_f) \rangle_A = \frac{1}{\pi R^2} \int_0^R f(\tau_f) 2\pi r dr \tag{5.11}$$

where, $l = 2\sqrt{R^2 - r^2}$ is the chord length intercepted at a distance r from the centre of the fuel kernel of radius R , $\tau_f = \Sigma_f l$ is the optical path intercepted and \bar{l} is the mean chord length in a sphere. The symbols A and V refer to averaging over an area perpendicular to the ray and

the volume of the fuel kernel respectively. In view of Eqs. (5.10) and (5.11), it is possible to rewrite the last factor in Eq. (5.9) in the alternative form of an area average as follows

$$\left\langle \left(\frac{1 - \exp(-\tau_f)}{\tau_f} \right) \right\rangle_V = \frac{(1 - \langle \exp(-\tau_f) \rangle_A)}{\bar{l}\Sigma_f} \quad 5.12$$

Assuming an exponential distribution of the intervals, permits us to write

$$P_m(x)dx = \exp(-\lambda x)\lambda dx \quad 5.13$$

$$C(x) = \exp(-\lambda x) \quad 5.14$$

The integrals over the moderator are in the form of convolutions and are best evaluated in the Laplace domain. The Laplace transform of the above expression in Eq. (5.9) (as a function of L) is easily evaluated and we get

$$\begin{aligned} \widetilde{P}_{FF1}(n_i, k, s) &= \int_0^\infty P_{FF1}(n_i, k, L) \exp(-sL) dL = \\ &= [1 - \langle \exp(-\tau_f) \rangle_A] \left(\frac{1 - \langle \exp(-\tau_f) \rangle_A}{\bar{l}\Sigma_f} \right) \frac{\lambda^{n_i} \langle \exp(-\tau_f) \rangle_A^k}{(s + \Sigma_m + \lambda)^{k+1} (s + \lambda)^{n_i - k}} \end{aligned} \quad 5.15$$

There will be several such terms contributing to the fuel-to-fuel collision probability and we have to sum over all of them. For the above case, there are $n_i - k - 1$ such terms and k can vary from 0 to $n_i - 2$ terms. Finally, we sum over n_i and k . Carrying out these operations, we obtain

$$\widetilde{P}_{FF1}(s) = \frac{(1 - \langle \exp(-\tau_f) \rangle_A)^2}{\langle \tau_f \rangle} \sum_{n_i=2}^{\infty} \lambda^{n_i} \sum_{k=0}^{n_i-2} \frac{(n_i - k - 1) \langle \exp(-\tau_f) \rangle_A^k}{(s + \Sigma_m + \lambda)^{k+1} (s + \lambda)^{n_i - k}} \quad 5.16$$

The summation of Eq. (5.16) is easy and we finally obtain

$$P_{FF1} = \frac{\lambda^2 (1 - a)^2}{\langle \tau_f \rangle (s)^2 (s + \lambda - a\lambda + \Sigma_m)} \quad 5.17$$

Where,

$$a = \langle e^{-\tau_f} \rangle_A = \frac{1}{\pi R^2} \int_0^R 2\pi r dr \exp(-2\Sigma_f \sqrt{R^2 - r^2}) = \frac{1 - e^{-2R\Sigma_f}(1 + 2R\Sigma_f)}{2R^2\Sigma_f^2} \quad 5.18$$

and,

$$\langle \tau_f \rangle = \Sigma_f \bar{l} = \frac{\Sigma_f}{\pi R^2} \int_0^R 2\pi r l dr = \frac{4R\Sigma_f}{3} \quad 5.19$$

The mean optical chord length $\langle \tau_f \rangle$ in a sphere is defined in the Eq. (5.19). On inverting, the Laplace transform of Eq. (5.17) and dividing by the quantity λL , as there are λL kernels on an average that are intersected by the line; we get fuel-to-fuel collision probability.

$$P_{FF1}(L) = \frac{\lambda^2(1-a)^2[\{\lambda(1-a) + \Sigma_m\}L - 1 + e^{-[\lambda(1-a) + \Sigma_m]L}]}{(\lambda L)\langle \tau_f \rangle[\lambda(1-a) + \Sigma_m]^2} \quad 5.20$$

Another contribution comes from collision probability from the second type of terms (collision within the same fuel kernel in which the neutron is born) and is the same for each kernel viz.,

$$P_{FF2}(L) = \frac{(\langle \tau_f \rangle - (1-a))}{\langle \tau_f \rangle} \quad 5.21$$

If there are n_i kernels, there will be n_i equal contributions. Averaging over the Poisson statistics for the distribution of the number of kernels clearly does not change this quantity.

Hence, the total contribution of the two terms to the fuel-to-fuel collision probability is given by Eq. (5.22)

$$P_{FF}(L) = \frac{\lambda L[\langle \tau_f \rangle - (1-a)]}{(\lambda L)\langle \tau_f \rangle} + \frac{\lambda^2(1-a)^2[\{\lambda(1-a) + \Sigma_m\}L - 1 + e^{-[\lambda(1-a) + \Sigma_m]L}]}{(\lambda L)\langle \tau_f \rangle[\lambda(1-a) + \Sigma_m]^2} \quad 5.22$$

5.5.2 Contribution to Fuel Kernel to Mesh Surface Probability $P_{FB}(L)$

A similar method gives the other probabilities. For example, with n_i fuel kernels lying along the ray of length L_i in mesh i the expression for the probability of a neutron starting from the k^{th} fuel kernel to reach the mesh surface is given by Eq. (5.23)

$$\int_0^L dx_1 \int_0^{L-x_1} dx_2 \int_0^{L-x_1-x_2} dx_3 \dots \int_0^{L-x_1-x_2-\dots-x_{n_i-1}} dx_{n_i} P_m(x_1) \dots P_m(x_{n_i}) C(L-x_1-x_2-\dots-x_{n_i}) \langle \exp(-\tau_f)_A \rangle^{n_i-k} \exp(-\Sigma_m(L-x_1-x_2-\dots-x_k)) \left\langle \frac{1-\exp(-\tau_f)}{\tau_f} \right\rangle_V \quad 5.23$$

The total probability is given by summing over k and n_i . The Laplace transform of the above expression is easily written down using the convolution theorem, we get

$$\begin{aligned} \widetilde{P}_{FB}(n_i, k, s) &= \int_0^\infty P_{FB}(n_i, k, L) \exp(-sL) dL \\ &= \left(\frac{1 - \langle \exp(-\tau_f) \rangle_A}{\bar{l}\Sigma_f} \right) \frac{\lambda^{n_i} \langle \exp(-\tau_f) \rangle_A^{n_i-k}}{(s + \lambda + \Sigma_m)^{n_i-k+1} (s + \lambda)^k} \end{aligned} \quad 5.24$$

After summing over, k and n_i we get

$$P_{FB} = \left(\frac{1 - \langle \exp(-\tau_f) \rangle_A}{\bar{l}\Sigma_f} \right) \sum_{n_i=1}^\infty \sum_{k=1}^{n_i} \frac{\lambda^{n_i} \langle \exp(-\tau_f) \rangle_A^{n_i-k}}{(s + \lambda + \Sigma_m)^{n_i-k+1} (s + \lambda)^k} \quad 5.25$$

The summations are easily carried out and we obtain

$$P_{FB} = \frac{(1-a)\lambda}{\langle \tau_f \rangle (s + \lambda - a\lambda + \Sigma_m)(s)} \quad 5.26$$

On inverting the Laplace transform of Eq. (5.26) and dividing by the average number of kernels intercepted by the ray of length L i. e. (λL) , we get final expression of fuel to surface probability

$$P_{FB}(L) = \frac{\lambda(1-a)[1 - e^{-L[(\lambda(1-a) + \Sigma_m)]}]}{(\lambda L)\langle\tau_f\rangle[(\lambda(1-a) + \Sigma_m)]} \quad 5.27$$

5.5.3 Contribution to Mesh Surface to Surface Probability $P_{BB}(L)$

The surface-to-surface probability is the simplest. There is no moderator integral since moderator length (L) and hence the attenuation is fixed viz. $\exp(-\Sigma L)$. The attenuation in the fuel depends on the number of fuel kernels encountered. Averaging this over the Poisson distribution for the number of kernels intercepted, we have for the surface-to-surface probability

$$\begin{aligned} P_{BB}(L) &= \exp(-\Sigma L) \exp(-\lambda L) \sum_{n_i=0}^{\infty} \frac{(\lambda L)^{n_i}}{n_i!} \langle \exp(-\tau_f) \rangle^{n_i} \\ &= \exp[\lambda L \langle e^{-\tau_f} \rangle - (\Sigma_m + \lambda)L] \\ P_{BB}(L) &= \exp(-(\lambda(1-a) + \Sigma_m)L) \end{aligned} \quad 5.28$$

Note that the above expressions in Eqs. (5.22), (5.27) and (5.28) refer to the collision probabilities associated with the segment of a particular ray drawn across the cell falling in one particular mesh. By using Eq. (5.2) (which again refers to that particular ray and hence does not require the cosine current assumption) and integrating over all such rays (as is done for obtaining exact collision probabilities and is illustrated in Figure 5-1), we obtain (within mesh and across meshes) collision probabilities between fuel kernels and the graphite. Note that we do not assume the cosine current approximation of neutrons entering or exiting the kernels, as is done in other solutions to this problem [67], [142] and in this sense the calculation of the

collision probabilities is exact. Further we do not attempt to obtain an equivalent transport equation which has been the attempt in several approaches to transport in a random medium[99], [100], [140], [141]. Hence, we do not invoke assumptions such as no scattering etc. The various assumptions are only about the statistical properties of the medium, which we have seen are quite accurate at least for the case at hand. The method can easily be generalized to other chord length distributions.

5.6 Alternative Method for Obtaining Integrands in the CP Calculations

This method uses simple arguments for writing down an integral equation for the mesh boundary to region (and mesh boundary to mesh boundary probability). The equation is solved by converting it to a differential equation. Finally, the region-to-region collision probabilities are obtained as integrals over the mesh boundary to region probabilities. Some of the arguments are somewhat heuristic but the simplicity of the method justifies the presentation. Throughout this section, we use the notation $a = \langle \exp(-\tau_f) \rangle_A$ (See Eqs. 5.11 and 5.18).

5.6.1 Integrand for the Mesh Surface-to-Surface Probability $P_{BB}(L)$

A neutron path may cross the medium without encountering a fuel kernel at all or after crossing one or more kernels. The probability of the former event is $\exp(-\lambda L)$ and the probability of crossing without collision in this case is $\exp(-\Sigma_m L)$. Thus, the probability of reaching the mesh boundary is $\exp(-(\lambda + \Sigma_m)L)$. In the latter of the two possibilities, let us assume that the first kernel is encountered at a distance between x and $x + dx$ for which the probability is $\exp(-\lambda x)\lambda dx$. To this we multiply the probabilities of crossing the moderator length x and the kernel without collision viz. $\exp(-\Sigma_m x)$ and $a = \langle \exp(-\tau_f) \rangle_A$ and since the

neutron is now at a distance $L - x$ from the outgoing boundary, we further multiply it by $P_{BB}(L - x)$ and integrate over x . We thus have

$$\begin{aligned}
 P_{BB}(L) &= \exp(-(\lambda + \Sigma_m)L) + a \int_0^L \exp(-(\lambda + \Sigma_m)x) P_{BB}(L - x) \lambda dx \\
 &= \exp(-(\lambda + \Sigma_m)L) \left[1 + a \int_0^L \exp((\lambda + \Sigma_m)x) P_{BB}(x) \lambda dx \right]
 \end{aligned} \tag{5.29}$$

On differentiating Eq. (5.29) w.r.t. L we can write down the following differential equation

$$\frac{dP_{BB}(L)}{dL} = -[\lambda(1 - a) + \Sigma_m]P_{BB}(L) \tag{5.30}$$

Since for zero length the crossing probability is unity, we use this initial condition to obtain the solution

$$P_{BB}(L) = \exp[-\{\lambda(1 - a) + \Sigma_m\}L] \tag{5.31}$$

5.6.2 Integrands for the Collision Probabilities $P_{BF}(L)$ and $P_{BM}(L)$

Using arguments similar to those of the previous section, we can write down the following equation for $P_{BF}(L)$

$$\begin{aligned}
 P_{BF}(L) &= \int_0^L \exp(-(\lambda + \Sigma_m)x) [(1 - a) + aP_{BF}(L - x)] \lambda dx \\
 &= \frac{\lambda(1 - a)(1 - e^{-(\lambda + \Sigma_m)L})}{\lambda + \Sigma_m} \\
 &\quad + \lambda a e^{-(\lambda + \Sigma_m)L} \int_0^L \exp((\lambda + \Sigma_m)x) P_{BF}(x) \lambda dx
 \end{aligned} \tag{5.32}$$

On differentiating Eq. (5.32) w.r.t. L we obtain the following differential equation

$$\frac{dP_{BF}(L)}{dL} = \lambda(1-a) - [\lambda(1-a) + \Sigma_m]P_{BF}(L) \quad 5.33$$

$P_{BF}(L)$ clearly tends to zero as L tends to zero and hence the solution is

$$P_{BF}(L) = \frac{\lambda(1-a)(1 - e^{-(\lambda(1-a)+\Sigma_m)L})}{\lambda(1-a) + \Sigma_m} \quad 5.34$$

Using the sum rule on probabilities we can now write

$$P_{BM}(L) = \frac{\Sigma_m(1 - e^{-(\lambda(1-a)+\Sigma_m)L})}{\lambda(1-a) + \Sigma_m} \quad 5.35$$

5.6.3 Integrands for the Collision Probabilities $P_{FF}(L)$ and $P_{FM}(L)$

A fuel kernel can be anywhere in the interval 0 to L with equal probability i.e. $\frac{dx}{L}$.

The fuel-to-fuel probability consists of two parts. The self-collision probability is given by

$(\langle\tau_f\rangle - 1 + a)/\langle\tau_f\rangle$ (where $\langle\tau_f\rangle = \Sigma_f \bar{l}_f = \frac{4\Sigma_f R}{3}$) and the probability of escaping this kernel

and colliding in another kernel. The former is simply $(1-a)/\langle\tau_f\rangle$ while the latter is $P_{BF}(L-x)$. Multiplying various factors and integrating over x we get

$$\begin{aligned} P_{FF}(L) &= \int_0^L \frac{dx}{L} \left[\frac{\langle\tau_f\rangle - 1 + a}{\langle\tau_f\rangle} + \frac{1-a}{\langle\tau_f\rangle} P_{BF}(L-x) \right] \\ &= \frac{\lambda L (\langle\tau_f\rangle - (1-a))}{(\lambda L) \langle\tau_f\rangle} \\ &\quad + \frac{\lambda^2 (1-a)^2 [\{\lambda(1-a) + \Sigma_m\}L - 1 + e^{-(\lambda(1-a)+\Sigma_m)L}]}{(\lambda L) \langle\tau_f\rangle [\lambda(1-a) + \Sigma_m]^2} \end{aligned} \quad 5.36$$

Similar arguments give us the following expressions for $P_{FM}(L)$ and $P_{FB}(L)$

$$P_{FM}(L) = \frac{\lambda(1-a)\Sigma_m [\{\lambda(1-a) + \Sigma_m\}L - 1 + e^{-(\lambda(1-a)+\Sigma_m)L}]}{(\lambda L) \langle\tau_f\rangle [\lambda(1-a) + \Sigma_m]^2} \quad 5.37$$

$$P_{FB}(L) = \frac{\lambda(1-a)[1 - e^{-(\lambda(1-a)+\Sigma_m)L}]}{(\lambda L)\langle\tau_f\rangle[\lambda(1-a) + \Sigma_m]} \quad 5.38$$

5.6.4 Integrands for the Collision Probabilities $P_{MF}(L)$, $P_{MB}(L)$ and $P_{MM}(L)$

Finally, we write down these probabilities using reciprocity and sum rules. They can also of course be obtained using the arguments of Section [5.6.3](#).

$$P_{MF}(L) = \frac{\lambda(1-a)[\{\lambda(1-a) + \Sigma_m\}L - 1 + e^{-(\lambda(1-a)+\Sigma_m)L}]}{L[\lambda(1-a) + \Sigma_m]^2} \quad 5.39$$

$$P_{MB}(L) = \frac{(1 - e^{-(\lambda(1-a)+\Sigma_m)L})}{L[\lambda(1-a) + \Sigma_m]} \quad 5.40$$

$$P_{MM}(L) = \frac{\Sigma_m[\{\lambda(1-a) + \Sigma_m\}L - 1 + e^{-(\lambda(1-a)+\Sigma_m)L}]}{L[\lambda(1-a) + \Sigma_m]^2} \quad 5.41$$

The first thing we note is that the expressions for the various probabilities derived in this section agree with those obtained in Section [5.5](#). This gives us confidence in the method used for deriving these expressions. The other thing to be noted is that the above expressions represent probabilities for a given ray of length L in the mesh. Hence, they may not be used as such for the integrands in the calculation of collision probabilities by the routine. At the end of the routine, each of the (integrated) probabilities is divided by the product of volume and cross-section of the region of birth of the neutron. Since the integration is over the area perpendicular to the direction of flight, and the volume of a tube of a region is proportional to the chord length in that region, all integrands corresponding to region i to another region j or a

mesh boundary must be multiplied by the total macroscopic cross-section and chord length of region i . In the case of fuel this is $(\lambda L)\langle\tau_f\rangle$ while in the case of the moderator this is $\Sigma_m L$.

5.7 Corrections to the Distribution of Fuel Kernels due to the Coatings

In Sections [5.5](#) and [5.6](#), we assumed that the kernels are randomly distributed and hence the distribution of the kernels along any line is a Poisson point process. For the problem discussed in this thesis ($\frac{1}{\lambda} \cong 100\text{mm}$ is large as compared to a TRISO particle diameter that is 0.92mm or 0.66mm), the results obtained are perfectly adequate as we shall see in the next section. However, for sake of completeness of results and for applicability to larger sized kernels or higher packing densities, we sketch a method to obtain corrections to the Poisson distribution results.

The presence of coatings introduces a minimum gap equal to twice the total coating thickness (approximately the same as diameter of a TRISO particle). Hence, we replace the interval distribution[91] between two fuel kernels by

$$R_F(x) = 0 \text{ for } x < D \tag{5.42}$$

$$R_F(x) = \lambda \exp(-\lambda(x - D)) \text{ for } x > D \tag{5.43}$$

The above expression is justified as the kernels are small compared to the TRISO particle and hence rays passing through fuel kernels are almost diametrical through the TRISO particles. We will also need an interval distribution for the next interception starting from a point chosen at random (the random interval distribution). This is obtained by integrating the above expression and multiplying by the average number of kernels per unit length $\mu = \lambda/(1 + \lambda D)$

$$R_R(x) = \mu \text{ for } x < D \tag{5.44}$$

$$R_R(x) = \mu \exp(-\lambda(x - D)) \text{ for } x > D \quad 5.45$$

It may be recalled that the situation is similar to that of the statistical distribution of counts along the time axis in the presence of a non-extending dead time. Mueller[143] has given exact expressions for the distribution of the number of counts (kernels in our context) in a randomly chosen interval of length L . Using this distribution, it is possible to evaluate the surface-to-surface collision probability as in Eq. (5.28). With the probability $P_{BB}(L)$, obtained as above, we can derive other probabilities required. However, the evaluation is tedious and would lead to rather complicated expressions for this probability.

Hence, we look for a simpler alternative that would be easy to use in practice. Instead, we start from Eq. (5.29) and rewrite it for the present case. We paraphrase the argument used to obtain Eq. (5.29) for the present case. A neutron path may cross the medium without encountering a fuel kernel at all or after crossing one or more kernels. Since the starting point is randomly chosen, the probability of the former event is $\int_L^\infty R_R(x)dx$ and the probability of crossing without collision in this case is $\exp(-\Sigma_m L)$. Thus, the probability of reaching the mesh boundary is $\exp(-\Sigma_m L) \int_L^\infty R_R(x)dx$. In the latter of the two possibilities, let us assume that the first kernel is encountered at a distance between x and $x + dx$ for which the probability is $R_R(x)dx$. To this we multiply the probabilities of crossing the moderator length x and the kernel without collision viz. $\exp(-\Sigma_m x)$ and $a = \langle \exp(-\tau_f) \rangle$ and since the neutron is now at a distance $L - x$ from the outgoing boundary, but since we are starting from a kernel point and not a random point, we must now multiply it by $P_{BF}(L - x)$ and integrate over x . Here $P_{BF}(L)$ is the equivalent of $P_{BB}(L)$ with the starting point being at the surface of a fuel kernel rather than located randomly in the moderator. We thus have

$$P_{BB}(L) = \exp(-\Sigma_m L) \int_L^\infty R_R(x) dx + a \int_0^L \exp(-\Sigma_m x) R_R(x) P_{BF}(L-x) dx \quad 5.46$$

If instead of starting from a randomly chosen point in the moderator, we started from a point at the surface of the fuel kernel, we get on using an identical argument, the following equation for $P_{BF}(L)$

$$P_{BF}(L) = \exp(-\Sigma_m L) \int_L^\infty R_F(x) dx + a \int_0^L \exp(-\Sigma_m x) R_F(x) P_{BF}(L-x) dx \quad 5.47$$

We first note that the attenuation in the moderator is unaffected and hence we can try out the following factorization for $P_{BB}(L)$ and $P_{BF}(L)$

$$P_{BB}(L) = \exp(-\Sigma_m L) Q_R(L) \quad 5.48$$

$$P_{BF}(L) = \exp(-\Sigma_m L) Q_F(L) \quad 5.49$$

Where, the subscript R indicates starting from a random point and F indicates a point on the fuel surface. On substituting the forms (5.48) and (5.49) in (5.476) and (5.47) we can write down the following two equations for the functions $Q_R(L)$ and $Q_F(L)$.

$$Q_R(L) = \int_L^\infty R_R(x) dx + a \int_0^L R_R(x) Q_F(L-x) dx \quad 5.50$$

$$Q_F(L) = \int_L^\infty R_F(x) dx + a \int_0^L R_F(x) Q_F(L-x) dx \quad 5.51$$

Our task essentially amounts to solving the second of this pair of equations [Eq. (5.49)] and using the first to evaluate $Q_R(L)$ [Eq. (5.50)]. For $L < D$, $Q_F(L) = 1$, since another kernel cannot lie within one diameter of an earlier one. On introducing, the form of Eq. (5.45) for $R_F(x)$, Eq. (5.51) becomes

$$\begin{aligned}
Q_F(L) &= \exp(-\lambda(L - D)) [1 + a\{\exp(\lambda D) - 1\}] \\
&\quad + a\lambda \exp(-\lambda(L - D)) \int_D^{L-D} \exp(\lambda x) Q_F(x) dx
\end{aligned} \tag{5.52}$$

for $L > 2D$, and

$$Q_F(L) = \exp(-\lambda(L - D)) + a\{1 - \exp(-\lambda(L - D))\} \tag{5.53}$$

for $D < L < 2D$

It is clear from Eq. (5.53) that it is possible to obtain a recursive solution for Eq. (5.52) in successive intervals $2D < L < 3D, 3D < L < 4D$ and so on by substituting previously obtained solutions. For example, for $2D < L < 3D$ we obtain

$$\begin{aligned}
Q_F(L) &= \exp(-\lambda(L - D)) + a\{\exp(-\lambda(L - 2D)) - \exp(-\lambda(L - D))\} \\
&\quad + a^2\{1 - \exp(-\lambda(L - 2D)) - \lambda(L - 2D)\exp(-\lambda(L - 2D))\}
\end{aligned} \tag{5.54}$$

However, it is clear that the expressions will get more and more complicated as we proceed. However, we observe from Eqs. (5.53) and (5.54) that the function $Q_F(L)$ has discontinuities in various derivatives at $D, 2D, 3D$, etc. Thus while $Q_F(L)$ is itself continuous at $L = D$, its first derivative is discontinuous. At $L = 2D$, the function and its first derivative are continuous but the second derivative is discontinuous and so on. On differentiating Eq. (5.52) with respect to L we obtain

$$Q'_F(L) = -\lambda Q_F(L) + a\lambda Q_F(L - D) \tag{5.55}$$

Since $Q'_F(L)$ exist and is continuous for all $L > D$, at least for to $L > 2D$, we can write

$$Q'_F(L) = -\lambda(1 - a)Q_F(L) - a\lambda D Q'_F(L) \tag{5.56}$$

The solution is

$$Q_F(L) = C \exp\left(\frac{-\lambda(1-a)L}{1+a\lambda D}\right) \quad 5.57$$

The constant can be written by using the initial condition at $L = 2D$ from Eq. (5.53). However, on doing this it is seen that to the first order in λD the solution is not different from what is obtained by using the initial condition at $L = D$ viz. $Q_F(L) = 1$. Hence, we obtain finally for $L > D$,

$$Q_F(L) = \exp\left(\frac{-\lambda(1-a)(L-D)}{1+a\lambda D}\right) \equiv \exp(-\alpha(L-D)) \quad 5.58$$

Moreover, we have already seen that for $L < D$,

$$Q_F(L) = 1 \quad 5.59$$

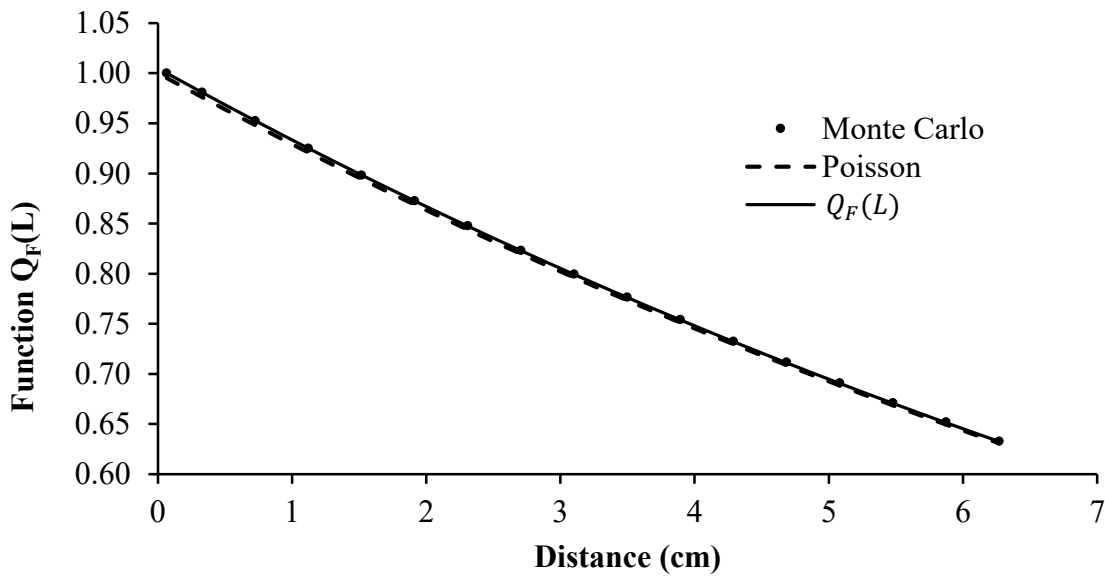


Figure 5-2: Variation of $Q_F(L)$ with distance (L): Comparison between Eq. (5.58) and Monte Carlo for smaller kernel radius (0.012cm) and lower kernel density (15000 Kernels). The result based on the assumption of Poisson statistics is also included.

The variation of the function $Q_F(L)$ with L as obtained by Eqs. (5.58) and by Monte Carlo calculations is shown in Figure 5-2 at low packing fraction (~ 0.022) of the TRISO particles and for the smaller kernel radius (0.12mm). The mean distance between any two kernels ($\frac{1}{\lambda} \cong 96\text{mm}$) for this configuration and it is very large as compared to the TRISO diameter 0.66mm. It can be seen from Figure 5-2 that at low packing of TRISO and for small kernels the Poisson statistics shows very good agreement with that of the Eq. (5.58) and with the Monte Carlo results as well. In Figure 5-3, we show a variation of the function $Q_F(L)$ with L as obtained by Eqs. (5.58) and by Monte Carlo calculations for $\frac{1}{\lambda} \cong 11\text{mm}$ and a TRISO particle diameter that is 1.0mm corresponding to a large value of the kernel radius (0.25 mm) and a high value of packing fraction (0.24).

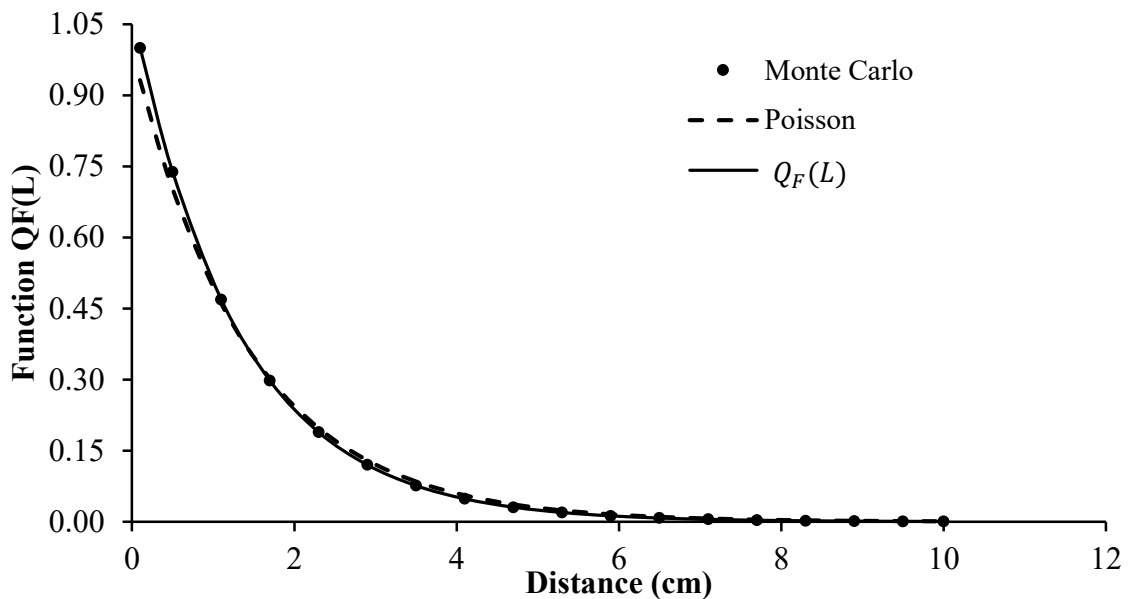


Figure 5-3: Variation of $Q_F(L)$ with distance (L): Comparison between Eq. (5.58) and Monte Carlo for larger kernel radius (0.025cm) and higher kernel density (30000 Kernels). The result based on the assumption of Poisson statistics is also included.

For the sake of comparison, we also show the function obtained assuming Poisson statistics. It is clear that while Poisson statistics gives a fair approximation to the Monte Carlo results, Eq. (5.58) shows excellent agreement. Now, we can obtain the probability for the random interval case and $P_{BB}(L)$ by substituting the expression for $Q_F(L)$ Eq. (5.58) in Eq. (5.46)-(5.47) and using Eqs. (5.44) and (5.45). For the three cases, viz. $L < D$, $D < L < 2D$ and $L > 2D$ we respectively obtain.

$$P_{BB}(L) = \exp(-\Sigma_m L) \left[\mu(D - L) + \frac{\mu}{\lambda} + a\mu L \right] \quad 5.60$$

$$P_{BB}(L) = \exp(-\Sigma_m L) \left[\frac{\mu e^{-\lambda(L-D)}}{\lambda} + \frac{a\mu}{\alpha} (1 - e^{-\alpha(L-D)}) + \frac{a\mu}{\lambda} (1 - e^{-\lambda(L-D)}) + a\mu(2D - L) \right] \quad 5.61$$

$$P_{BB}(L) = \exp(-\Sigma_m L) \left[\frac{\mu e^{-\lambda(L-D)}}{\lambda} + \frac{a\mu}{\alpha} (e^{-\alpha(L-2D)} - e^{-\alpha(L-D)}) + \frac{a\mu}{\lambda} (e^{-\lambda(L-2D)} - e^{-\lambda(L-D)}) + \frac{a\mu}{\lambda - \alpha} (e^{-\lambda(L-2D)} - e^{-\lambda(L-D)}) \right] \quad 5.62$$

The probability $P_{BM}(L)$ is obtained by multiplying the above expressions for $P_{BB}(L)$ by $\Sigma_m dx$ and integrating over x from 0 to L . We thus write

$$P_{BM}(L) = \Sigma_m \int_0^L P_{BB}(x) dx \quad 5.63$$

We assume that $L > 2D$, as this is practically the only important case of interest. The integration is carried out by splitting the range over the intervals $[0, D]$, $[D, 2D]$ and $[2D, L]$.

The moderator-to-moderator probability $P_{MM}(L)$ can be obtained by averaging $P_{BM}(x)$ over the length L of the interval. This implies a double integration of $P_{BB}(x)$ as shown below

$$P_{MM}(L) = \frac{1}{L} \int_0^L P_{BM}(x) dx = \frac{\Sigma_m}{L} \int_0^L \int_0^x P_{BB}(x') dx' dx \quad 5.64$$

Where, we have used Eq. (5.63). By changing, the order of integration of the two variables $P_{MM}(L)$ can be written as a single integration as follows

$$P_{MM}(L) = \frac{\Sigma_m}{L} \int_0^L (L-x) P_{BB}(x) dx = P_{BM}(L) - \frac{\Sigma_m}{L} \int_0^L x P_{BB}(x) dx \quad 5.65$$

We again assume as before that $L > 2D$ and carry out the integration by splitting the range over the intervals $[0, D]$, $[D, 2D]$ and $[2D, L]$. The final expressions for $P_{BM}(L)$ and $P_{MM}(L)$ are given in APPENDIX-B. Other probabilities can be obtained using reciprocity and sums rule.

5.8 Results and Discussions

The treatment of double heterogeneity in the resonance region was incorporated in an earlier version of the code as outlined in Sections 4.4 and 5.1. Results of analysis of the OECD benchmark[105] (phase 1 and phase 5) were presented in Ref.[135]. In this section, we present results of analysis of benchmarks for validation of the methodology described in the previous section. The modified expressions for the collision probabilities in the random heterogeneous medium (fuel kernels dispersed in a graphite matrix) described in Section 5.5 were incorporated in the code BOXER3. This allows us to treat the double heterogeneity for fuels having large cross-sections in the thermal region. In particular, it applies to fuels having a high concentration of plutonium. We have studied a number of Pu fueled HTR benchmarks using the modified code and the results are discussed in the following sub sections.

5.8.1 Analysis of an OECD Benchmark

The details of benchmark definitions are provided by the Organization for Economic Cooperation and Development, Nuclear Energy Agency (OECD NEA), Nuclear Science Committee, Working Party on the Physics of Plutonium Fuels and Innovative Fuel Cycles[105]. The specifications of fuel pebbles and coated particles of these benchmarks used in the present study are reproduced in [APPENDIX-A](#). The benchmark consisting of an infinite array of pebble containing plutonium fuels, described in phase 2a, has been used for validation of BOXER3 code using the 69 and 172 group WIMSD-formatted library based on evaluated nuclear data files recommended by WLUP participants [38].

Table 5-1 Results of BOXER3 code with new method of self-shielding and comparison with other codes

Pebble Model		Boxer		MCNP	WIMS9	APPOLO
		JEF2.2	IAEA	ENDF-B/VI	JEF2.2	JEF2.2
		172g	172g	Point data	172g	172g
Homogeneous		1.22835	1.20864	1.4573 ± 0.001	1.46154	1.46369
Doubly heterogeneous (present work with 2,3,4 meshes in fuel)	2	1.46876	1.45147			
	3	1.46868	1.45159			
	4	1.46882	1.45150			
Doubly heterogeneous (based on Dancoff)		1.22849	1.20897			

Table 5-1 shows a comparison of results obtained using BOXER3 and those of other contributors using various codes. As was observed in Ref.[135], the equivalence principle / Dancoff factor based methodology used for double heterogeneity treatment in the resonance region of Pu fueled pebble bed HTRs, showed no significant improvement in the results which showed gross under prediction of k_{∞} . This is clearly seen in Table 5-1. The BOXER3 result for the homogeneous pebble model and the heterogeneous model with conventional resonance treatment based on the Dancoff and Bell corrections have no significant difference in the calculated values of the k_{∞} . This is mainly due to fact that the standard resonance treatment, based on the equivalence principle and resonance tables, using the WIMS-D library does not account for the variation of the cross-section around the resonances at 0.3 eV and 1.0 eV of Pu. This problem has been the principal motivation for developing the present method.

However, with the implementation of the modified expressions for collision probabilities in a heterogeneous medium, derived in Section 5.5 or 5.6, we see a substantial improvement in the results. In the heterogeneous model the meshes in the heavy scatterer, the coolant and the graphite moderator regions are ordinary homogeneous meshes, whereas the meshes falling in the fuel zone of the pebble are split into two sub meshes viz. fuel sub mesh and matrix sub mesh.

The BOXER3 results shown in Table 5-1 are computed with two, three and four meshes in the fuel zone. The results show that k_{∞} is insensitive to the number of meshes in the fuel zone for this particular problem. It can also be seen from Table 5-1 that BOXER3 results using 172 group IAEA (mostly based on ENDF-B/VI data) library show closer agreement with the MCNP result based on ENDF-B/VI point data, the difference being about 0.4 % whereas with JEF2.2 library the difference is larger about 0.8%. Likewise, the BOXER3 results with the 172

group JEF2.2 library agree better with the APPOLO2, and WIMS9 values (the difference being about 0.34%, 0.49% respectively) than with the results with the 172 group JEF2.2 library. This is due to the use of the same library (JEF2.2) with these two codes. Certainly, there is a tremendous improvement over the results obtained by homogenizing the fuel kernels and graphite matrix with and without the heterogeneous resonance treatment.

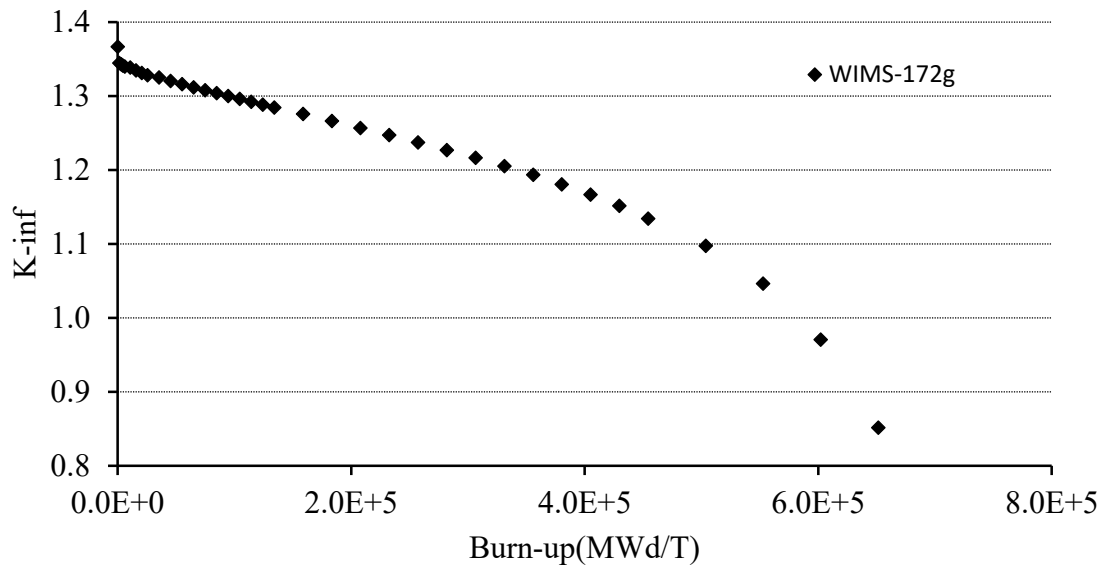


Figure 5-4: Variation of k_{∞} as a function of fuel burn-up for the benchmark defined in the phase 2a.

Burnup of the benchmark cell was studied up to 65000 MWd/ton. The variation of k_{∞} is shown in Figure 5-4. A comparison of our results for the variation of the concentrations of the isotopes of Pu, Am, and Cm with burnup with benchmark (WIMS9) data is shown in Figure 5-5. The average percentage difference between the ^{239}Pu , ^{240}Pu and ^{241}Pu concentrations computed by BOXER code and the reference code WIMS9 is of the order of 0.38%, 0.02% and 0.24% respectively.

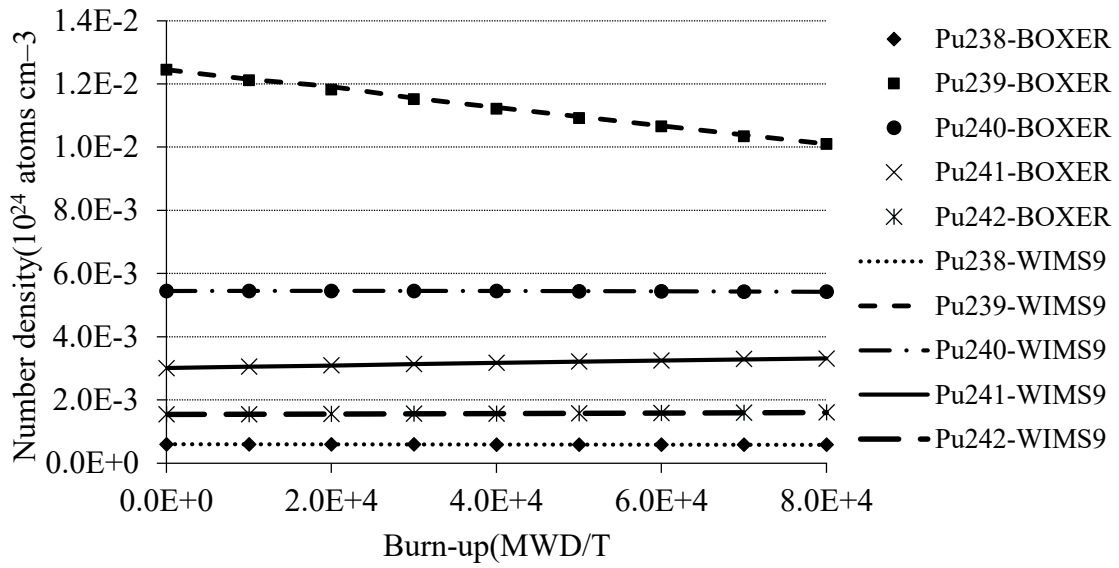


Figure 5-5: Variation of Plutonium isotopes density as a function of fuel burn-up for the benchmark defined in the phase 2a.

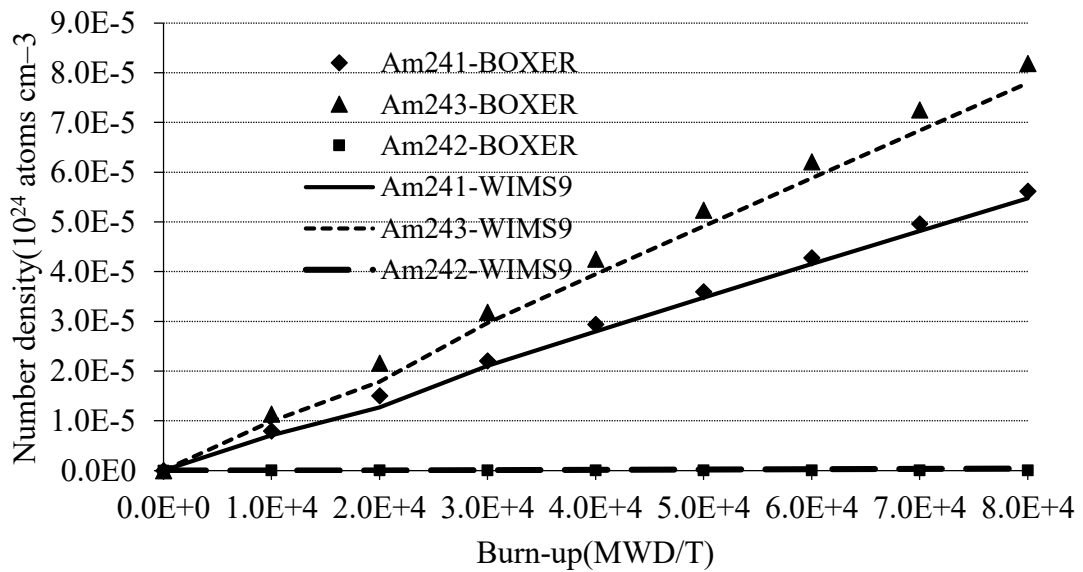


Figure 5-6: Variation of Americium isotopes density as a function of fuel burn-up for the benchmark defined in the phase 2a.

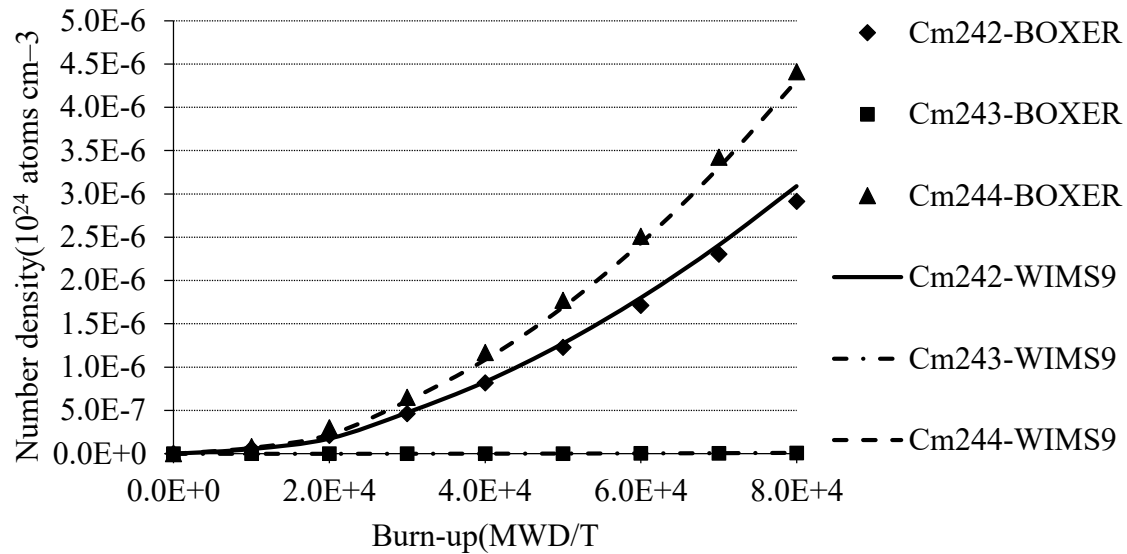


Figure 5-7: Variation of Curium isotopes density as a function of fuel burn-up for the benchmark defined in the phase 2a.

Again, the good agreement lends confidence in the new methodology for treating double heterogeneity in the thermal region for the case of plutonium fuels.

5.8.2 Analysis of Other Benchmarks

Another validation of the proposed method has been carried out for the pebble lattice cell problems discussed in the thesis of Bende [134]. We have studied four cases using BOXER3. In the first two cases, 1 gram of plutonium is loaded per pebble [by packing 25829 and 19406 TRISO particles with kernels of radius 0.01cm and 0.011cm respectively]. The other two cases have 2-gram plutonium loaded per pebble [by packing 51659 and 38812 TRISO particles with kernels of radius 0.01cm and 0.011cm respectively]. The geometrical specifications of the pebble and TRISO particles are taken from Ref.[134]. A uniform temperature of 600K is taken over the pebble for all the cases. A comparison of BOXER3

results with the reference [134] results obtained from the MCNP code for these cases is presented in Table 5-2.

Table 5-2 Comparison of k_{∞} of pebble with MCNP results

Pu mass→		1g per pebble		2g per pebble	
Codes	Library	Kernel Radius (cm)		Kernel Radius (cm)	
		0.01	0.011	0.01	0.011
BOXER	Jef2.2-172group	1.4106	1.4216	1.2426	1.2550
MCNP	Jef2.2 Point Data	1.403	1.418	1.233	1.247
% difference		0.54	0.25	0.78	0.64

Here the agreement with MCNP results is somewhat similar to that of the previous benchmark, the maximum difference is about 0.78%. The differences must be attributed to the different modeling methods used in the codes. The collision probability method used in BOXER3 takes into account the fact that fuel kernels are randomly distributed in the graphite matrix based on a Poisson distribution. Whereas in the reference analysis with MCNP, a simple cubic lattice cell [with each of the unit cells consisting of a fuel kernel followed by coating layers], is used to represent the random distribution of kernels. We have observed in our earlier studies, that a difference of a few hundred pcm can be observed between lattice and randomized distribution of fuel kernels in HTR lattice cell calculations.

5.9 Conclusions

A new method for thermal neutron transport in the random heterogeneous lattice cells of HTRs containing high concentration Pu fuel as is the case in Pu burning HTRs has been

described in the chapter. The method is based on the collision probability approach. Exact expressions for collision probabilities in the random heterogeneous medium have been obtained by two independent methods under realistic assumptions of the statistical distribution of fuel kernels in the graphite matrix. Results based on the use of these formulae in the lattice code BOXER3 show generally good agreement HTR benchmarks involving Pu fuel.

The method developed in this chapter does not make use of any free parameters such as the Bell factor used in the equivalence principle approach for resonance treatment. This is a major advantage and hence, for calculating resonance absorption in HTR cells, the method could be used in conjunction with the subgroup approach or ultra-fine group approach. The method also suggests a new Monte Carlo approach to solving transport problems in High Temperature Reactors that is a subject of [Chapter 6](#).

Chapter 6 **A NEW APPROACH TO MONTE CARLO IN HTRs: sampling kernel position during a random walk process**

In this chapter, we use some of the collision probability formulae, derived in Chapter 5, to construct a fast Monte Carlo algorithm for high temperature reactors applications. This chapter discusses the theoretical basis of the Monte Carlo algorithm, its implementation for the case of a lattice cell with a multigroup library and the results obtained.

6.1 Introduction

Monte Carlo methods are increasingly being used for obtaining solutions to criticality and other problems of reactor physics due to their ability to exactly handle complex variation of cross-sections with energy and geometrical layout of various materials[106], [144], [145]. While this is true in situations where the material distribution is precisely defined, it may not always be the case. One such example is when the core has undergone burnup and there is a continuous variation of the fuel composition. Clearly some modelling of the variation of fuel composition is necessary as the exact variation is neither available nor is it practically feasible to model such a variation. A fairly common form of modelling is to divide the fuel into a number of burnup zones and use the flux tallies in these zones to obtain the average burnup in each zone and subsequently use this average fuel composition in each zone [146], [147]. Another example is when the distribution of materials in the reactor is statistical as is the case

in high temperature reactors (HTRs), that is the subject of the present thesis. The core of HTRs consists of thousands of fuel elements (pebbles or small slugs called compacts) each of which in turn consists of thousands of tiny fuel kernels dispersed randomly in a graphite matrix. Since it is not permissible to replace this dispersion of tiny fuel kernels by a homogeneous mixture (as it often results in unacceptably large errors), it is necessary to model the variation of material composition of such a reactor.

Various methods have therefore been used to explicitly model the fuel kernels in HTRs by the Monte Carlo method. One of the most common methods is to replace the random distribution of fuel kernels by a regular lattice arrangement and use the lattice features of Monte Carlo codes[148]. This type of modelling has two problems. The first is that detailed tracking through the lattice is time consuming. The other problem is that the calculated K_{eff} is significantly different from that of a random distribution. Another approach is to use a lattice but to randomly locate the fuel particle within each cell [148], [149], or a more detailed approach [150] involving generation of a random medium and carrying out tracking through it. These approaches partially or fully mitigate the second problem but not the first. Finally, there is the option of using the delta algorithm [151], [152] in place of detailed tracking after modelling the fuel arrangement in one of aforementioned ways. However, the delta algorithm slows down whenever there is any material with a very large cross-section. Moreover, it does not permit calculations of the track length estimator of the flux.

This chapter describes a new approach to the modelling of this complex arrangement of the fuel in the HTR. The method uses a new technique for sampling the next collision point that avoids having to prepare a model of the arrangement of fuel particles and tracking in detail the neutrons through this medium. The method draws upon various formulae for collision probabilities in random media derived in [Chapter-5](#)[153]. It may be emphasized that the present

method is not an exact representation of the system, but like the methods described above, is a way of modelling the spatial distribution of materials in the HTR core. Nevertheless, the new method has the statistical element inherent in it and is expected to be faster than the one involving detailed tracking methods described above. At the same time, the proposed new method does not have any of the limitations of the delta algorithm that is commonly used to avoid detailed ray-tracing through the problem geometry required in tracking particles in Monte Carlo.

The sampling methods used for tracking neutron histories are described in Section [6.2](#). Although the presentation is for pebble bed reactors, it may be used for prismatic type reactor lattice and core calculations as well. To demonstrate the method, we describe its implementation for solving the criticality problem of a pebble-bed lattice cell using a multigroup library in Section [6.4](#). The method can be easily extended to more general problems with continuous energy data and to core calculations in pebble-bed reactors as described in Section [6.5](#). Results and comparisons with other methods are presented in Section [6.6](#). In Section [6.7](#), we present a summary of the work and the conclusions drawn.

6.2 Theoretical Basis of the Method: The new algorithm for neutron tracking for Poisson statistics of kernels

6.2.1 The Next Collision of a Neutron Starting at a Point in the Graphite Matrix

In [Chapter 5](#), we obtained an expression giving the attenuation (probability of surviving up to a distance x) of neutrons initially at a point chosen randomly within the graphite matrix of the fuel zone of a pebble of a pebble bed HTR. The derivation was based on the assumptions that the fuel kernels are very small compared to a mean free path in graphite, and are distributed

completely randomly inside the graphite matrix (Poisson statistics). It is assumed that the distributions of the intervals intercepted by any chord in the medium follows a renewal process, i.e., the successive intercept length distributions are independent of one another. It is also assumed that the outer coatings of a TRISO particle that surround the fuel kernel have been homogenized with the graphite matrix and hence the fuel zone medium consists of tiny fuel kernels embedded randomly in the homogenized graphite matrix. We show how some of these assumptions can be relaxed in the next Section [6.2.2](#).

Accordingly, the probability of a neutron not colliding up to a distance x is given by

$$P(x) = \exp[-\{\lambda(1 - a) + (1 - \lambda\bar{l})\Sigma_m\}x] \quad 6.1$$

Where,

\bar{l} is the mean chord length in a sphere

a_k is the fuel kernel radius

$\lambda = n\pi a_k^2$; n is kernel density

Σ_m is moderator total cross-section

Σ_f is fuel total cross-section

$$a = \frac{1}{\pi a_k^2} \int_0^{a_k} 2\pi r dr e^{-2\Sigma_f \sqrt{a_k^2 - r^2}} = \frac{1 - e^{-2a_k \Sigma_f} (1 + 2a_k \Sigma_f)}{2a_k^2 \Sigma_f^2} \quad 6.2$$

Note that Eq. (6.1) is slightly different from the equation obtained in Ref.[153] in that it includes a small correction factor $(1 - \lambda\bar{l})$ to the moderator cross-section to compensate for the assumption of an infinitesimally small kernel in the derivation of the equation in Ref. [153].

The ending point could be anywhere. By considering a distance $x + dx$

$$P(x + dx) = \exp[-\{\lambda(1 - a) + (1 - \lambda\bar{l})\Sigma_m\}(x + dx)] \quad 6.3$$

And subtracting Eq. (6.1) from (6.2) we obtain the collision probability in the distance interval x to $x + dx$

$$P(x)dx = \exp[-\{\lambda(1 - a) + (1 - \lambda\bar{l})\Sigma_m\}x]\{\lambda(1 - a) + (1 - \lambda\bar{l})\Sigma_m\}dx \quad 6.4$$

We interpret the above equation as follows. Starting from a point in the graphite matrix part of the fuel zone, the distance to the next collision will be sampled using the above distribution. The probability that the collision takes place in a fuel kernel or in the graphite matrix are then respectively given by

$$\frac{\lambda(1 - a)}{\lambda(1 - a) + (1 - \lambda\bar{l})\Sigma_m} \quad 6.5$$

$$\frac{(1 - \lambda\bar{l})\Sigma_m}{\lambda(1 - a) + (1 - \lambda\bar{l})\Sigma_m} \quad 6.6$$

In Section 6.4.1, we describe details of the implementation of the location of the collision based on Eqs. (6.4) - (6.6). We also describe a somewhat different procedure in Section 6.4 that is based on the same philosophy but does not explicitly use the above equations. This alternative procedure is somewhat more convenient for finding track length estimates.

6.2.2 The next collision of a neutron starting at a point in the fuel kernel

Consider a fuel kernel and a coordinate system in which the centre of the kernel is at the origin. Let the neutron start at a point $\mathbf{r} = (x, y, z)$ inside the kernel in the direction $\mathbf{\Omega} = (\Omega_x, \Omega_y, \Omega_z)$. If the neutron is an initial source neutron, we determine $\mathbf{\Omega}$ by sampling from an isotropic distribution and \mathbf{r} by sampling from a uniform distribution within the volume of the kernel. If

the neutron is a secondary neutron due to collision of a neutron in the fuel kernel, then determination of the collision and direction is done as discussed in Section [6.2.3](#).

The point of intersection of the neutron trajectory is given by solving the equations of the trajectory and the sphere.

$$\mathbf{R}^2 = a_k^2 \quad 6.7$$

$$\mathbf{R} = r + s \boldsymbol{\Omega} \quad 6.8$$

i.e. the positive root of Eq. (6.9)

$$s^2 + 2r \cdot \boldsymbol{\Omega} s - (a_k^2 - r^2) = 0 \quad 6.9$$

given by Eq. (6.10)

$$s = \sqrt{(r \cdot \boldsymbol{\Omega})^2 + (a_k^2 - r^2)} - r \cdot \boldsymbol{\Omega} \quad 6.10$$

s gives the maximum distance travelled within the fuel kernel. This suggests the following sampling scheme. We sample a distance given by $D = -\frac{1}{\Sigma_f} \ln \xi$. If $D < s$, the neutron again collides in the fuel kernel and the process can be repeated for the secondaries arising from the collision. If $D > s$, the neutron escapes the kernel and enters the graphite matrix, in which case we use the sampling scheme of Section [6.2.1](#).

6.2.3 Sampling of the collision point in a fuel kernel

Two cases arise. The first in which the starting point is within the same kernel. This is dealt with the method described in Section [6.2.2](#). If the starting point is outside the kernel in which next collision occurs, we use the following method.

We assume that the centre of the kernel in which the collision occurs is distributed with a probability proportional to its distance from the trajectory of the colliding neutron up to a

distance equal to its radius. This follows from the probability being proportional to the area presented perpendicular to the direction of the trajectory. With this assumption, the cylindrical coordinates (ρ, z) of the point of collision within the sphere are obtained by the following sampling scheme.

Determine $\rho = a_k \sqrt{\xi_1}$ and accept if

$$\xi_2 < (1 - \exp(-2\Sigma_f \sqrt{a_k^2 - \rho^2})) / (1 - \exp(-2\Sigma_f a_k)) \quad 6.11$$

The rejection condition is due to the fact that we are considering neutrons that have collided in the kernel whose probability depends upon the track length within the sphere that in turn depends upon the distance of the trajectory from the centre.

Determine z by sampling x from the distribution

$$\frac{\exp(-\Sigma_f x) \Sigma_f}{(1 - \exp(-2\Sigma_f \sqrt{a_k^2 - \rho^2}))} \quad 6.12$$

and write

$$z = x - \sqrt{a_k^2 - \rho^2} \quad 6.13$$

Transforming to the coordinates $r = (x, y, z)$ relative to a coordinate system that is parallel to a fixed coordinate system and whose origin is located at the centre of the fuel kernel under consideration is in general fairly complicated just as is the transformation of the new direction after scattering. Fortunately, this is not required. We note from the equation giving the distance travelled by the neutron in the kernel that this depends upon r^2 and $r \cdot \Omega$. Without loss of generality, we may assume that the centre of the sphere is in the xz plane of the frame moving with the neutron before the collision. The standard method for sampling the direction of the neutron in the case of anisotropic scattering involves sampling the direction vector components in this frame and transforming to the fixed frame as follows

$$\begin{pmatrix} \mu_f \\ \eta_f \\ \xi_f \end{pmatrix} = \begin{pmatrix} \frac{uv}{\sqrt{1-w^2}} & -\frac{v}{\sqrt{1-w^2}} & u \\ \frac{vw}{\sqrt{1-w^2}} & \frac{u}{\sqrt{1-w^2}} & v \\ -\sqrt{1-w^2} & 0 & w \end{pmatrix} \begin{pmatrix} \mu_s \\ \eta_s \\ \xi_s \end{pmatrix} \quad 6.14$$

where u, v, w are the components of the initial direction with respect to the fixed frame and the vectors with subscripts f and s referring to the components of the outgoing direction in the fixed and moving (sampling) frames respectively. ξ_s is sampled as per the scattering law and the other components are obtained by sampling the azimuthal angle uniformly between 0 and 2π and using

$$\mu_s = \sqrt{1 - \xi_s^2} \cos \varphi \quad 6.15$$

$$\eta_s = \sqrt{1 - \xi_s^2} \sin \varphi \quad 6.16$$

Since the components of the collision point relative to the sphere centre are available in the moving frame, we can write the scalar product $\mathbf{r} \cdot \boldsymbol{\Omega}$ as

$$\mathbf{r} \cdot \boldsymbol{\Omega} = \rho \mu_s + z \xi_s \quad 6.17$$

and

$$r^2 = \rho^2 + z^2 \quad 6.18$$

For the special case of isotropic scattering, calculation of the components of the scattered direction as well as the (maximum) distance that can be traversed in the sphere is simple. Since the initial direction is unimportant in isotropic scattering, we can sample the components of the scattered direction in any system of coordinates. While the transformation will change the components of an individual direction vector, it does not change the distribution of directions. Thus, suppose we sample the components of the outgoing direction in the fixed

system of coordinates as for an isotropic distribution. Such a distribution has the property that the cosine of the angle relative to any direction is distributed uniformly in the interval $[-1, 1]$.

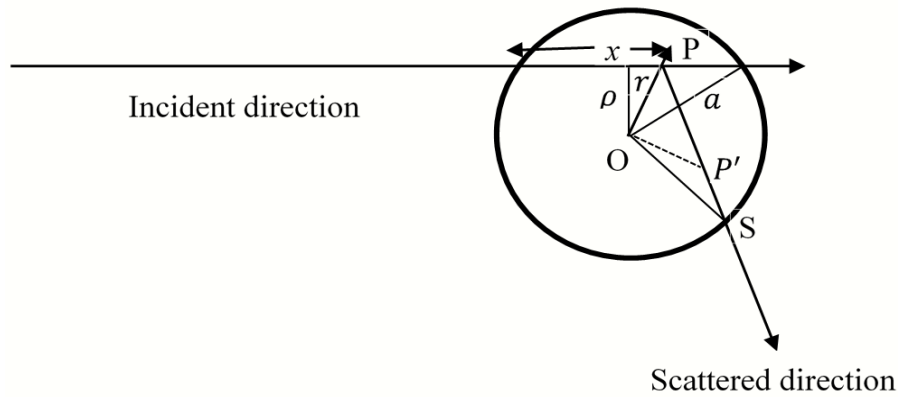


Figure 6-1: The cylindrical coordinates (ρ, z) of the point of collision within the fuel kernel.

Further the distance (s) to the surface of the fuel kernel depends on the radial distance of the collision point from the center (r) and the cosine of the angle (μ) that the outgoing direction makes with the radial vector of the point of collision [as per Eq. (6.19) and shown in Figure 6-1]. Now r can be determined using the (ρ, z) coordinates as simply

$$r^2 = \rho^2 + z^2 \quad 6.19$$

Since the isotropic distribution of particles emitted from the collision point necessarily has a distribution of μ that is uniform in the interval $[-1, 1]$, we obtain μ by sampling it from this distribution. The distance s is then determined by solving the triangle OPS as follows

$$a_k^2 = r^2 + s^2 + 2rs\mu \quad 6.20$$

Where, s is obtained as the positive root of this equation as

$$s = -\mu r + \sqrt{a_k^2 - r^2(1 - \mu^2)} \quad 6.21$$

Once the distance to the surface of the kernel has been determined, the distance travelled in the fuel kernel medium is determined and if it happens to be larger than the distance

to the surface, the particle exits the kernel into the moderator and the next distance is sampled using Eqs. (6.4) - (6.6). However, if the collision is within the same kernel, one must determine the point of collision which is at a point on the neutron path [at the end of the dotted line]. Since the initial distance from the centre (r), the distance travelled by the neutron (D) and the cosine of the angle between them are known, the distance of the point of collision from the centre (r'), is easily calculated using Figure 6-1 and Eq. (6.22).

$$r'^2 = r^2 + d^2 + 2dr\mu \quad 6.22$$

The other quantities viz., ρ' and z' are now easily determined as follows

$$\rho' = r\sqrt{1 - \mu^2} \quad 6.23$$

$$z' = \sqrt{r'^2 - \rho'^2} \quad 6.24$$

An approximate alternative approach that avoids tracking within the kernel

Since the kernel is small, it is expected that there would be at the most one or two successive collisions in it. If the first collision is in an energy region where the cross-section is not very large, but scattering leads to an energy in which the cross-section is large, we may have a second collision. Otherwise, the probability of a second collision is rather small. In the former case, the neutron will most probably undergo absorption (fission or capture) and hence the probability of a scattering leading to an energy where the cross-section is high is extremely small. This observation enables us to introduce a simpler alternative procedure that completely avoids tracking in the kernel.

For the case of isotropic scattering, using Eq. (6.21) and the assumption that the direction of emission after collision and the quantity μ are not correlated, we can write the following expression for the probability of escape from the kernel

$$P_{esc}(r) = \int_{-1}^1 \exp \left[-\Sigma_f \left(\sqrt{a_k^2 - r^2(1 - \mu^2)} - \mu r \right) \right] d\mu \quad 6.25$$

The integral is easily evaluated by substituting

$$l = \left(\sqrt{a_k^2 - r^2(1 - \mu^2)} - \mu r \right) \quad 6.26$$

Or

$$\mu = \frac{a_k^2 - r^2 - l^2}{2rl} ; d\mu = \left(-\frac{1}{2r} - \frac{a_k^2 - r^2}{2rl^2} \right) dl \quad 6.27$$

Which finally gives

$$P_{esc}(r) = \frac{1}{2\Sigma_f r} \left[\exp[-\Sigma_f(a_k - r)] - \exp[-\Sigma_f(a_k + r)] \right] + \frac{a_k + r}{2r} E_2[\Sigma_f(a_k - r)] - \frac{a_k - r}{2r} E_2[\Sigma_f(a_k + r)] \quad 6.28$$

Where, $E_2(r)$ is the second order exponential integral.

This way one computes $P_{esc}(r)$ and checks whether the next collision is in the (same) kernel or not. In the latter case, no second collision is recorded in the (same) kernel and the distance to the next collision etc. are sampled as per Eqs. (6.4) - (6.6). In the former case, a second collision is recorded in the same kernel without transporting the particle (i.e. without changing the local or global coordinates). The energy and direction of any secondary originating from the second collision are computed and its subsequent transport is treated as per Eqs. (6.4) - (6.6).

A similar method can be used for the case of anisotropic scattering. However, the expression for the escape probability involves complicated integrals. Hence, it is best to calculate the distance s to the boundary using Eqs. (6.10), (6.17) and (6.18) [after having

sampled the direction variables (μ_s, η_s, ξ_s)] and check whether there is a second collision within the fuel kernel [i.e. whether $\xi < \exp(-\Sigma_f s)$] or that there is no second collision [i.e. whether $\xi > \exp(-\Sigma_f s)$]. The method may be used for the case of isotropic scattering as well, in case computation of the E_2 function is deemed to be too complicated or expensive.

6.3 The new algorithm for neutron tracking for coating corrected Poisson statistics of kernels

In Section [6.2](#), with regard to the third assumption we showed how to sample collision points in the case of Poisson statistics as regards the distribution of kernels. This would be exact if the kernel (or rather the entire TRISO particle) is small enough to be treated as a point object. We had seen in Ref. [153] that for the typical kernel densities, the assumption is quite good. However, a better approximation is to account for the TRISO particle coating that is typically 1-2 mm in diameter due to which two kernels cannot lie within one TRISO particle diameter. This changes the distribution of kernels along a line in the medium from Poisson to a ‘dead time corrected Poisson’. While such a distribution continues to have the character of a renewal process, there are two types of interval distributions of encountering a kernel viz., the random origin interval and the interval originating at a fuel kernel. Similarly, there are two types of probabilities of reaching a distance L without collision starting from a random point of origin and a point at a fuel kernel. In this section, we deduce algorithms for sampling the distance to the next collision starting from a random point in the moderator and from a point in the fuel kernel.

6.3.1 The next collision of a neutron starting at a randomly chosen point in the graphite matrix

We do this calculation in parts. The first part involves determining the distance to the first fuel kernel along the neutron flight. In the second part, we check whether the neutron collides in the graphite before the kernel or in the first kernel. If yes, the flight is terminated at the collision point. Else, the flight continues and the collision point is determined based on the distribution

$$\exp(-\Sigma_m L) \tag{6.29}$$

for $L < D$

$$\exp\left(-\left(\Sigma_m + \frac{\lambda(1-a)}{1+a\lambda D}\right)(L-D)\right) \tag{6.30}$$

for $L > D$

The distance to the first kernel is determined by sampling from the distribution¹¹

$$R_R(x) = \mu_k \quad \text{for } x < D \tag{6.31}$$

$$R_R(x) = \mu_k \exp(-\lambda(x-D)) \quad \text{for } x > D \tag{6.32}$$

Where, $\mu_k = \frac{\lambda}{1+\lambda D}$

The first kernel is within $[0, D]$ if $\xi_1 < \mu_k D$ and outside otherwise, where ξ_1, ξ_2 are two uniformly distributed random numbers in $[0, 1]$. If the kernel is within $[0, D]$, its distance from the starting point is $x = \xi_2 D$. Else if the kernel falls beyond D , we obtain the distance using the sampling formula for an exponential and $x = D - \left(\frac{1}{\lambda}\right) \log_e(\xi_2)$.

If $\xi_3 < \exp(-\Sigma_m x)$ or $\exp(-\Sigma_m x) < \xi_3 < \exp(-\Sigma_m x) + 1 - a$, the neutron collides in the moderator up to the point x or in the kernel respectively. Else, it crosses the first kernel and its collision point is determined using the expression in Eqs. (6.29)-(6.32) as exponential distributions for the two cases. The distance to the next collision is determined using

$$x = -\left(\frac{1}{\Sigma_m}\right)\log_e(\xi_2) \quad 6.33$$

If $x > D$, the distance is recomputed using

$$x = D - \left(\frac{1}{\beta}\right)[\log_e(\xi_2) + \Sigma_m D] \quad 6.34$$

where,

$$\beta = \Sigma_m + \frac{\lambda(1-a)}{1+a\lambda D} \quad 6.35$$

After a collision, secondary neutrons may emerge in different directions and the collision point is treated as being random if it lies in the graphite moderator and if it is within the fuel kernel it is treated by the method of Sections 6.2.2 and 6.2.3. The only difference is that after emerging from the kernel, since we are at a fuel point, further tracking of its collision point is done using the distribution in Eqs. (6.29) - (6.32).

6.4 Implementation for a pebble-bed HTR lattice cell

While implementation of the above methodology is planned for the general case with continuous energy, here we describe the implementation in the simplest non-trivial case of a spherical lattice cell of a pebble bed HTR. Several benchmarks were studied by us recently using the code BOXER3 [61], [74] employing the multi-group WIMS library [38]. For PuO₂, BOXER3 result is readily available [153] while for (Th-²³³U)O₂ and UO₂ fuels types, it has

been used to calculate the reference results for comparison with results of the proposed Monte Carlo method. Hence, the implementation is carried out in a spherical geometry using multigroup fuel and moderator and coolant cross-sections from the WIMS library after processing the resonance group cross-sections in the usual way. We also use the (transport corrected) isotropic scattering option as it considerably simplifies the modelling as discussed above.

The criticality calculation starts with an initial (guess) spatial distribution of source neutrons that could simply be unity in the fuel and zero elsewhere with an isotropic angular distribution and an energy distribution corresponding to the fission spectrum. Since we do not deal with individual fuel kernels, we start with a source distributed uniformly in the fuel zone. Each of the neutrons is tracked till it is absorbed or leaks out. At each collision the neutron is either absorbed or slows down. The probability of the events is determined by the ratio of the respective cross-section and the total cross-section.

6.4.1 The algorithm used in development of PebMC Code

While much of the k_{∞} calculation algorithm is the same as in standard Monte Carlo methods, the specifics associated with tracking in the random medium, the method of obtaining track length estimates are different. For the sake of completeness, we have included a description the entire algorithm used in our program.

1. Definitions

- (i) History: The sequence of events from birth to absorption or leakage of a particle
- (ii) Cycle: A set of M histories corresponding to a generation of particles.

2. Initialization

(i) Initial source distribution: uniform in fuel region having isotropic distribution and fission spectrum

(ii) Initial number of particles: N each of weight $W=1.0$.

(iii) Initial k_∞ (guess): any reasonable value as close to the expected value

3. If M particles are generated in a new cycle, make each of their weights equal to N/M so total weight is $M(N/M) = N$, which is the same as the initial weight.

4. Following a history:

(a) Initialising

(i) Sampling initial positions of (first cycle) source particles \mathbf{r}_0

For a spherical cell centered at $(0, 0, 0)$ (cell radius $=R_c$, fuel zone radius $=R_f$),

If

$$(2\xi_1 - 1)^2 + (2\xi_2 - 1)^2 + (2\xi_3 - 1)^2 < 1 \quad 6.36$$

Then

$$x = R_f(2\xi_1 - 1), y = R_f(2\xi_2 - 1), z = R_f(2\xi_3 - 1) \quad 6.37$$

For subsequent cycles initial positions are generated from fissions sites of previous cycle

(ii) Sampling direction (all cycles):

$$\Omega_z = 2\xi_1 - 1, \Omega_x = \sqrt{1 - \Omega_z^2} \cos\varphi, \Omega_y = \sqrt{1 - \Omega_z^2} \sin\varphi \quad 6.38$$

(iii) Sampling energy group (all cycles):

Prepare and store a cumulative distribution of the fission spectrum:

$$c_0 = 0, c_1 = p_1, c_2 = c_1 + p_2, c_3 = c_2 + p_3, \dots \dots \quad 6.39$$

If $c_{g-1} < \xi < c_g$, then the sampled energy group is g .

(b) Collision point using

$$\mathbf{r} = \mathbf{r}_0 + \boldsymbol{\Omega}s \quad 6.40$$

Where s is distance to next collision and is sampled using

$$s = -\frac{1}{\Sigma_e} \log_e \xi_1 \quad 6.41$$

If initial point is in the fuel zone, where the effective cross-section $\Sigma_e = [\Sigma_m + \lambda(1 - a)]$ the collision point is in the graphite matrix or fuel depending upon whether $\xi_1 < \Sigma_m/\Sigma_e$ or $\xi_1 > \Sigma_m/\Sigma_e$.

For initial point in any other material with total cross-section Σ , the distance to the next collision is sampled using

$$s = -\frac{1}{\Sigma} \log_e \xi \quad 6.42$$

Note 1. If trajectory crosses the boundary of the material region, distance (from the crossing point) is resampled using one of these equations and the corresponding cross-section. If trajectory crosses the cell boundary the trajectory is continued inward (from the crossing point) as discussed in Section [6.4.2](#).

Note 2. Obtaining track length estimate of the k_∞ using this method of locating the collision point is a little tricky as discussed in Section [6.4.3](#). Hence, we also provide an alternative method in which the usual track length estimator is used. The alternate method is described in Section [6.4.4](#).

6.4.2 White Boundary Condition used in PebMC Code

The problem considered is that of a spherical cell of a pebble bed HTR as shown in [Figure 6-2](#). The central fuel zone is a random dispersion of fuel kernels in a graphite matrix and tracking within this zone is done by the special method. Tracking from the fuel zone to the

moderator and coolant zones or vice versa and reflection from the boundary may be done by the usual methods. If a neutron collision point falls outside the outermost boundary, it is returned inside with a cosine current distribution. Such reflection of particles is called white boundary condition.

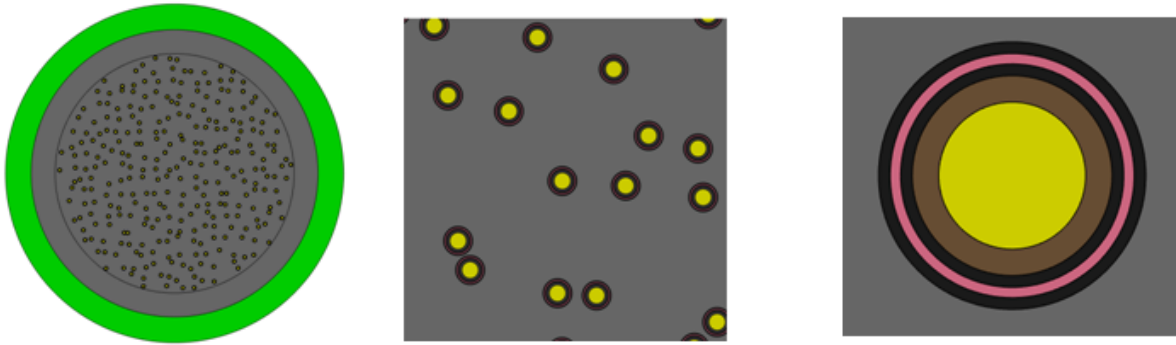


Figure 6-2: (a) HTR pebble unit cell (b) Graphite matrix with TRISO particles (c) Different coating layers of TRISO particle

The distribution of white reflected direction of particles is defined as in Eq. (6.43).

$$f(\mu, \varphi) = 2\mu d\mu \frac{d\varphi}{\pi} \quad 6.43$$

Where, $\mu = \cos(\theta)$, $0 \leq \mu \leq 1$; $0 \leq \varphi < 2\pi$, θ is the polar angle and φ is the azimuthal angle with respect to normal to the surface. Here, the cosine of angle (θ) with respect to the normal and azimuthal angle can be sampled independently since they are mutually independent. Thus, $f(\mu, \varphi)$ can be written as product of distributions $P(\mu)$ and $P(\varphi)$

$$f(\mu, \varphi) = 2\mu d\mu \frac{d\varphi}{\pi} = P(\mu)P(\varphi) \quad 6.44$$

Now, we can sample μ using the distribution $P(\mu)$ and φ using the distribution $P(\varphi)$ as follows

$$\mu = \sqrt{\xi} \text{ and } \varphi = 2\pi\xi \quad 6.45$$

The direction cosines of particles can be determined using relations obtained in Section [2.7.2](#). If the direction cosines of the normal to a surface is $(\Omega_x, \Omega_y, \Omega_z)$, then the direction cosines of the particle's new white reflected direction $(\Omega'_x, \Omega'_y, \Omega'_z)$, are given by Eqs. (6.46)-(6.48) [86] .

$$\Omega'_x = \Omega_x \mu + \frac{\Omega_x \Omega_z \sqrt{1 - \mu^2} \cos(\varphi) - \Omega_y \sqrt{1 - \mu^2} \sin(\varphi)}{\sqrt{1 - \Omega_z^2}} \quad 6.46$$

$$\Omega'_y = \Omega_y \mu + \frac{\Omega_y \Omega_z \sqrt{1 - \mu^2} \cos(\varphi) + \Omega_x \sqrt{1 - \mu^2} \sin(\varphi)}{\sqrt{1 - \Omega_z^2}} \quad 6.47$$

$$\Omega'_z = \Omega_z \mu - \sqrt{1 - \Omega_z^2} \sqrt{1 - \mu^2} \cos(\varphi) \quad 6.48$$

6.4.3 Track length estimator used with the first algorithm

The track length estimator is found to be little complicated in the case when we use the first algorithm, as discussed in Section [6.2](#), for tracking neutrons in randomly distributed fuel particles. When the neutron travels a distance L starting from a random point (including boundary of the fuel zone), the expected (mean) track length in the fuel might appear to be $T_L = \lambda L \bar{l}$, where \bar{l} is the mean chord length of a fuel kernel, since the mean number of kernels intercepted in a length L is λL and the neutron travels an average distance \bar{l} in each kernels. However, this estimator does not agree with the collision estimator but the use of $\lambda L (1 - a) / \Sigma_f$ gives an estimate that is consistent with the collision estimator.

To understand this, we first try and obtain the average distance travelled in any kernel by a neutron incident on it. We first note that the distribution of chord lengths is given by Eq. (6.49)

$$P(l)dl = \frac{ldl}{2R^2} \quad 6.49$$

A neutron may collide in the kernel or escape. Thus, the average track length \bar{T}_{L1} travelled in the kernel will be given by Eq. (6.50)

$$\bar{T}_{L1} = \int_0^{2R} \frac{ldl}{2R^2} \left[l \exp(-\Sigma_f l) + \int_0^l x \exp(-\Sigma_f x) \Sigma_f dx \right] = \frac{1-a}{\Sigma_f} \quad 6.50$$

where the subscript 1 in \bar{T}_{L1} stands for the track length through one kernel. Now one may easily argue that since the average number of kernels in a total track length L is λL , the expected track length in the fuel kernels is given by Eq. (6.51)

$$\frac{\lambda L(1-a)}{\Sigma_f} \quad 6.51$$

We make the argument more precise as follows. A neutron starts out in the matrix region of the fuel zone, that is assumed to be of infinite extent for the present argument. We wish to estimate the average total distance \bar{T}_L that the neutron travels in all the kernels it encounters (up to its first collision in the matrix or a kernel). Clearly, the neutron has a probability $\lambda/(\lambda + \Sigma_m)$ of reaching the first kernel without collision. The neutron either collides in the kernel or crosses it. In the process, it travels an average track length \bar{T}_{L1} obtained above in the kernel and emerges from the kernel (into the matrix) with a probability a . After emerging from the kernel, it may encounter other kernels through which it will again traverse the track length \bar{T}_L . The expected track length up to the first collision \bar{T}_L may then be written as

$$\bar{T}_L = \frac{\lambda}{\lambda + \Sigma_m} [\bar{T}_{L1} + a\bar{T}_L] = \frac{\lambda}{\lambda + \Sigma_m} \left[\frac{1-a}{\Sigma_f} + a\bar{T}_L \right] \quad 6.52$$

This equation can be easily solved for \bar{T}_L to give

$$\bar{T}_L = \frac{\lambda(1-a)}{\Sigma_f[\Sigma_m + \lambda(1-a)]} = \frac{\lambda L_c(1-a)}{\Sigma_f} \quad 6.53$$

Where, L_c is the average distance travelled by a neutron before collision in the medium (in the matrix or a kernel) and is given by the reciprocal of the effective attenuation cross-section in the random medium. Both the above arguments show that on starting from a randomly chosen point in the matrix of the fuel zone (that also include points of entry into the fuel zone) the average track length in the kernel per unit length travelled in the fuel zone is $(1-a)/\Sigma_f$, irrespective of whether the track ends without a collision or in a collision in a kernel or the matrix.

However, if the starting point is in the fuel, we must add the additional distance travelled in the starting kernel before the neutron exits the kernel. The starting distance (s) is computed as per Eq. (6.51). If both starting and ending points are in the same kernel (without emergence from the kernel), the quantity to be added to track length is simply the distance travelled between these two points.

$$K_{inf}^{(T_L)} = K_{inf}^{(T_L)} + \frac{W\bar{T}_L\nu\Sigma_f g}{N} \quad 6.54$$

6.4.4 Alternative algorithm for sampling collision point

For two random numbers ξ_1 and ξ_2 , calculate the distances to the first kernel (s_k) intercepted by the path and collision point (s_c) by using Eq. (6.55) and Eq. (6.56) respectively,

$$s_k = -\frac{1}{\lambda} \ln \xi_1 \quad 6.55$$

$$s_c = -\frac{1}{\Sigma_m} \ln \xi_2 \quad 6.56$$

If $s_c < s_k$, the collision occurs at a point in the matrix before the kernel (i.e. there is no intersection with the kernel). Calculate the collision point using $\mathbf{r} = \mathbf{r}_0 + \boldsymbol{\Omega}s_c$ and check if it is within the fuel zone and record this as the collision point. If the point is outside the fuel zone, move the particle to the boundary point on the trajectory and sample the distance in the medium outside the fuel zone.

If $s_c > s_k$, calculate the kernel position $\mathbf{r} = \mathbf{r}_0 + \boldsymbol{\Omega}s_k$ and check if it is within the fuel zone. If the position is outside the fuel zone, move the particle to the boundary point on the trajectory and sample the distance in the medium outside the fuel zone. If it is within the fuel zone it means the particle crosses the first kernel. Sample the chord length (l) in the kernel from the distribution given by Eq. (6.57)

$$P(l)dl = \frac{ldl}{2R^2} \quad 6.57$$

using the formula in Eq. (6.58)

$$l = 2R\sqrt{\xi_3} \quad 6.58$$

Sample the distance to the collision in the kernel fuel medium using Eq. (6.59)

$$s = -\frac{1}{\Sigma_f} \ln \xi_4 \quad 6.59$$

(Where ξ_3, ξ_4 are new random numbers, and R is the radius of the kernel).

If $s < l$, the particle collides at a distance s inside the kernel. The values of (ρ, z) and global coordinates for the collision point are given by Eqs. (6.60) - (6.62)

$$\rho = \sqrt{R^2 - \left(\frac{l}{2}\right)^2} \quad 6.60$$

$$z = \frac{l}{2} - s \quad 6.61$$

$$\mathbf{r} = \mathbf{r}_0 + \boldsymbol{\Omega}s_k \quad 6.62$$

Add the quantity s to the track length estimate and follow the trajectory within the fuel kernel as in the earlier procedure till it exits the kernel. Add the actual distance travelled within the kernel each time to the track length estimate. If $s > l$, the particle does not collide in the kernel and in this case the process is repeated starting from the new point i.e. $\mathbf{r} = \mathbf{r}_0 + \boldsymbol{\Omega}s_k$. Add the quantity l to the track length estimate in this case.

6.5 Extension to pebble bed HTR core calculations

Extension to core calculations and to continuous energy Monte Carlo does not seem to present any special problems. Several authors [129], [154] have proposed methods for randomly packing pebbles in the reactor vessel of a pebble bed HTR. Once one such a packing arrangement has been made, it is possible to track neutrons from pebble to pebble without any difficulty as in normal Monte Carlo calculations. The main difficulty of having to handle thousands of spheres per pebble can be taken care of by the method of Section [6.2.1](#). Thus, unlike cell calculations in which we reflect isotropically the neutron from the cell boundary, we track it uninterrupted till it collides with a coolant atom or enters another pebble. The rest of the procedure is the same.

6.6 Results

The methods discussed in Section [6.2](#) have been implemented in a Monte Carlo code (PebMC) and we present the results of calculations performed with this code for demonstrating the utility of the method. Since the purpose of this section is to demonstrate the method, a

number of simplifications have been made in the implementation. The implementation has been done in multigroup form and we restrict ourselves to lattice cell calculations. Moreover, we limit ourselves to isotropic scattering. The multigroup cross-sections are based on the IAEA WIMS 172 group library [38], with the transport corrected cross-section. The problems studied are the same benchmarks that were presented in Ref. [153] using BOXER3 [61], [74] as modified for use in HTRs [135]. In addition to presenting comparisons with BOXER3, we also study the effect of various approximations and their corrections that were discussed in Section [6.3](#).

6.6.1 Brief description of the benchmarks studied

The benchmark problems are defined by the OECD Nuclear Energy Agency Nuclear Science Committee working party on the Physics of Plutonium Fuels and Innovative Fuel Cycles [105]. The following benchmark problems have been studied out of the five phases of the OECD NEA benchmark -

- Phase1a- Uranium fuel: Cell calculation employing a spherical outer boundary.
- Phase2a- Plutonium fuel: Cell calculation employing a spherical outer boundary.
- Phase5a-Thorium/uranium fuel: Cell calculation employing a spherical outer boundary.

The specifications of fuel pebbles and coated particles of these benchmarks used in the present study are reproduced in [APPENDIX-A](#). The relative percentage difference of Monte Carlo result with respect to the reference code BOXER3 is defined as follows-

$$Rel. \% Diff. = \left(\frac{K_{MC} - K_{BOXER3}}{K_{BOXER3}} \right) \times 100\%$$

6.6.2 Comparison of the k_{∞} obtained using Monte Carlo with BOXER3 results

In Table 6-1, we show a comparison of our Monte Carlo results with the BOXER3 results obtained in Ref. [153]. We present results obtained using collision as well as track length estimators. The cross-section library and Dancoff corrections used are the same as in Ref. [153]. It is seen that for all three-fuel types, the Monte Carlo results agree within the statistical error with BOXER3 estimates. This provides confidence in our proposed algorithm and its implementation.

Table 6-1 Comparison of k_{∞} obtained using Monte Carlo and BOXER3. Numbers in brackets show % deviation from the reference result.

Fuel Types	Sampling collision point in Random mixture of Kernel and Matrix using effective cross-section Σ_e		BOXER3
	Detailed Tracking in Kernel		
	Collision-Estimator	Track-Length-Estimator	CP method
UO ₂	1.512699 ± 0.000193 (-0.018)	1.512811 ± 0.000367 (-0.011)	1.512978
(Th- ²³³ U)O ₂	1.456409 ± 0.000142 (-0.059)	1.457111 ± 0.000272 (-0.011)	1.457271
PuO ₂	1.451957 ± 0.000144 (0.018)	1.452447 ± 0.000355 (0.052)	1.451691

6.6.3 Effect of using reduced track length $(1 - \lambda\bar{l})$ in graphite matrix

In Table 6-2, we present the effect of using the correction in the track length in graphite to overcome the approximation of point kernels. This involves reduction of the track length in graphite by the factor $(1 - \lambda\bar{l})$. Practically speaking this is achieved by reducing the graphite cross-section by this factor so that the number of collisions in graphite is reduced to their correct value. Since the total kernel volume is about 1% of the fuel zone volume, this is equivalent to having a lower V_m/V_f ratio by about 1%. In the present instance, the effect on k_∞ is clearly not very large. The two results are practically indistinguishable for the smaller sized kernels of Pu and Th. For the larger uranium kernels, the difference is larger and the corrected results differ by 0.2% from the uncorrected and BOXER3 results. This is because the BOXER3 result is also based on the uncorrected formulae. The same correction can be applied in BOXER3 and the corrected BOXER3 result shows closer agreement.

Table 6-2 Effect of using reduced track length $(1 - \lambda\bar{l})$ in graphite matrix. Numbers in brackets show % deviation from the reference result.

Fuel Types	Sampling collision point in Random mixture of Kernel and Matrix using effective cross-section Σ_e		BOXER3 results	
	Monte Carlo (Collision-Estimator)		No correction	With correction $(1 - \lambda\bar{l})$
	No correction	With Correction $(1 - \lambda\bar{l})$		
UO ₂	1.512699±0.00019	1.510810±0.00020	1.512978	1.510669

	(-0.018)	(0.009)		
(Th- ²³³ U)O ₂	1.456409±0.00014 (-0.059)	1.457309 ± 0.00015 (-0.022)	1.457271	1.457630
PuO ₂	1.451957±0.00014 (0.018)	1.451999 ± 0.00017 (0.036)	1.451691	1.451476

6.6.4 Study of the need for tracking within a kernel

In this section, we show that tracking in the kernel once collision is detected in it is important. The reason is that the probability of collision in the same kernel, though small, is not zero. Table 6-3 shows the effect of ignoring tracking in the kernel and basing the algorithm on Eqs. (6.1)-(6.5) alone. The results are significantly different in the two cases thereby clearly demonstrating the need for tracking within the kernel. However, the method of tracking is not particularly important as is seen from Table 6-4. This shows that the radial position dependent formula for $P_{esc}(r)$ as well as flat source-based formula gives about the same results as the detailed tracking in the kernel.

Table 6-3 Results showing the need for tracking within a kernel. Numbers in brackets show % deviation from the reference result.

Fuel Types	Sampling collision point in Random mixture of Kernel and Matrix using effective cross-section Σ_e		BOXER3 results
	Tracking in Kernel	Kernel Tracking ignored	
UO ₂	1.512699±0.000193	1.516724 ± 0.000199	1.512978

	(-0.0184)	(0.25)	
(Th- ²³³ U)O ₂	1.456409±0.000142 (-0.059)	1.455823±0.000152 (-0.10)	1.457271
PuO ₂	1.451957±0.000144 (0.018)	1.459163±0.000202 (0.51)	1.451691

Table 6-4 Effect of different methods of tracking within a kernel. Numbers in brackets show % deviation from the reference result.

Fuel Types	Sampling collision point in Random mixture of Kernel and Matrix using effective cross-section Σ_e		BOXER3
	Use of Escape probability to avoid tracking in kernel		
	Flat Source based (P_{esc})	$P_{esc}(r)$	CP method
UO ₂	1.512970± 0.000193 (-0.0005)	1.51301± 0.00021 (0.0021)	1.512978
(Th- ²³³ U)O ₂	1.456067±0.000151 (-0.083)	1.456183±0.000143 (-0.075)	1.457271
PuO ₂	1.451542±0.000208 (-0.010)	1.452333 ±0.000149 (0.044)	1.451691

6.6.5 Alternative method for sampling the point of collision

In this section, we describe the results using the alternative method for sampling the next collision point starting from a point in the random mixture. As explained there, this method

gives track length estimates more directly than the one based on Eqs. (6.3) - (6.5). Table 6-5 presents the collision and track length estimates of the k_{∞} for various fuel types based on the alternative scheme. We see from Table 6-5 that though the scheme is slightly more involved, the results are in good agreement with BOXER3.

Table 6-5 Results using alternative method for sampling the point of collision. Numbers in brackets show % deviation from the reference result.

Fuel Types	Alternative scheme of sampling collision point in Random mixture of Kernel and Matrix		BOXER3
	Tracking in Kernel		CP method
	Collision	Track-Length	
UO ₂	1.513307± 0.000192 (0.022)	1.514486 ± 0.000348 (0.099)	1.512978
(Th- ²³³ U)O ₂	1.458675±0.000169 (0.096)	1.458912±0.000313 (-0.083)	1.457271
PuO ₂	1.451553±0.000195 (-0.010)	1.451418±0.000542 (-0.010)	1.451691

6.6.6 Studies on the effect of the coatings

In Chapter 5, describing the collision probability approach, we had obtained the distribution of kernels taking their coating into account. We saw that instead of the Poisson distribution, we obtain a dead time corrected Poisson distribution. In Table 6-6, we show the effect of employing this distribution on the k_{∞} . Table 6-6 shows that at least for the fuel density in the current set of benchmarks analysed by us, the effect is indeed very small. This may

however increase as the density increases. Table 6-6 also shows a fictitious result corresponding to a very thin coating. It is seen that this result is almost the same as the one in Table 6-1, that is for a Poisson distribution.

Table 6-6 The effect of the kernel distribution. Numbers in brackets show % deviation from the reference result.

Fuel Types	Sampling collision point in Random mixture of Kernel and Matrix with coating Modified Poisson distribution (Collision-Estimator)				BOXER3
	Coating Thickness (cm)	k_{∞}	Coating Thickness (cm)	k_{∞}	k_{∞}
UO ₂	0.0205	1.512476±0.000166 (-0.033)	0.002	1.513228 ±0.000171 (0.0165)	1.512978
(Th- ²³³ U)O ₂	0.021	1.457427±0.000149 (0.011)	0.002	1.456221±0.000169 (-0.072)	1.457271
PuO ₂	0.021	1.451329±0.000158 (-0.025)	0.002	1.452455±0.000147 (0.053)	1.451691

6.6.7 Discussion of the results

The study of lattice cell benchmarks of a pebble bed reactor involving plutonium, enriched uranium and thorium fuel and two different sizes of the fuel kernel with the proposed Monte Carlo method shows very good agreement with the reference results obtained using the BOXER3 code. A number of points such as the importance of tracking within the kernels (if the previous collision has been in it), and the method used to do the tracking, the correction to

account for the finite volumes of the kernels and the effect of coatings on the statistical distribution of the kernels have been studied. The results of these studies are along more or less expected lines. Tracking within the kernels is seen to be important and therefore necessary irrespective of the size of the kernel. However, the exact method used is not important and simplified models may also be used. The correction due to the finite volume of the kernel is obviously more important for the larger sized kernels of uranium fuel and is not significant for the other smaller sized kernels. The change in statistical distribution of the kernels due to the presence of coatings is found to be small at least for the packing fractions in the benchmarks. Finally, we have shown that the alternative tracking method gives the same results.

6.7 Conclusions

A new approach to Monte Carlo calculations in high temperature reactors has been presented. The proposed new method avoids detailed tracking through the millions of TRISO particles distributed throughout the reactor. It also avoids the limitations of the delta algorithm that may be used in place of detailed tracking. While the method is based on some assumptions that introduce some approximation in the theory, the effects of these has been seen to be very small, being mostly of the order of typical statistical errors and is actually less than the errors in many standard Monte Carlo calculations that make some approximations in describing the statistical distribution of TRISO particles. The results for the case of a pebble-bed reactor lattice cell using multigroup cross-section data are encouraging.

This chapter summarises the highlights of the results obtained in this thesis and outline the ways the present work can be extended in the future.

7.1 Summary and Conclusions

HTRs present unusual challenges concerning the neutronic simulations. It might appear that both deterministic and stochastic methods are inapt to deal efficiently with the peculiar configuration of HTRs. The major challenge is to devise a new efficient method to perform neutron transport in random dispersion of fuel lumps. This also includes resonance self-shielding both in thermal and resonance regions in HTR lattice cell calculations. To provide an appreciation of these challenges, we first gave an overview of HTRs in [Chapter 1](#).

In [Chapter 2](#), traditional neutronics methods and literature review on specific methods used in HTR neutronic calculations were discussed. Two comprehensive objectives of the thesis were defined in [Section 2.9](#). The first is that the thesis sought to improve upon the existing tools to treat HTRs unusual challenges. The second is to develop new deterministic and stochastic methodologies as well as computational tools for HTR analysis. This includes the development of new theoretical models, algorithms and computer codes based on the models, and analysis of benchmark problems.

[Chapter 3](#) presented a new method for computing the Dancoff factors using the Monte Carlo method for the treatment of resonance self-shielding in the resonance energy region. We have described the development of a new scheme (CLR) method using the Monte Carlo to

generate the randomly distributed TRISO particles in the fuel zones of the pebble and the compact shaped graphite. The principal advantage of the method described in the thesis is that it can be used for low as well as high particle densities (~70%). This method is implemented in the Monte Carlo program, called **MCDanc**. The method is very efficient as the randomisation scheme is based on nearest neighbours search algorithm to eliminate any overlapping of particles. This method can also be used to randomly stack pebbles to form pebble-bed in the reactor core for neutronics simulations.

The **MCDanc** program is used to compute the Dancoff factors to conserve the resonance self-shielding in pebble-bed HTR lattice cell calculations. A new method to deal with self-shielding in the thermal energy region using the Equivalent Spherical Shell model is developed in [Chapter 4](#). The results of the equivalent spherical shell model used in BOXER3 code for the HTR benchmark problems show satisfactory agreement with that of the reference results. The BOXER3 code with the equivalent shell method takes about 5sec per HTR lattice cell calculation for pre-computed outer shell radius of a given problem that gives acceptable results. However, the equivalent shell method is somewhat heuristic in nature and does not give a detailed variation of neutron flux in the fuel zone except a single mesh. Another shortcoming of this method is that the calculation of the equivalent radius of the spherical shell is not straightforward as it depends on fuel cross-section.

After this, [Chapter 5](#) discussed the development of a new and rigorous theoretical model to solve the neutron transport equation in the random medium of the HTR lattice cell using the collision probability method. This includes the derivation of several collision probability formulae using two independent methods based on Poisson and coating corrected Poisson distribution of fuel particles in the graphite matrix. The lattice code BOXER3 is extended to implement the new formulae to solve the neutron transport equation in HTR lattice

cells. Multigroup neutron transport equation solution using BOXER3 code with new collision probabilities is a major theoretical improvement and requires slightly more time (about 7sec per HTR lattice cell calculation) as compared to the Equivalent Spherical Shell model. In addition, this method allows to compute flux in several radial meshes in random medium of HTR pebble. Results show that the new method can efficiently perform HTR analysis for any combination of fertile (Th^{232} , U^{238}) and fissile isotopes (U^{233} , U^{235} and Pu). This method is equally suitable with subgroup or ultrafine cross-section data libraries, as it does not require any free parameters such as the Bell factor. In fact, the proposed method presents a novel solution of the double heterogeneity effect involved in HTR lattice analysis. Hence, the equivalent spherical shell method and the one involving solution of transport equation in random medium using new collision probabilities are well suited for the scoping studies as the computational time is short compared to the MC methods.

These formulae laid the foundation of a very efficient new Monte Carlo approach for neutron transport in random medium, which was presented in [Chapter 6](#). Further, we discussed the theoretical basis of the Monte Carlo algorithm and its implementation in **PebMC** code for the case of a lattice cell with a multigroup library. The proposed method has the statistical nature inherent in it and is faster than the methods requiring detailed neutron tracking through the millions of fuel particles randomly distributed in HTR. K-inf calculation using the PebMC code takes about 39min, 50min and 123min for HTR lattice benchmark problems, Phase1a-Uranium fuel, Phase2a- Plutonium fuel and Phase5a-Thorium/uranium fuel, respectively. The explicit modelling of fuel kernels and detailed neutron tracking is almost 4 to 5 times computationally more expensive as compared to the formulae-based tracking.

At the same time, the new method does not have any of the limitations of the delta algorithm. These features of the proposed method make it a better alternative to the traditional

Monte Carlo neutron tracking in HTRs. While all studies in the thesis pertain to lattice cell calculations, the MC method described in the thesis is easily extendable to solve core problems with continuous energy cross section data and full capability of the present method will be utilized with continuous data library and parallel computing.

7.2 Future Work

The collision probability method derived in [Chapter 5](#) is applied to the HTR lattice cell in conjunction with the equivalence principle based WIMSD multigroup library. It will be very interesting to implement this method in the subgroup approach for resonance treatment. We have already obtained the expression for the collision probabilities based on the coating modified Poisson distributions. Implementation of these formulae to further improve the applicability in the higher packing range of TRISO particles is proposed to be carried out in future.

Another important aim for the future is to extend the Monte Carlo development to core calculations for HTR. This requires development of a method for stacking pebbles in the core under gravity. Another aim is to compare the results of our method with a Monte Carlo calculation based on detailed tracking within a fixed (random) configuration of fuel particles. The method will also include a study of the effect of explicit modelling of coatings. It is also proposed to evaluate the effect of packing density of fuel particles on HTR lattice cell results using the collision probability formulae for neutron tracking derived using the Poisson and modified Poisson statistics for random fuel particles dispersions. Since Monte Carlo is most effective together with continuous energy cross-section data, extension of the work to include this capability is envisaged in future.

APPENDIX-A

TABLE A.1 The specifications of fuel pebble for the phase 2a of the benchmark [105]

Fuel pebble specification				
Fuel Type	UO ₂	PuO ₂	(Th- ²³³ U)O ₂	Unit
mass per pebble	10.210	1.129	1.129	g
Packing fraction of coated particles	9.043	3.45	3.45	%
Unit cell coolant outer radius	3.5373			cm
Pebble diameter	3.0			cm
Radius of fuel zone	2.5			cm
Outer carbon coating thickness	0.5			cm
Outer carbon natural boron impurity	0.5			ppm
Number of coated particles per pebble	15000			---
Graphite matrix density	1.75			g/cm ³
Graphite matrix natural boron impurity	0.5			ppm
Outer carbon coating density	1.75			g/cm ³
Coated particle specification				
Outer coated particle radius	0.0455	0.033	0.0455	cm
Fuel kernel radius	0.025	0.012	0.012	cm
Coating thickness	0.09/0.04/0.035/0.0 4	0.095/0.04/0.035/0.04		mm

Coating density	1.05/1.9/3.18/1.9	g/cm ³
Coating materials	C/C/SiC/C	
Fuel natural boron impurity by mass	1	ppm
Fuel density	10.4	g/cm ³

TABLE A.2 OECD/NEA No.6200 HTR benchmark specifications [105]

Nuclide number density data		
Material	Nuclides	Atoms per cm ³ (10 ⁻²⁴)
PuO ₂ fuel	²³⁸ Pu	6.01178e-04
	²³⁹ Pu	1.24470e-02
	²⁴⁰ Pu	5.44599e-03
	²⁴¹ Pu	3.00965e-03
	²⁴² Pu	1.54539e-03
	O	4.60983e-02
	¹⁰ B	1.14694e-07
	¹¹ B	4.64570e-07
UO ₂ fuel	O	4.64272E-02
	²³⁵ U	1.92585E-03
	²³⁸ U	2.12877E-02
	¹⁰ B	1.14694E-07
	¹¹ B	4.64570E-07

(Th- ²³³ U)O ₂ fuel	O	4.74279E-02
	²³² Th	2.19473E-02
	²³³ U	1.76668E-03
	¹⁰ B	1.14694E-07
	¹¹ B	4.64570E-07
Inner low-density carbon kernel coating	C	5.26449e-02
Pyro carbon kernel coatings (inner and outer)	C	9.52621e-02
Silicon carbide kernel coating	C	4.77240e-02
	Si	4.77240e-02
Carbon matrix	C	8.77414e-02
	¹⁰ B	9.64977e-09
	¹¹ B	3.90864e-08
Carbon pebble outer coating	C	8.77414e-02
	¹⁰ B	9.64977e-09
	¹¹ B	3.90864e-08
Helium coolant (at 273.16 K,105 Pa)	³ He	3.71220e-11
	⁴ He	2.65156e-05

APPENDIX-B

Here we write the final expressions for $P_{BM}(L)$ after integrating the Eq. (5.63) using Eqs. (5.60), (5.61) and (5.62).

$$\begin{aligned}
P_{BM}(L) = & \frac{e^{-D\Sigma_m}}{\Sigma_m} [\Sigma_m(e^{D\Sigma_m} - 1) - (1 - a)\mu\{e^{D\Sigma_m} - (1 + D\Sigma_m)\}] \\
& + \Sigma_m\mu \left[\frac{a(1 - e^{-D\alpha})}{\alpha(\Sigma_m + \alpha)} (e^{-2D\Sigma_m} + e^{-L(\alpha+\Sigma_m)+D\alpha}) \right. \\
& + \frac{1 + 2a\lambda(e^{D\lambda} - 1) + \alpha(a - 1 - ae^{D\lambda})}{\lambda(\lambda - \alpha)(\Sigma_m + \lambda)} (e^{-(\lambda+2\Sigma_m)D} \\
& \left. - e^{-L(\lambda+\Sigma_m)+D\lambda}) \right] \tag{B.1} \\
& + \mu e^{-2D\Sigma_m} \left[\frac{a(\alpha\lambda - \alpha - \lambda)}{\Sigma_m\alpha\lambda} + \Sigma_m\alpha\lambda \left(\frac{a\lambda e^{-D\alpha}}{(\Sigma_m + \alpha)} - \frac{(1 - a)\alpha e^{-D\lambda}}{(\Sigma_m + \lambda)} \right) \right. \\
& + \alpha\lambda e^{D\Sigma_m} \left\{ \frac{\Sigma_m\alpha}{\Sigma_m + \lambda} \right. \\
& \left. \left. - a \left(\frac{\alpha\lambda}{\Sigma_m} - (\alpha + \lambda + D\alpha\lambda) + \frac{\lambda\Sigma_m}{(\Sigma_m + \alpha)} + \frac{\alpha\Sigma_m}{(\Sigma_m + \lambda)} \right) \right\} \right]
\end{aligned}$$

The final expressions for $P_{MM}(L)$ after integrating the Eq. (5.48) using expressions of $P_{BM}(L)$ and $P_{BB}(L)$ is given in Eq. (5.50).

$$\begin{aligned}
P_{MM}(L) = & P_{BM}(L) - \frac{e^{-D\Sigma_m}}{L\Sigma_m^2} [(2\mu(1 - a)(1 - e^{D\Sigma_m}) + \Sigma_m e^{D\Sigma_m} - (1 + D\Sigma_m)\Sigma_m + \\
& \mu D\Sigma_m(1 - a)(2 + D\Sigma_m)] + \frac{\mu e^{-D\Sigma_m}}{\alpha\lambda L} \left[\alpha\lambda D^2(4e^{-D\Sigma_m} - 1) + \right. \tag{B.2} \\
& \left. \frac{a(1+2D\Sigma_m)(-2\alpha\lambda+\Sigma_m(\alpha+\lambda+2D\alpha\lambda))}{\Sigma_m^2} (1 - e^{-D\Sigma_m}) + \frac{\lambda a \Sigma_m e^{-D(\alpha+\Sigma_m)}}{(\Sigma_m+\alpha)^2} \{(1 + D\Sigma_m + \right. \\
& \left. D\alpha)(1 - e^{D(\Sigma_m+\alpha)}) + D\Sigma_m + D\alpha\} + \frac{(a-1)\alpha\Sigma_m e^{-D(\lambda+\Sigma_m)}}{(\Sigma_m+\lambda)^2} \{(1 + D\Sigma_m + D\lambda)(1 - \right.
\end{aligned}$$

ACKNOWLEDGEMENTS

I would like to take this opportunity to convey my thanks of gratitude towards several people without their direct or indirect support this work would not have been possible.

I would like to express my great appreciation and deepest regards to my thesis supervisor Dr S.B. Degweker for all his support, motivations, encouragements and guidance. I sincerely thank him for providing me the opportunity to carry out my research under his professional expertise. I will always be indebted to him for all he taught to me, untiring efforts to clarify my doubts and invaluable help in writing the thesis.

I sincerely thank my co-guide Dr Anurag Gupta, Head RPAS, RPDD for his care, motivation, encouragement and for providing all the freedom I needed to work in my own ways. He is my guide after superannuation of Dr S. B. Degweker. I am particularly thankful to Dr Umasankari Kannan, Head RPDD and chairman of my doctoral committee for her insightful comments and technical suggestions. I am thankful to Dr Palani Selvem, BARC and Dr Deven, IGCAR for their time, suggestions, efforts in reviewing my progress of the research and serving on my doctoral committee.

I am grateful to Shri Amod Kishore Mallick and Smt. Argala Srivastava, RPDD for always being helpful and friendly for any problem. I sincerely acknowledge to Shri D.K. Dwivedi, Shri Kapil Deo, Shri A. K. Srivastava, Shri Amit Thakur, Shri Vishal Bharti and Shri Arindam Chakraborti for all their support and help. I want to thanks to RPDD colleagues and friends in BARC for all their help and encouragements.

Thanks are due to my cousin and friend Sunil Singh for his time, support and encouragements. I would like to record high respect and admiration to my parents for their unconditional love and several cheerful sacrifices for my success. I highly appreciate to numerous friends for being supportive, giving unforgettable happy moments in my life and having faith in me.

Thanks, finally but not least, to my son Viresh and wife Chandra Prabha for providing emotional support and great care during the work of this thesis. Above all, I pray and thanks to God Almighty for blessing me the mental ability, courage and knowledge to complete this work.

Thesis Highlight

Name of the Student: Indrajeet Singh

Name of the CI: Bhabha Atomic Research Centre

Enrolment No.: PHYS01201504003

Thesis Title: Development of Deterministic and Stochastic Methods for Physics Analysis of High-Temperature Reactors

Discipline: Physical Science

Date of viva voce: 29th June-2021

High Temperature Reactors (HTR) present unusual challenges concerning the neutronic simulations. It might appear that both deterministic and stochastic methods are inapt to deal efficiently with the peculiar configuration of HTRs. The major challenge is to devise a new efficient method to perform neutron transport in random dispersion of fuel lumps in form of Tri-Structural Isotropic (TRISO) particles. This also includes resonance self-shielding both in thermal and resonance regions in HTR lattice cell calculations.

This research work had led to the new theoretical models, equally suitable to the two alternative methods of reactor physics, the deterministic and Monte Carlo (MC) methods, are developed to address the challenges involved in the HTR lattice cell. This effort includes the derivation of Collision Probabilities (CPs) in random media to solve the integral transport equations for pebble-bed lattice cell. Exact expressions for CPs in the random heterogeneous medium have been obtained by two independent methods under realistic assumptions of the statistical distribution of fuel kernels in the graphite matrix. The primary assumption in the derivation of CPs is that the distribution of the fuel kernels along the length of the intercept follows renewal statistics, more specifically, Poisson statistics. The merit of Poisson statistics is that it corresponds fairly close to the actual situation and allows a simple analytical treatment.

The conventional MC methods are not practical for routine analysis, in particular for HTR lattice cell, due to the high computational cost. To address this challenge, a new MC methodology based on CP formulae derived for random medium, is developed and benchmarked to demonstrate its validity and efficiency. This new method avoids detailed tracking through the millions of TRISO particles distributed through the reactor. It also avoids the limitations of the delta algorithm that may be used in place of detailed tracking. These new methods have been successfully implemented in the multigroup code PeBMC for the pebble bed reactor lattice cell to demonstrate its utility. Thus, it may be expected to serve as an important alternative formulation of MC in HTRs analysis.

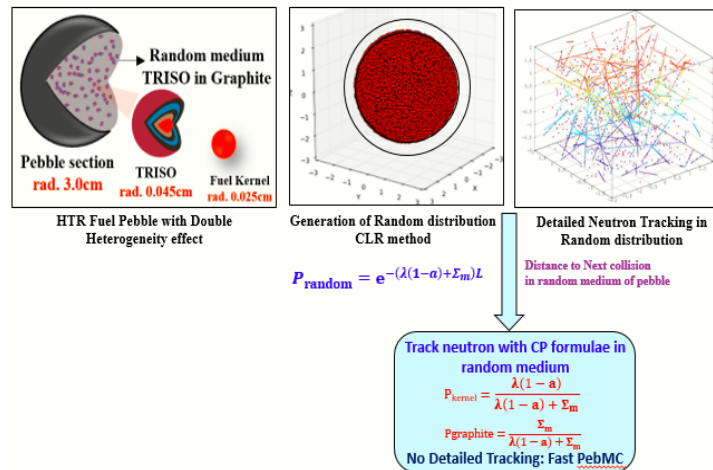


Figure 1 Double heterogeneous HTR lattice cell simulation using new collision probability formula based Monte Carlo code PebMC

These new methods have been successfully implemented in the multigroup code PeBMC for the pebble bed reactor lattice cell to demonstrate its utility. Thus, it may be expected to serve as an important alternative formulation of MC in HTRs analysis.